Surface State Electron Dynamics on Deformed Liquid Helium Films

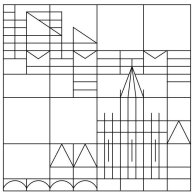

DISSERTATION

zur Erlangung des akademischen Grades
des Doktors der Naturwissenschaften (Dr. rer. nat.)
an der Universität Konstanz, Fachbereich Physik

vorgelegt von

Spyridon Koutsoumpos

Konstanz, 2010

Konstanzer Online-Publikations-System (KOPS)
URN: http://nbn-resolving.de/urn:nbn:de:bsz:352-opus-130195
URL: http://kops.ub.uni-konstanz.de/volltexte/2011/130197

Datum der mündlichen Prüfung: 7. Februar 2011
I. Referent: **Prof. Dr. Paul Leiderer**
II. Referent: **Prof. Dr. Johannes Boneberg**

This thesis was typeset with $\mathcal{A}\mathcal{M}\mathcal{S}$LaTeX.
Text was set in 10pt *Minion Pro* with *Euler* math.
Plots were generated with PyXPlot.
A PDF/A-1b file suitable for electronic archiving was produced with pdfLaTeX.
Printed in Athens, February 10, 2011.

Surface State Electron Dynamics on Deformed Liquid Helium Films

Spyridon Koutsoumpos

Universität Konstanz, Fachbereich Physik, 78457-Konstanz

The financial support of the EU-RTN *Surface Electrons on Mesoscopic Structures* is gratefully acknowledged.

Abstract. Electrons can form stable two-dimensional systems above the surface of dielectric substances like *superfluid liquid helium* (LHe). Due to the extreme purity and smoothness of the LHe surface, electrons on bulk LHe proved to be a versatile (with respect to the facility for changing physical parameters like temperature and magnetic field, but especially electron density) and clean (with respect to electron interactions) system.

In this thesis, we model the dynamics of *two-dimensional electron systems* (TDES) on deformed *superfluid liqui helium* (LHe) films that wet a periodically structured surface exhibiting troughs and peaks and report measurements of the admittance of such TDES for different electron densities and temperatures, as a function of a magnetic field perpendicular to the TDES. We develop the necessary formalism regarding the profile first of an uncharged and then of a charged LHe film (i.e when TDES are present) that wets an idealized profile of the substrate surface. We show that a sufficiently thin LHe film is deformed so that periodical troughs and peaks develop. We find that the trough profile is parabolic. We present the general form of the potential profile that would have been experienced by a *single* electron (i.e interactions among electrons are ignored) both in the troughs and on the peaks of a LHe film that wets a *perfect* substrate (i.e substrate roughness is ignored). Electron potential is parabolic in the troughs and constant on the peaks; thus, a parabolic potential well forms inside the troughs. Having obtained the potential, we proceed to derive the hamiltonian of a single electron both inside a trough and on a peak, in the presence of a static electric and magnetic fields perpendicular to the substrate surface. The energy spectrum of the resulting *Darwin-Fock* hamiltonian indicates that electron motion is essentially a two-dimensional quantum oscillator, but the cyclical frequency (equivalently, the quantum of oscillation) is much greater inside the troughs than on the peaks. We introduce the statistical equilibrium equation for TDES on a deformed LHe film. This equation determines the fraction of electrons that reside on the troughs and peaks at any instant in equilibrium for a given magnetic field, electron density and temperature. We also introduce the concept of *flow admittance*, which arises for TDES on deformed LHe films when the magnetic field is altered. In summary, we suggest that TDES on deformed LHe films partition themselves in two fractions, one for electrons in troughs and another for electrons on the peaks of the film surface. Electrons perform Landau oscillations on the peaks and Darwin-Fock oscillations in the troughs: the latter have a smaller classical radius (localization is stronger) than the former. For changing magnetic field, electrons flow to and from the peaks: an additional "flow admittance" arises, that should be dominant for very high magnetic fields, low temperatures and low electron densities. The behavior of the experimentally measured admittance can be attributed to changes in the fraction of peak electrons and the flow admittance.

Contents

Introduction

Die Kraft des Geistes ist nur so groß als ihre Äußerung, seine Tiefe nur so tief, als er in seiner Auslegung sich auszubreiten und sich zu verlieren getraut.

Phänomenologie des Geistes
G. W. F. Hegel

One of the main ambitions of physicists is to understand and explain the properties of the materials that surround us. Much empirical knowledge has been collected ever since humans learned how to found and process iron and copper, and create alloys. This knowledge was greatly expanded by the alchemists who laid the foundations of modern metallurgy and chemistry and the body of knowledge that would bring about the scientific revolution. It is then perhaps surprising that the first coherent framework for explaining the properties of the three major classes of materials (metals, semiconductors and insulators) became available only after quantum theory was established and especially after the second world war.

In particular, the structure of metals and semiconductors is nowadays understood as a blend of a positively charged immobile ion grid that is filled with negatively charged mobile electrons, so that the net charge remains equal to zero. The system of mobile electrons is the 'dynamic' part that is largely responsible for most properties of metals and semiconductors. The transport properties[1] of these electron systems are crucial as they determine, among others, the thermal and electrical properties of metals and semiconductors and for this reason they are extensively studied.

Except for the study of transport properties *per se*, an objective in recent years—related to the statistical nature of transport properties—has been to identify and study N-particle systems at the smallest possible scale needed, in order

[1]Transport properties of a system of N particles are those properties that depend on physical quantities with a collective, statistical nature. For example, each electron has a certain energy, spin, charge and can exert a force, but speaking of the temperature, resistance, and pressure of a single electron is absurd. Transport properties arise out of the interactions of a large number of particles. Thus, energy exchange and spin interactions give rise to temperature, while the kinetics of charged carriers give rise to conductance.

for transport properties to emerge. These systems are large enough to be studied at the particle level yet not so large for particle-level fluctuations to be ignored: they are a bridge between the microscopic and the macroscopic level and for this reason they are called *mesoscopic systems*.

Transport properties of an N-particle system are statistical properties that also depend on the degrees of freedom the motion of the particles has. A particle can have at most seven degrees of freedom, in a universe with three spatial dimensions, made up of three space coordinates, three momentum coordinates and one angular momentum coordinate. If the maximum number of degrees of freedom cannot be increased further, as this would require an other universe, it is interesting to consider systems whose particles have less degrees of freedom. An obvious possibility would be systems where one, two, or all three spatial degrees of freedom are suppressed, so that the particles are constrained to move in a plane, a line, or not move at all, being constrained to a point, respectively. Depending on the available spatial degrees of freedom, such N-particle systems are characterized as two-, one-, or zero-dimensional, respectively.

The characterization of an N-particle system as mesoscopic, or low-dimensional, is not absolute, but it should be understood in a relative sense. A system of colliding billiard balls on a relatively frictionless table could have been termed mesoscopic, had the number of billiard balls been large enough to just permit a treatment by means of statistical mechanics. This system is also two-dimensional, because the balls have two spatial degrees of freedom, since they move on a plane (the motion of billiard balls vertically is insignificant compared to their motion horizontally). A system of electrons, moving on the plane surface of superfluid helium is also mesoscopic and two-dimensional, because electron motion in the z-direction (the motion *to* and *from* the surface) is insignificant compared to the motion in the x- and y-direction. Clearly, the absolute size of the billiard-ball system and the electron system differs by many orders of magnitude, but this does not affect their characterization as two-dimensional mesoscopic systems.

Low dimensional mesoscopic systems that have been experimentally realized include colloidal suspensions, emulsions, foams, polymers and liquid crystals. An advantage of these systems is that in many cases the particle size is large enough, so that it is possible to investigate particle kinetics optically, by means of a microscope and a VCD-camera. Moreover, these systems find important technological applications and they are significant in chemistry and biology.

Another class of low-dimensional mesoscopic systems has been realized with electrons in heterostructures and electrons on the surface of dielectric substances. The benefits of using heterostructures, in order to create a high-density, two-dimensional electron system were analyzed theoretically by *Kroemer* [**64**] in 1963, but the technical demands for constructing a heterostructure delayed experimental studies until 1967, when *Rupprecht et al.* [**92**] paved the way for the

fabrication of the GaAs-AlGaAs heterostructure. At around the same time, *Cole et al.* [**19, 21**] and independently *Shikin* [**96**] proposed the use of electrons on the surface of dielectric substances for creating a two-dimensional mesoscopic system. The first experimental demonstration, using electrons on liquid helium, followed in 1971 by *Williams et al.* [**116**]. In the following years, several other dielectric substances were used, including solid neon, solid hydrogen and liquid ^{3}He.

The properties of two-dimensional electron systems (henceforth TDES) are extensively studied (a classic review article covering the state of research up to 1982 is *Ando et al.* [**7**]). The study of TDES led to the demonstration of expected phenomena like the Wigner crystallization (*Wigner* [**114**]) and of unexpected phenomena like the integer (*von Klitzing et al.* [**109**]) and fractional quantum Hall effect (*Tsui et al.* [**108**], theoretically explained by *Laughlin* [**69**]). Electrons on liquid helium have also been proposed as a system for quantum computation by *Platzman et al.* [**91**].

Theoretically, the transport properties of TDES are studied by means of the quantum field theory and the scaling theory. Quantum field theory is usually associated with elementary particle physics, but the renormalization group and the Feynman diagram techniques are valuable tools for the study of phase transitions, interactions and correlations of an N-particle system as well (*Zinn-Justin* [**119**] develops quantum field theory without an elementary particle physics bias). *Datta* [**27**] focuses in the theory of transport properties of TDES in heterostructures from a quantum field theoretic perspective, while *Monarkha and Kono* [**81**] do the same for TDES on liquid helium. The scaling theory, developed by *Thouless* and coworkers (see the review article by *Thouless* [**106**]) relies on dimensional analysis arguments and the effects of dimensionality in transport properties, in order to derive general formulas for transport properties that explicitly contain the dimension $d = 1, 2, 3$ of the system. The formulas provided by scaling theory can be used for comparison and guidance with the more demanding quantum field theoretic approach.

A two-dimensional electron system, according to *Abrahams et al.* [**1**], should be an insulator[2] in the absence of a magnetic field. This means that conductivity drops for a decreasing temperature, becoming zero at the limit $T \longrightarrow 0$. The exciting possibility of superconductivity in two-dimensional systems is therefore excluded, although there have been theoretical claims for the contrary by *Tanatar et al.* [**103**]. Moreover, the *Kosterlitz-Thouless* theory of melting [**59**] predicts that TDES on liquid helium would undergo a liquid-to-solid phase transition as the electron density increases for a given temperature. This phase transition

[2]This is a general result of scaling theory for two-dimensional systems. A metallic state, in the sense that the resistance drops for decreasing temperature, cannot exist in two dimensions. It is perhaps an irony that a system made up exclusively of electrons, the principal carriers of conduction in metals, is an insulator!

was indeed observed by *Grimes et al.* [**39**]. Conductivity is abruptly reduced in the transition from liquid to solid. Further increase of electron density for a constant temperature should lead to another, purely quantum solid-to-gas phase transition, which has not been observed, due to the difficulty of bringing electron density at the required value.

One-dimensional electron systems, or *quantum wires* have been created with electrons in nanotubes, as well as with TDES in heterostructures and on liquid helium. The research on quantum wires is pursued vigorously, because these systems are the primary candidates for the detection of the Luttinger liquid (*Luttinger* [**76**]), a strongly correlated Coulomb liquid that can nevertheless be theoretically analyzed in detail. One-dimensional electron systems on liquid helium were created by *Kovdrya et al.* [**62, 63**], using substrates whose surface was periodically structured in the form of long channels. A thin superfluid helium film wet the substrate surface, following its pattern. Measurements of electron mobility confirmed that electrons moved preferentially along the channels rather than across them, but failed so far to indicate the existence of the Luttinger liquid.

A zero-dimensional electron system, or *quantum dot*, is created from a TDES, if additional electric or magnetic fields rip off all degrees of freedom of electrons. Quantum dots, containing several thousand electrons, have been demonstrated for TDES in heterostructures and their physics is reviewed by *Alhassid* [**3**]. Ideally, a quantum dot should contain exactly one electron, but this is not easily achieved, because of the high electron densities of TDES in heterostructures.

Electron systems on liquid helium are advantageous, because electron density is easily varied and it can be made low enough to create quantum dots that accommodate a single electron. This would have been particularly important for quantum computation, because such a quantum dot could be used as a qubit (the quantum analog of a conventional boolean switch).

This thesis presents an attempt towards the zero-dimensional localization of electrons on liquid helium. Electron localization is topological, in the sense that the surface of liquid helium is deformed, its profile exhibiting periodic troughs and peaks, so that electrons are more likely to be trapped inside troughs. The deformation of the liquid helium surface is achieved by using a silicon substrate whose surface is periodically structured into troughs and peaks. Then, the periodically structured substrate is wet by a superfluid helium film whose thickness is adjusted, so that the helium film follows the periodic structure of the substrate. The fact that superfluid liquid helium is a universal wetting agent, allows a fine adjustment of the film thickness just by raising or lowering the level of bulk liquid helium under the substrate.

Electron localization is perfected by applying a magnetic field with nonzero component only in the direction perpendicular to the surface of liquid helium. The ensuing Landau quantization causes electrons in the troughs to move in

quantized circular orbits, whose radius can be made smaller when the magnitude of the magnetic field increases.

The silicon substrate (and ultimately the TDES) is laid on two golden electrodes that are connected to a lockin amplifier. An AC-excitation voltage is applied by the lockin amplifier at one of the electrodes and the response of the TDES is collected by the second electrode. The admittance of the TDES can then be determined. From the behavior of conductivity when the magnetic field is altered one can draw conclusions about the physical properties of zero-dimensional electron localization.

The present thesis is structured in two parts containing five chapters. The first part reviews the basic theory of and experiments on electrons on liquid helium and it can be skipped by readers with experience in the field, although we certainly hope that the exposition of the material, which was *intended* to be logical and perspicuous, will provoke some interest. The second part contains the main theoretical and experimental results of our research.
In more detail:

Chapter 1 reviews basic experimental and theoretical properties of TDES on bulk liquid helium with an emphasis on the interactions of TDES electrons and how these interactions affect electron mobility and the thermodynamics of the TDES. A fundamental shortcoming of TDES on bulk liquid helium is that there exists a maximum attainable electron density, after which the surface of liquid helium becomes unstable and the TDES is destroyed.

Chapter 2 continues the experimental and theoretical review for the case of TDES on helium films, with an emphasis on the effect of different substrates on electron mobility and the thermodynamics of the TDES. The behavior of TDES on helium films in the presence of a magnetic field is analyzed and the important phenomena of weak localization and cyclotron resonance are examined.

Chapter 3 introduces the apparatus utilized for the measurements and analyzes the experimental methods used for determining the conductivity. The basic models for data analysis (with their limitations and advantages) and the way in which raw experimental data are turned into the conductivity of the TDES are examined in detail.

Chapter 4 develops the theoretical foundations of the experiment on zero-dimensional localization. The derivation of the profile of the liquid film that wets the substrate by means of the Young-Laplace equation is presented. The effect of a DC-electric field, pushing electrons towards the deformed surface of liquid helium is examined. Then, the combined effect of a DC-electric field and a magnetic field perpendicular to the surface of liquid helium is treated, leading to a model for determining the distribution of localized electrons inside the troughs and on the peaks. A critical finding is that the partial fraction of electrons in the troughs (and consequently also on the peaks) depends on the magnitude of the

applied magnetic field. It is shown that changing the magnetic field leads to an electron flow to and from the peaks, which contributes to the admittance.

Chapter 5 presents preparatory measurements of parameters of the experimental apparatus that influence the behavior of TDES and, of course, admittance measurements as a function of the magnetic field. Admittance measurements are subsequently discussed and analyzed in view of the theoretical insights gained from the previous chapter.

Two appendices provide some useful theoretical elaboration on the surface states of a single electron on liquid helium (appendix A) and Landau quantization (appendix B).

The SI (or MKSA) units are used everywhere in this thesis, except for seldom occasions, which are clearly labeled. The use of SI units in experimentally oriented work (and especially in diagrams) is not uncommon, because these units are widespread both in everyday life and in experimental physics. However, most theoretical papers are written with the gaussian (or CGS) system of units in mind. This is especially problematic for the equations of electromagnetism, because factors of $4\pi\epsilon_0$ and c must be divided or multiplied out, in order to transform to SI units. The possibility of errors is very high. Therefore, all theoretical equations were transformed for use with SI units, and they may appear different than their original form in the research literature. If, for some reason, the reader would like the CGS form of the equations it suffices to consult the original research papers.

Part I

Foundations

CHAPTER 1

Electrons on Bulk Liquid Helium

1.1. Electron potential

A stable two-dimensional electron system (TDES) can be generated on the surface of liquid helium that partially fills the free space between two metallic plates (the *top plate* and the *bottom plate*, a realization of which is depicted in fig. 3.1). Assume that the surface of liquid helium lies at $z = 0$. Liquid helium extends down to a depth $z_1 < 0$ where the bottom plate is reached. Vacuum, or gas helium atoms of low pressure, are encountered from $z = 0$ up to $z_2 > 0$ where the top plate is reached. Electrons of the TDES levitate at a height $z > 0$ above the surface of liquid helium.

Electrons can interact with liquid helium, with other electrons of the TDES, and external electric or magnetic fields. Therefore, in the most general case, the potential of a single electron will be the sum $V = V_{He} + V_C + V_{ex}$, with obvious notation.

For clarity, the contribution of each term will be examined separately in the immediately following sections. The effects of an external magnetic field are important and varied; they are discussed extensively in section 2.5.

1.1.1. Electron potential due to the surface of liquid helium. Assume that external fields are absent and consider a single electron at a distance $z > 0$ above an ideal[1] liquid helium surface located at $z = 0$. Two phenomena are essential in deriving the potential V_{He}, experienced by the approaching electron.

- The first phenomenon is the polarization of the liquid helium surface by the approaching electron that leads to a weak attracting Coulomb potential term of the form $-\Lambda/z$. The exact value of Λ is obtained by considering that the electron induces an image charge inside helium and, if the dielectric constant of helium is denoted with $\epsilon_{He} = 1.0572$ and the electron charge with e, it is equal to

$$\Lambda = \frac{\epsilon_{He} - 1}{4(\epsilon_{He} + 1)} e^2 \text{ [CGS]} = \frac{\epsilon_{He} - 1}{16\pi\epsilon_0(\epsilon_{He} + 1)} e^2 \text{ [SI]} \approx 7 \times 10^{-3} e^2. \qquad (1.1)$$

[1] This means that the surface does not have any structure and constitutes an abrupt discontinuity.

- The second phenomenon is a strong repulsion at short distances, due to Pauli principle, between the free electron and the *s*-electrons of the helium atom. This repulsion imposes a positive potential barrier the free electron has to overcome, in order to penetrate in liquid helium. In an ideal surface, the potential barrier may be approximated as being practically infinite. The potential due to the surface of liquid helium in every region is then,

$$V_{He}(z) = \begin{cases} -\Lambda/z & z > 0, \\ \infty & z \leqslant 0. \end{cases} \tag{1.2}$$

The potential as given by eq. (1.2) captures the basic physics of a TDES and it is simple enough to permit an analytical solution of the Schrödinger equation for the system (see appendix A). The Coulomb form of the potential for $z > 0$ in eq. (1.2) suggests the existence of a spectrum of discrete z values that define a discrete family of equilibrium planes above the surface of liquid helium. Electrons are allowed to move only at these equilibrium planes, meaning that motion along the z-direction is quantized.

Spectroscopic measurements performed by *Grimes et al.* [**40**] validated the Coulomb form of the electron potential due to the surface of liquid helium. However, *Grimes et al.* [**40**] found that their experimental data are better described by a phenomenological potential of the form

$$V_{He}(z) = \begin{cases} -\Lambda/(z+\beta) & z > 0, \\ V_0 & z \leqslant 0. \end{cases} \tag{1.3}$$

where the values of β and V_0 that provide the best fit for experimental data are 1.01Å and 1eV respectively. The potential barrier $V_0 = 1\text{eV}$ is three orders of magnitude greater than any other energy of the TDES, justifying the idealization $V_0 \longrightarrow \infty$ of eq. (1.2).

1.1.2. Microscopic electron potential due to the surface of liquid helium (CGS Units). The more general case of a strongly interacting electron gas near a nonuniform granular interface is an intractable N-body problem. *Cheng, Cole and Cohen* [**16**] (CCC) have ignored electron-electron interactions and studied the case of electrons that interact with a granular helium interface.

In the CCC approach, the surface of liquid helium is no longer considered ideal, but rather a profile described by the density function $\rho_{He}(z)$. At a given temperature, $\rho_{He}(z)$ becomes equal to the density of helium gas for $z \gg 0$, whereas for $z < 0$ it quickly assumes the density of bulk liquid helium. The density profile of the liquid-to-gas interface of ^{4}He is known from X-ray scattering experiments of *Lurio et al.* [**74, 75**].

The single-electron potential can then be written as the sum $V(z) = V_0\big(\rho_{He}(z)\big) + V_p(z)$ of a local term $V_0\big(\rho_{He}(z)\big)$ that expresses the influence of

helium atoms in the immediate neighborhood of the electron, plus a nonlocal term $V_p(z)$ that incorporates any other long range influence upon the electron from helium atoms.

The local term is therefore responsible for what was *ad hoc* stated in section 1.1.1 as "the strong repulsion at short distances, due to Pauli principle, between the free electron and the *s*-electrons of the helium atom" and it can be calculated as a function of microscopic parameters (for the details of that calculation the reader is deferred to [**16**]). Especially interesting is the numerical value of V_0 near the liquid helium surface, calculated from the asymptotic formula

$$V_0\left(\rho_{He}(z \longrightarrow 0)\right) \approx \frac{2\pi\hbar^2}{m}\rho_{He}a. \tag{1.4}$$

In the equation above, m is the electron mass, ρ_{He} the density of liquid helium and $a = 0.62\text{Å}$ the total scattering length of a helium atom-electron collision. The theoretical numerical value for V_0, calculated from eq. (1.4), is 1.16eV, in good agreement with the experimental value $V_0 = 1\text{eV}$ that *Grimes et al.* [**40**] determined.

The nonlocal term $V_p(z)$ is the polarization energy of an electron, arising from the long range polarization of helium atoms caused by electron charge. In deriving the image charge potential of eq. (1.2), it had been just stated that the approaching electron leads to a weak polarization of liquid helium surface. The nonlocal term is given by

$$V_p(z) = -\frac{\pi\alpha_{He}e^2}{2}\int_{-\infty}^{+\infty} dz' \frac{\rho_{He}(z') - \rho_{He}(z)}{(z-z')^2}. \tag{1.5}$$

The static polarizability α_{He} of helium that appears in the equation above is defined by

$$\alpha_{He} = \frac{1}{2\pi\rho_{He}}\frac{\epsilon_{He}-1}{\epsilon_{He}+1}. \tag{1.6}$$

Although the integrand in eq. (1.5) has a double pole at $z = 0$, the integral's Cauchy principal value can be determined and a $1/z$ Coulomb behavior is obtained for $z > 0$, in agreement with both the experimental phenomenological potential of eq. (1.3) and the theoretical image-charge potential of eq. (1.2).

In view of the CCC approach and the completely different microscopic form of the electron potential found, it is even more surprising that such a simple phenomenological potential like eq. (1.3) is established through experiments. Here, as in other areas of physics, the complicated details of the individual particle's dynamics, due to their inherent randomness, get "washed out" at larger scales, so that in the end only relatively simple features emerge.

1.1.3. Electron potential due to other electrons (CGS Units). Electrons on the surface of liquid helium form a two-dimensional system where electrons interact with each other through Coulomb forces. Let the surface density of the

electron sheet be denoted with n, and consider the uniform continuous charge distribution ne. The potential of this charge distribution is equal to $-2\pi ne^2 z$, if the vertical distance z is larger than the mean distance between the electrons of the sheet ($z \gg 1/\sqrt{n}$). If z is comparable or even smaller than the mean distance, the charge distribution is neither uniform nor continuous and the details of the local charge density should be taken into consideration, as was done by *Iye et al.* [**50**] in the *correlation hole model*.

According to the correlation hole model, electrons that belong to a two-dimensional gas cannot approach each other closer than a certain correlation distance r_0. The correlation hole can then be defined as the disc with radius equal to r_0 around an electron. Correlation distance is determined from the condition $g(r_0) = 1/2$, where the pair correlation function $g(r)$ gives the probability that two electrons are at a distance r apart. The pair correlation function has been computed for the two-dimensional electron gas by *Totsuji* [**107**]. The existence of correlation holes decreases charge density around electrons and it modifies the potential V_C due to the electron sheet in the vertical z-direction, as in

$$V_C(z) = -2\pi ne^2 \times \begin{cases} z^2/2r_0 & 0 < z \leqslant r_0, \\ z - r_0/2 & z > r_0. \end{cases} \tag{1.7}$$

Correlation holes are augmented for an increasing electron density. For low electron densities, electron-electron interactions are weak and the correlation radius r_0 very small, whence the lower branch of V_C in eq. (1.7) dominates completely. For high electron densities, the correlation radius r_0 could eventually become comparable with the distance between the electrons and the surface of liquid helium. In this case, V_C will be dominated by the upper branch of eq. (1.7), which has a quadratic dependence on z instead of the linear dependence one would expect from a uniform, continuous charge distribution.

Information on electron potential can be obtained experimentally, by measuring the escape rate of electrons when a controlled amount of electric energy is provided. Assuming that all other escape mechanisms have been brought under control, electrons will escape only when the provided energy is greater or equal to the potential. Experiments of that kind have been performed by *Iye et al.* [**49, 50**] and they revealed a dependence of the escape rate on electron density, as predicted by the correlation hole model.

1.1.4. Electron potential due to external electric fields. The motion of electrons above the surface of liquid helium is free parallel to the surface, but quantized vertically (see appendix A). Each quantum state is a plane parallel to, and at a certain height above the surface of liquid helium, with higher planes associated with higher energy as well.

If energy levels are expressed in terms of temperature (by means of the fundamental equation $E = k_B T$), one obtains (cf. also [**20**])

$$E_\nu = -\frac{7.5\text{K}}{(\nu+1)^2}, \quad \text{for} \quad \nu = 0, 1 \ldots \tag{1.8}$$

The ground state ($\nu = 0$) is characterized by an equivalent thermal energy of temperature $(-)7.5$K, whereas the thermal energy of the first excited state ($\nu = 1$) has a temperature approximately equal to $(-)1.8$K.

The properties of TDES on liquid helium are normally studied at temperatures lower than 2.1K, so that the advantage of the calm surface of superfluid helium is exploited. This means that the available thermal energy should not be enough for electrons to populate excited states, since $T(\nu = 1) - T(\nu = 0) = 5.7\text{K} > 2.1\text{K}$, and electrons ought to be at the ground state exclusively.

However, measurements of the TDES mobility by *Ostermeier et al.* [**87**], using a direct time-of-flight method, suggested that the majority of electrons resided at excited, almost free states. According to *Ostermeier et al.* [**87**], bound electrons at the ground state—if they existed at all—would be stable for less than 10ms.

These results were intriguing, especially in view of earlier mobility measurements by *Sommer et al.* [**101**] and TDES lifetime measurements by *Williams et al.* [**116**], which suggested that TDES at their ground state were stable for many hours.

A more careful analysis of the experimental conditions in the experiments reported in [**87, 101, 116**] resolved the apparent paradox and revealed the importance of TDES statistical mechanics. The thermodynamic properties and statistical mechanics of TDES on liquid helium are important and rich, affecting the mobility of TDES electrons for different combinations of electron density and temperature (see section 1.4) and quasi one- and zero-dimensional electron localization [**10**].

Crandall et al. [**24**] studied how TDES states are populated with electrons. They considered a classical, saturated, two-dimensional electron gas of density n_s, obeying the Maxwell-Boltzmann distribution. From statistical mechanics, the partial fraction n_ν/n_s of electrons of a TDES that belong to the ν-th state is found to be

$$\frac{n_\nu}{n_s} = \frac{1}{Z} \exp\left(-\frac{E_\nu}{k_B T}\right), \quad \text{for} \quad \nu = 0, 1 \ldots \tag{1.9}$$

where Z is the partition function of the system and E_ν the eigenenergy of the ν-th quantum state.

Crandall et al. [**24**] notice that the partition function can be decomposed into a sum over the quantized bound states plus a term for free (continuous) motion along the direction perpendicular to the surface of liquid helium. Both bound and continuous states are those that fit in the space between the top plate and the bottom plate. If the distance that separates the top and bottom plates is

denoted with L, and a_0 is the equivalent Bohr radius of TDES on liquid helium (see appendix A), the partition function results in

$$Z_0 = \left(\frac{mk_BT}{2\pi\hbar^2}\right)^{1/2} L + \sum_{\nu=1}^{\nu_{max}} \exp\left(-\frac{1}{\nu^2}\frac{E_0}{k_BT}\right), \quad \text{where} \quad L = a_0\nu_{max}^2. \quad (1.10)$$

Substituting eq. (1.10) into eq. (1.9) and considering a realistic value $L = 10\text{mm}$, one finds that $n_0/n_s \approx 0$ for $T > 0.9\text{K}$, meaning that most electrons populate excited states and are almost free, in that electron motion in the direction perpendicular to the surface of liquid helium is almost continuous[2]. Thus, the experimental results of *Ostermeier et al.* [**87**] who failed to detect a stable TDES at the ground state for $T > 1\text{K}$ appear to be theoretically vindicated.

But then, the question that arises is why *Sommer et al.* [**101**] and *Williams et al.* [**116**] were successful in detecting stable TDES on liquid helium even at temperatures $T > 1\text{K}$. The answer is that these experimenters applied a constant electric field perpendicular to the liquid helium surface that attracted electrons towards the bottom plate (such an electric field will be hereafter referred to as the *holding field*). The electron potential due to a holding field $\mathcal{E}_\perp$ is

$$V_{ex}(z) = -e\mathcal{E}_\perp z, \quad (1.11)$$

where the minus sign indicates that for positive electric field ($\mathcal{E}_\perp > 0$) electrons are attracted from the bottom plate, whereas for negative electric field ($\mathcal{E}_\perp < 0$) electrons are repelled.

The existence of a holding field modifies the Schrödinger equation for an electron above the surface of liquid helium and the resulting energy spectrum. A potential as in eq. (1.11) will be appended in the electron potential, an analytic solution of Schrödinger equation is no longer possible and perturbation methods need to be employed (appendix A). The approach is similar to the one followed in the analysis of the Stark effect in atomic physics and the outcome is a general shift of the energy levels towards higher (when $\mathcal{E}_\perp < 0$) or otherwise lower values.

But, even when the modified energy spectrum is taken into account, the energy difference between the ground state and the first excited state remains much larger than the available thermal energy. Moreover, from the fact that the energy levels are all shifted to lower values (when $\mathcal{E}_\perp > 0$) the situation is qualitatively the same as in the experiment of *Ostermeier et al.* [**87**]. The apparent paradox with regard to the experiments [**101, 116**] is not yet resolved.

Cole [**20**] calculated the partition function $Z_\mathcal{E}$ for a TDES in the presence of a holding field $\mathcal{E}_\perp$. Due to the analytically intractable energy spectrum (Schrödinger equation is solvable only by perturbation method for $\mathcal{E}_\perp \neq 0$),

[2]It is a common observation that the properties of quantum systems approach the properties of their continuous, classical counterparts for big quantum numbers (large number of quanta).

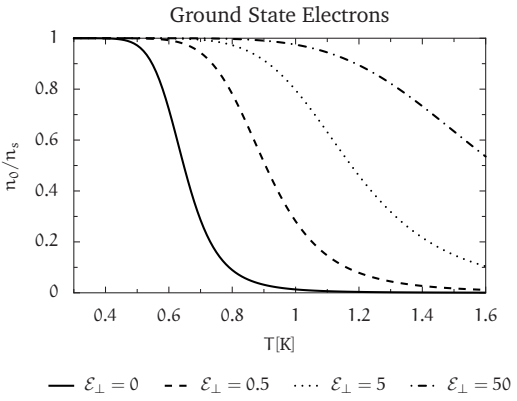

FIGURE 1.1. Partial fraction n_0/n_s of ground state electrons as a function of temperature T, for holding fields $\mathcal{E}_\perp$[V/m]. For $\mathcal{E}_\perp = 0$ most electrons reside in excited states for $T > 0.9$K. However, even very weak $\mathcal{E}_\perp$ alter electron distribution, so that most electrons reside in the ground state for $T > 0.9$K as well.

the partition function $Z_\mathcal{E}$ is also an approximate expression of the form

$$Z_\mathcal{E} \approx \exp\left(-\frac{E_0 + e\mathcal{E}_\perp \langle z\rangle_0}{k_B T}\right) + \frac{k_B T}{\hbar e \mathcal{E}_\perp}\left(\frac{2mk_B T}{\pi}\right)^{1/2} \exp\left(\frac{e\mathcal{E}_\perp \langle z\rangle_0}{k_B T}\right), \quad (1.12)$$

where $\langle z\rangle_0 = 114$Å is the mean distance of the ground state from the surface of liquid helium.

Replacing $Z_\mathcal{E}$ as given in eq. (1.12) into eq. (1.9), the partial fraction of ground state electrons results in values $n_0/n_s \approx 1$ for $T > 1$K, even for weak holding fields (see fig. 1.1), and the apparent paradox posed by the experiments in [**87, 101, 116**] is finally resolved.

It is interesting to note that in the early experiments [**101, 116**] the holding field was intuitively applied, in order to "push" electrons towards the bottom plate (and, thus, towards the ground state). Nevertheless, the argumentation in the previous paragraphs makes clear that electrons populate the ground state because $\mathcal{E}_\perp$ increases the probability weight of the ground state compared to the excited states. This is a purely statistical property of the TDES, with no connection to electron dynamics, or the modification of the energy spectrum.

The electrons of a TDES repel each other with Coulomb forces. If the repulsion is greater than the binding energy, electrons will disperse on the plane parallel to the surface of liquid helium. A first estimation of the relative strength between Coulomb repulsion and binding energy, according to *Cole* [**20**], gives rise to a critical electron density n_c for a disk-shaped TDES to remain stable that is equal to

$$n_c = \Lambda^2 R/a_0 \approx 6.37 \times 10^7 \, m^{-2}, \quad \text{for } R = 1\text{cm}. \quad (1.13)$$

In the equation above, the radius of the TDES was denoted with R and the equivalent Bohr radius with a_0 (see appendix A).

Typical values of n_c are at least four orders of magnitude lower than the desired electron densities for mobility measurements. An external potential

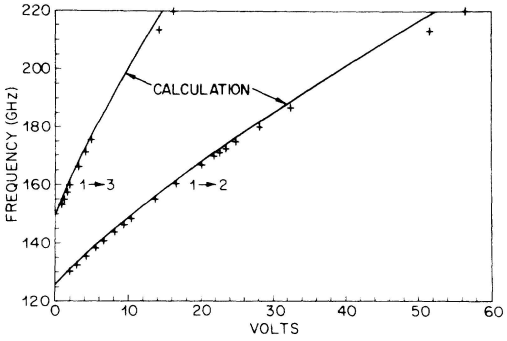

FIGURE 1.2. Measurements by *Grimes et al.* [**41**], confirming the hydrogenic energy spectrum of TDES and the Stark-effect shift when a holding field is applied. Cyclic transition frequencies from the ground state to the first ($1 \longrightarrow 2$) and second ($1 \longrightarrow 3$) excited states were measured.

barrier (the *guard voltage*) around the TDES must be applied on the plane of the TDES, such that the maximum number of electrons can be constrained in the area of interest. Theoretically, the presence of a guard voltage is unwelcome, because it complicates the analysis of TDES dynamics. But, in practice, the capacity of the electron gas to screen external fields very effectively means that only electrons in the immediate neighborhood of the boundary will experience the electric field. Therefore, if the area of the two-dimensional electron system is large, edge effects that relate to the guard voltage will not arise.

1.1.5. Experimental observation of electron potential. The hydrogen-like energy spectrum of electrons on helium was confirmed after direct spectroscopic measurements by *Grimes et al.* [**41**] shown in fig. 1.2. If the energies eq. (A.10) are transformed to (cyclic) frequencies through the elementary relation $E_\nu = 2\pi\hbar f_\nu$ one finds that the first three states correspond to frequencies 159.0GHz, 39.8GHz and 17.7GHz. A transition to a higher state would take place, if the ground state electrons were excited by a wave of a frequency equal to the difference between the excited and the ground state (119.2GHz for $1 \longrightarrow 2$ and 141.3GHz for $1 \longrightarrow 3$). Furthermore, if a holding field is applied, it is expected that the transition frequencies will be affected as was referred in section 1.1.4 (linear Stark effect).

Both phenomena were observed, although the extrapolated zero-field transition frequencies were consistently higher than expected from eq. (A.10) and the Stark effect was not completely linear, especially at high fields. The weak nonlinearity of the frequency-field dependence in that region was attributed to electrons interacting stronger with the helium surface as the increasing electric field pushes them closer to it. The deviations of the zero-field transition frequencies are just manifest of the limitations of the elementary potential eq. (1.2) and disappear when the phenomenological potential eq. (1.3) is considered.

1.2. Scattering mechanisms

The transport properties of a system of particles depend on the nature of scattering mechanisms and the dimensionality of the system. It is known for example from the transport theory of metals that it is precisely the scattering of electrons with lattice imperfections which accounts for their finite conductivity (in an ideal metal, conductivity should be infinite). A second fundamental result is that electron-electron scattering is insignificant due to screening effects and, more critically, the Pauli principle.

A similar picture emerges for TDES over liquid helium, albeit for somewhat different reasons. The role of lattice imperfections is undertaken by helium gas atoms at high temperatures ($T > 0.7K$) and by quantized excitations of the helium surface in the low-temperature regime ($T < 0.7K$). Electron-electron scattering depends on the density of the electron system, which can be varied in a range of at least four orders of magnitude.

The wide span of the TDES-density range, means that the influence of electron-electron scattering ranges from negligible (for low electron densities) to crucial (for high electron densities). Interelectron scattering is manifest in the form of a phase transition from the liquid to the solid phase. For this reason, electron-electron scattering will be treated separately in section 1.4.

1.2.1. Electron-gas atom scattering. The electrons of a TDES interact with helium gas atoms. No other known substance can coexist in its gas phase with liquid helium and it suffices therefore to treat the scattering with helium gas atoms exclusively. Helium atoms are 10^4 times heavier than electrons and this huge mass difference means that the scattering of electrons with helium gas atoms is almost elastic, without a significant exchange of momentum.

The scattering rate τ_g^{-1} is proportional to the density n_{He} of scatterers (helium gas atoms). If it is assumed that the liquid helium phase is in equilibrium with the respective gas phase, the gas density of helium coincides with saturated vapor density. According to thermodynamics, saturated vapor density follows a Boltzmann-type dependence in temperature. If the latent heat of evaporation of liquid helium is denoted with $L_g = 7.17 k_B$, the radius of the helium atom with a_{He} and the scattering length with $a = 0.62\text{Å}$, the scattering rate τ_g^{-1} due to helium gas atom scattering is calculated from

$$\tau_g^{-1} = \frac{3\pi^2}{2} \frac{a_{He}^2 \hbar}{ma} n_{He} \left(\frac{m_{He} k_B T}{2\pi\hbar^2} \right)^{3/2} \exp\left(-\frac{7.17}{T} \right). \tag{1.14}$$

From eq. (1.14) it is obvious that electron-gas atom scattering becomes exponentially insignificant for a decreasing temperature, and essentially disappears below 0.7K. The scattering time τ_g decreases exponentially for an increasing temperature, and especially for $T > 1.2K$ (cf. fig. 1.3).

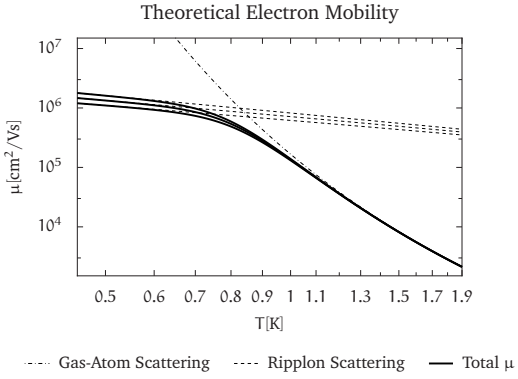

FIGURE 1.3. Electron mobility μ, as a function of temperature T. The ripplon scattering curves show mobility for $E_\perp$[V/cm] which, looking from bottom up, are equal to 200, 110 and 30. The total μ is calculated from Matthiesen rule. Axes scale is logarithmic.

1.2.2. Electron-ripplon scattering. Another scattering mechanism arises from the interactions of electrons with quantized excitations of the liquid helium surface. Surface excitations of a liquid turn out as solutions of the classical wave equation of motion for the surface and they are referred in this context as *capillary waves*. *Cole* [**19**] followed a completely quantum mechanical treatment for the interaction between the electrons of a TDES and the quantized capillary waves—which *Cole* [**19**] termed *ripplons*—of the liquid helium surface, and he derived the basic physical properties of electron-ripplon scattering.

If ρ_{He} is the density of liquid helium (gas density is ignored), σ_{He} the surface tension of liquid helium, g the acceleration of gravity, ω the cyclic frequency and k the wave vector, the dispersion relation of ripplon excitations is given by

$$\rho_{He}\omega^2 = \rho_{He} g k + \sigma_{He} k^3. \tag{1.15}$$

The dynamics of individual electrons of a TDES will be mostly affected by 'short'-range surface excitations that are characterized by a small wave length (big wave vector k) comparable to the interelectronic distance. For such big wave vectors, the $\sigma_{He}k^3$ term dominates and the dispersion relation can be written as

$$\omega_k \approx \left(\frac{\sigma_{He}k^3}{\rho_{He}}\right)^{1/2}. \tag{1.16}$$

The previous equation is used as a starting point for the construction of theories analogous to those that describe electron-phonon interactions in solids. A scattering rate τ_r^{-1} is obtained, which is proportional to a polynomial function of temperature, instead of the exponential dependence on temperature that was encountered in electron-gas atom scattering. The polynomial dependence on temperature explains why for low temperatures, $T \lesssim 0.7$K, ripplons are the main scattering mechanism.

Buntar et al. [**14**] summarize the theoretical results obtained by *Monarkha*[3] in the following formula for the rate τ_r^{-1} of electron-ripplon scattering:

$$\tau_r^{-1} = \frac{e^2}{4\hbar\sigma_{He}}\left(E_0^2 + \frac{4\sqrt{2}}{\pi}\left(\frac{k_B T}{\mathcal{E}}\right)^{1/2} E_0 E_\perp + \frac{k_B T}{\mathcal{E}} E_\perp^2\right), \tag{1.17}$$

where σ_{He} is the surface tension of liquid helium and $E_\perp$ is the holding field magnitude. Equation (1.17) takes into account the possibility that the TDES is not in thermal equilibrium with its surroundings. This is a possibility, because electron-ripplon scattering (like electron-gas atom scattering) is almost elastic and very weak. For this reason, the thermal energy $\mathcal{E}$ of the TDES is distinguished from the thermal energy $k_B T$ of the surrounding space. In thermal equilibrium it is, of course, $\mathcal{E} = k_B T$. In eq. (1.17), the parameter E_0, with the physical dimension of electric field [V/m] is defined from

$$E_0 = \frac{2\gamma\Lambda\sqrt{m k_B T}}{3e\hbar}. \tag{1.18}$$

It should be noted that Λ has been defined in eq. (1.1). In turn, the dimensionless number γ is calculated from

$$\gamma = \frac{\gamma_0}{3x}\left(x + \sqrt[3]{1+\sqrt{1-x^6}} + \sqrt[3]{1-\sqrt{1-x^6}}\right), \tag{1.19}$$

where

$$x = \gamma_0\left(\gamma_0^3 + 13.5\gamma_E^3\right)^{-1/3}, \quad \gamma_0 = \frac{m\Lambda}{\hbar^2}, \quad \gamma_E = \left(\frac{3meE_\perp}{2\hbar^2}\right)^{1/3}. \tag{1.20}$$

In contrast to electron-gas atom scattering, which depends on temperature only, the ripplon scattering rate τ_r^{-1} is also sensitive to the magnitude $E_\perp$ of holding field, which "pushes" electrons closer to the helium surface and, as a result, enhances the coupling of electrons to ripplons. Figure 1.3 depicts, essentially, the scattering times τ_g and τ_r due to gas atom and ripplon scattering, respectively. The plot in terms of mobility μ, which is simply the scattering time multiplied by e/m, was chosen, so that a direct comparison between theory and experiments is made possible (cf. fig. 1.6 and section 1.5).

1.3. Stability of the charged liquid helium surface

The solutions of the wave equation of motion for the uncharged helium surface are capillary waves with a dispersion relation given from eq. (1.15). When electrons are brought on the surface, an electrostatic pressure builds up because

[3]Published for the first time in [Fiz. Nisk. Temp. **5**, 994 (1974)].

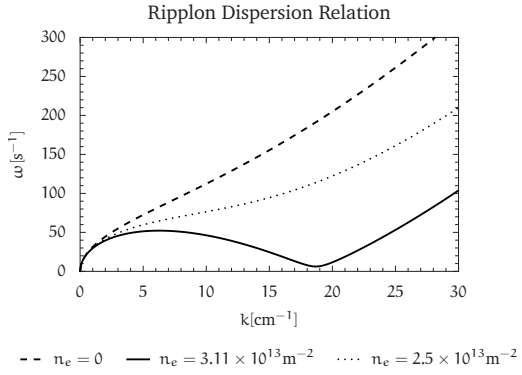

FIGURE 1.4. Ripplon frequency ω plotted against the wave vector k for different electron densities n_e. The theoretical ripplon dispersion relation, eq. (1.21), is applicable for the LHe-vacuum interface. *Wanner et al.* [**112**] have verified a similar ripplon dispersion relation for the ^{3}He/^{4}He interface.

helium is a dielectric substance. The dispersion relation of the capillary waves will be modified accordingly, obtaining the form

$$\rho_{He}\omega^2 = \sigma_{He}k^3 + \rho_{He}gk - \frac{(n_s e)^2}{2\epsilon_0}k^2, \tag{1.21}$$

where ρ_{He} and σ_{He} are the density and surface tension of liquid helium, k the wave vector and ω the cyclic frequency. Furthermore, in eq. (1.21), n_s is the saturated electron density, defined as the electron density that completely screens a given holding field and ϵ_0 is the dielectric constant of vacuum.

From eq. (1.21), it is seen that, for any given wave vector, the cyclic frequency steadily decreases for increasing electron densities. There will always exist a critical saturated electron density n_{sc}, such that $\omega = 0$. Using eq. (1.21), the condition $\omega = 0$ leads to a second order polynomial in k. The solution of this polynomial must be a unique critical wave vector, and the discriminant should therefore be set equal to zero. This leads immediately to the critical saturated charge density

$$n_{sc}e = \left(16\epsilon_0^2\rho_{He}\sigma_{He}g\right)^{1/4} \approx 4.985 \times 10^{-6}\mathrm{C/m^2}. \tag{1.22}$$

Replacing the expression $n_{sc}e$ as given in eq. (1.22) into the dispersion relation eq. (1.21) for $\omega = 0$, the critical (nonzero) wave vector k_{sc} that would completely suppress ripplons ($\omega = 0$) is given by

$$k_{sc} = \left(\frac{\rho_{He}g}{\sigma_{He}}\right)^{1/2} \approx 1873\mathrm{m}^{-1}. \tag{1.23}$$

It is evident from eq. (1.22) that the critical saturated electron density is determined from fixed properties of liquid helium and natural constants, not from experimentally controlled parameters. Therefore, $n_{sc} = 3.11 \times 10^{13}\mathrm{m}^{-2}$ is the maximum attainable electron density that can be supported over liquid helium.

Physically, when the cyclic frequency drops to zero, capillary waves (and their quantized analogs, the ripplons) cease to exist. However, the solution of the surface equation of motion suggests that capillary waves are an inherent property of a finite surface. This leads to the conclusion that the suppression of ripplons means that the surface itself becomes unstable and ceases to exist under these conditions. The electrons of the TDES can no longer be supported[4] and they penetrate in liquid helium, reaching finally the bottom plate. *Savignac et al.* [**95**] have captured interference patterns of the surface instability, where it can be seen that the surface of liquid helium is "wrinkled", before deep dimples develop, from where electrons eventually break through to the body of liquid helium.

Two-dimensional electron systems of densities higher than n_{sc} can nevertheless be created on helium films that wet a dielectric substrate. A surface instability occurs—if at all—at much higher electron densities in the case of helium films, because the van der Waals interaction between liquid helium and the substrate stabilizes the surface of liquid helium (see section 2.2).

1.4. Phase transitions of TDES on liquid helium

The common classification of matter as solid, liquid, or gas, is based on mainly qualitative characteristics: a gas does not have any form, it compresses easily and it expands in the available volume, whereas a liquid takes the form of its container and it is very difficult to compress. A solid retains its form and it is almost incompressible. Transitions between these states may be smooth (continuous) or abrupt (discontinuous). Discontinuous phase transitions are associated with the emission or absorption of energy (latent heat).

A more general classification of the solid, liquid, or gas state with quantitative content, is obtained by considering the potential and thermal energies of a system. By definition, the constituents of a gas interact very weakly with each other, meaning that the potential energy is close to zero, while the thermal energy due to the free motion of its particles is much larger. The interaction between the particles of a solid is much stronger than the interaction between the particles of a gas; for this reason, the potential energy of the particles of a solid should be much larger than its thermal energy. A liquid forms an intermediate state between a solid and a gas, because in a liquid the potential energy of its particles is comparable to their thermal energy.

A quantitative measure of "solidness", or "liquidness" is therefore the plasma parameter Γ that is defined as the ratio of the potential to the thermal energy of a particle system,

$$\Gamma = \frac{e^2 n}{4\sqrt{\pi}\epsilon_0 k_B T}, \tag{1.24}$$

[4]In a sense, electrons are 'wet' by liquid helium, in the same way a careless insect walking on the surface of a pond could be wet by water, usually with fatal consequences.

where n is the electron density and T the temperature of the TDES.

Plasma parameter values less than unity characterize weakly correlated systems, where the gaseous character dominates. Plasma parameter values in the range $1 \lesssim \Gamma \lesssim 100$ indicate progressively stronger correlations (liquid-like character), whereas values $\Gamma > 100$ are exhibited by highly correlated systems, which—if not already solid—are about to experience a phase transition to the solid state.

The phase transitions of a system depend crucially on its dimensionality and on the range of the interaction potential among the system's particles. Electrons on liquid helium form a classical two-dimensional system of N-particles, interacting through a Coulomb potential ($1/z$ interaction).

A theorem due to *Weeks* [**113**] states that there can be no liquid-to-gas phase transition for potentials of the form $1/z^n$, if n is smaller than the dimensionality of the system. As a consequence, it is impossible to define a clear transition from liquid to gas for TDES on liquid helium, although the nomenclature "electron gas" or "electron liquid" is often encountered in the literature, depending on somewhat vaguely defined ranges of Γ.

For some time, it was thought that a two-dimensional solid cannot exist, because long-range order had been proven to be impossible in two dimensions. However, order exhibits a weak, logarithmic decay as a function of the system's area, meaning that finite two-dimensional systems of moderate area (even macroscopically) might be able to experience a phase transition to the solid state.

The microscopic process of the solid-to-liquid phase transition in two-dimensional systems has been explained by *Kosterlitz and Thouless* [**58, 59**], as a two-step annihilation of the dislocations in a lattice (the number of dislocations is a measure of how brittle a solid is).

The first step involves the unbinding of dislocations in a continuous phase transition, where the solid ultimately loses its resistance to shear stress and starts flowing. In their publications, *Kosterlitz and Thouless* [**58, 59**] had identified the emerging phase as a liquid, but later *Halperin and Nelson* [**42**] and independently *Young* [**118**] observed that some order still persisted. Indeed, these authors showed that the unbinding of dislocations leads to another type of topological defect, the disclinations, making the emerging phase—which they named *hexatic*—similar to a liquid crystal.

Halperin et al. [**42**] and *Young* [**118**] proceeded then to complete the KT-theory, describing a second, continuous phase transition from the hexatic to the liquid phase, which involves the annihilation of disclinations. For this reason, the long acronym KTHNY-theory is often encountered in the literature.

It should be noted that the Kosterlitz-Thouless transition, although continuous, is not a second order phase transition, but rather an infinite order phase transition. The infinite order of KT-transition results from the fact that a rigorous

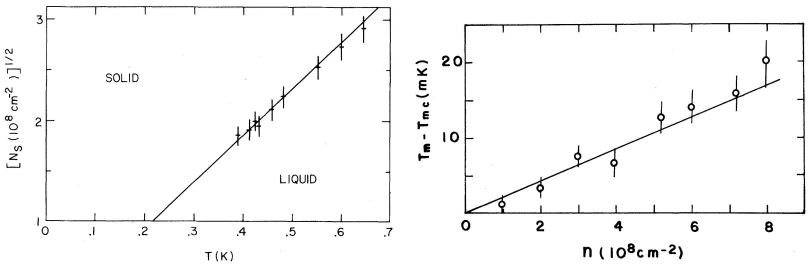

(A) Metallic electrodes (B) Glass substrate

FIGURE 1.5. Left: Liquid-solid phase boundary as a function of electron density N_s and temperature T, traced by *Grimes et al.* [**39**]. The line of coexistence corresponds to a plasma parameter value of 131 ± 7. Right: The same boundary as measured by *Mehrotra et al.* [**79**] through mobility measurements. The difference of the measured T_m minus the expected critical temperature T_{mc} is plotted versus electron density n. The absolute temperature range lies within the range 0.2K–0.7K. Their plasma parameter was found to be 124 ± 4.

(i.e non-divergent) order parameter in two-dimensional systems is impossible to be defined.

An important result of KT-theory is the association of the plasma parameter Γ_{KT} for which melting occurs, with the transverse (v_t) and longitudinal (v_l) phonon velocities in the lattice, by means of the equation

$$\Gamma_{KT} = \frac{1}{v_t^2}\left(\frac{1}{1 - v_t^2/v_l^2}\right). \tag{1.25}$$

The transverse and longitudinal velocities were theoretically derived by *Morf* [**83**], for the case of an isolated two-dimensional electron crystal, as a function of temperature. A plasma parameter $\Gamma_{KT} \approx 125$ was subsequently calculated for the liquid-to-solid phase transition of a TDES. The line of coexistence for the solid and liquid phases as a function of temperature T and electron density n could be obtained with the use of the theoretical, or experimental value of Γ_{KT} in eq. (1.24).

The plasma parameter, for the liquid-to-solid transition of a TDES on liquid helium, was measured by different experimental methods (cf. the review of *Peeters* in [**10**]), all of which converged to a value $\Gamma_{KT} \approx 137$, in excess of the theoretically predicted $\Gamma_{KT} \approx 125$. This deviation occurs, because *Morf* [**83**] considered only electron-electron interactions in the derivation of transverse and longitudinal velocities, ignoring electron interaction with ripplons.

The first experimental method employed for establishing and proving the solid TDES phase, involved the detection of ripplon resonances caused by oscillations of the electron crystal in the vertical z-direction and it was implemented by *Grimes et al.* [**39**] (left plot of fig. 1.5. Subsequently, the existence and properties of the electron crystal were investigated by different indirect methods, like mobility measurements (*Mehrotra et al.* [**79**], right plot of fig. 1.5).

Grimes et al. [**39**] understood that when the electron crystal is formed, the application of a uniform AC-electric field in the vertical direction will force the crystal to oscillate up and down with respect to the surface of liquid helium. However, for certain frequencies, the condition for the excitation of standing ripplon waves will be satisfied and a measurable resonance will develop. The condition for the excitation of standing ripplon waves can be formulated as $\lambda_n = 2L/n$, where λ_n is the wave length of the n-th mode and L is the nearest neighbor distance in the electron lattice. Ripplons are observed below 0.7K, meaning that the method of *Grimes et al.* [**39**] cannot be used for detecting the electron crystal at higher temperatures.

The continuity of the transition was investigated by *Glattli et al.* [**37**] through thermodynamic measurements. Electrons on liquid helium are in very good thermal insulation from their environment and it is possible to heat them at a higher temperature T_e for a relatively long time by applying a short pulse of power P (≈ 0.1nW) for a Δt period of time ($\approx 100\mu$s). The temperature T_e of the TDES can be determined from the phonon velocities by means of eq. (1.25) and the theoretical results of *Morf* [**83**]. The TDES specific heat is by definition $C = P\Delta t/\Delta T_e$ and its behavior near the melting point should reveal whether the transition involves the emission of latent heat, determining thus whether the transition were continuous or not. No latent heat of melting was observed, meaning that the transition is a continuous phase transition as predicted by KT-theory.

The experimentally accessible electron densities on bulk liquid helium vary in the range from $10^9 m^{-2}$ to $10^{13} m^{-2}$. One KT-type transition of a TDES from the liquid to the solid phase is then the only possible and the phase diagram is thus fully determined.

1.5. Electron mobility

The transport properties of electrons on liquid helium are determined by the scattering mechanisms and the dimensionality of the system. Electron mobility (μ) is a measure of transport properties, showing how easily an electron is moving and defined as

$$\mu = \frac{e\tau}{m^*}. \tag{1.26}$$

It should be noticed that electron mobility is defined in terms of the effective mass m^*, which might be greater or less than the usual bare electron mass.

However, for an electron on liquid helium it may be considered that the effective mass is with good accuracy equal to the bare electron mass.

The total single-electron mobility is fully determined, if one takes into account that the total inverse relaxation time τ^{-1} is, according to Matthiesen rule, $\tau^{-1} = \tau_g^{-1} + \tau_r^{-1}$, that is, the sum of the inverse relaxation time for each scattering mechanism, which for electrons on helium are scattering with ripplons, eq. (1.17), and helium gas atoms, eq. (1.14).

The collective, N-body nature of the system should provide an additional formula, relating the mobility of electrons on liquid helium with such collective properties as its density n and conductivity σ. The theories devised for that purpose treat electrons on liquid helium as a highly correlated, nondegenerate quantum fluid. Perhaps surprisingly, it is found that although electron correlations are strong, electron mobility follows essentially a classical Drude-type behavior, making it possible to write

$$\mu = \frac{\sigma}{ne}. \tag{1.27}$$

The previous equation implies the main method for the experimental determination of electron mobility: it suffices to measure the conductivity of a TDES under constant electron density. The resulting mobility values, in conjunction with eq. (1.26), give experimental information on the scattering mechanisms, enclosed in the total relaxation time τ.

Sommer et al. [**101**] measured electron mobility at temperatures ranging from 0.9K to 3.2K, for a liquid helium thickness of 1mm–2mm. Below 2K, electron mobility increases with decreasing temperature, following an activation-type law. This can be attributed to scattering of surface state electrons with helium gas atoms. Above 2K, electron mobility drops abruptly, in agreement with the findings of *Levine et al.* [**73**] who predicted and measured a transition to an electron complex, or a bubble state. Notably, the measured electron mobility is much lower for $T > 2K$ than the electron mobility measured by *Levine et al.* [**73**], a fact which *Sommer et al.* [**101**] attribute to the lower dimensionality of TDES in comparison to free electrons inside helium gas.

Grimes et al. [**38**], using plasmon resonance, excited standing wave resonances of surface state electrons and verified the two-dimensional plasmon dispersion relation $\omega_p \propto \sqrt{k}$, where ω_p is the plasmon cyclic frequency and k the wave vector. These resonances are observable as peaks of the experimentally measured quantity dA/dn_s, which is the derivative of the AC-electric field absorbtion A with respect to the density n_s of the TDES, when dA/dn_s is plotted against the cyclic frequency ω_p of the AC-electric field.

The resonance linewidth Γ_{pp} (peak-to-peak linewidth) gives the scattering time τ, which is equal to $\tau = (2\pi\sqrt{3}\Gamma_{pp})^{-1}$, if the resonance peak is assumed to obey a Lorentz distribution. Electron mobility can then be calculated by means of the fundamental eq. (1.26). By means of this methodology, *Grimes et al.* [**38**]

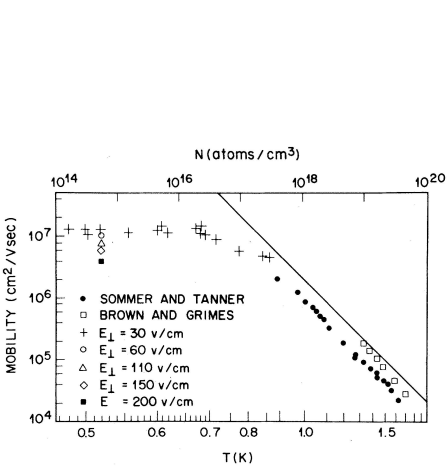

(A) Measured Electron Mobility

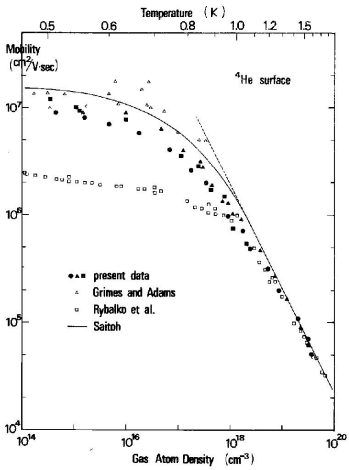

(B) Measured Electron Mobility

FIGURE 1.6. Electron mobility μ versus temperature T and helium-vapor density N. In (A), reprinted from *Grimes et al.* [**38**] (with data from *Sommer and Tanner* [**101**], and *Brown and Grimes* [**13**]), μ for different vertical holding fields $E_\perp$ are plotted. Below 0.68K the mobility is limited by ripplon scattering while at larger temperatures vapor-atom scattering predominates. The solid line is a theoretical calculation for vapor-atom scattering only. In (B), reprinted from *Iye* [**48**] (with data from *Grimes and Adams* [**38**], and *Rybalko et al.* [**93**]), μ is measured for excitation frequencies 100kHz (●) and 30kHz (▲) and liquid helium thickness $d = 1$mm, while measurement (■) has excitation frequency 100kHz and $d = 1.3$mm. The dashed line, indicates mobility due to gas atom scattering alone. The solid curve is the theoretical prediction of *Saitoh* [J. Phys. Soc. Japan **42**, 201 (1977)], for $E_\perp = 100$V/cm. Scale of both axes is logarithmic.

measured electron mobility for temperatures as low as 0.3K and verified the theoretical predictions with regard to electron-gas atom scattering and electron-ripplon scattering. In particular, for electron-ripplon scattering, it was found that:

- Electron mobility remains almost constant for $T < 0.68$K, where electron-ripplon scattering dominates, as predicted by *Cole* [**19**].
- Electron mobility decreases when the magnitude $\mathcal{E}_\perp$ of the holding field increases, as predicted by *Shikin* [Sov. Phys. JETP **31**, 936 (1970)].
- Electron mobility increases when guard voltage is set above a threshold value, as *Crandall* [**24**] predicted.

Inspection of eqs. (1.17) through (1.20) along with the associated fig. 1.3 suggests that—with the exception of guard voltage dependence, which is not

covered by these equations—the theoretical predictions are in good agreement with the experimental data shown in fig. 1.6.

Iye [**48**] measured electron mobility at low AC-excitation frequencies (in the kHz range, as compared to the MHz range of *Grimes et al.* [**38**]) for different AC-excitation frequencies and bulk liquid helium thicknesses. The temperature range from 0.5K to 1.8K included both the ripplon scattering regime and the gas atom scattering regime. Despite the different experimental methods the various experimenters followed, all mobility measurements establish the strong increase of electron mobility at the gas-atom scattering regime for decreasing temperature, and an almost constant electron mobility at the ripplon scattering regime for further decreasing temperatures (see fig. 1.6).

CHAPTER 2

Electrons on Liquid Helium Films

2.1. Electron potential in the presence of a dielectric substrate

Electrons can form stable two-dimensional equilibrium states at specific quantized distances above the surface of liquid helium. These states arise because liquid helium is slightly dielectric ($\epsilon_{He} = 1.057$) and its surface is polarized when electrons approach.

If liquid helium wets a solid dielectric substrate, electrons on liquid helium will also polarize the surface of the dielectric substrate. The extent of substrate polarization depends on the dielectric constant ϵ_s of the substrate and the thickness of the liquid helium film that wets the substrate.

A large part of the discussion for the electron potential over bulk liquid helium remains relevant also for substrates wet by helium films. The following sections focus on features of the electron potential that require modification for TDES on helium films supported by a dielectric substrate.

2.1.1. Electron potential due to the surface of liquid helium. Let d be the thickness of liquid helium wetting the substrate and z the distance of an electron from the surface of liquid helium. Define the induced image charge on the substrate as

$$\Lambda_s = \frac{\epsilon_s - \epsilon_{He}}{4(\epsilon_s + \epsilon_{He})} e^2 \text{ [CGS]} = \frac{\epsilon_s - \epsilon_{He}}{16\pi\epsilon_0(\epsilon_s + \epsilon_{He})} e^2 \text{ [SI]}, \tag{2.1}$$

in a manner completely analogous to the induced image charge Λ on liquid helium, which was defined in eq. (1.1).

The electron potential $V_{He}(z)$ due to liquid helium, in the presence of a dielectric substrate, results in

$$V_{He}(z) = \begin{cases} -\Lambda/z - \Lambda_s/(z+d) & z \geqslant 0, \\ \infty & z < 0. \end{cases} \tag{2.2}$$

The mean distance of an electron of a TDES at the ground state above the surface of liquid helium is approximately 114Å. If the thickness of the helium film that wets the substrate is much greater than 114Å, so that $d \gg z$, the term $\Lambda_s/(z+d)$ can be expanded in a Taylor series with respect to $z/d \ll 1$. Keeping only first order terms and after redefining the potential, so that a constant term

Λ_s/d is dropped, the electron potential $V_{He}(z)$ can then be approximated as

$$V_{He}(z) = -\frac{\Lambda}{z} - \frac{\Lambda_s}{d^2} z \quad \text{(thick film approximation, } z > 0\text{)}. \tag{2.3}$$

Comparing eq. (2.3) and the form of the potential in the presence of holding field eq. (1.11), it is seen that the solution of Schrödinger equation for an electron of a TDES on a helium film that wets a dielectric substrate will resemble the perturbation solution for an electron on bulk liquid helium in the presence of holding field.

The coefficient $\Lambda_s/d^2 > 0$ implies that strong dielectric substrates and thin helium films are able to shift electron states towards the surface of liquid helium, in exactly the same way a holding field $E_\perp$ would. If, in addition, a holding field is actually applied, the shift is of course further enhanced. Moreover, even without a holding field, the electron distribution is shifted in favor of the ground state for TDES on helium films that wet a dielectric substrate. This should be contrasted to the electron distribution of TDES on bulk liquid helium, which favors the excited states for temperatures higher than 0.9K.

2.1.2. Electron potential due to other electrons. Electrons on bulk liquid helium interact with Coulomb forces, generated from the potential $V_C(r) = e^2/4\pi\epsilon_0 r$, where r is the distance between any two electrons. Coulomb interactions are of course present also for TDES on helium films on a dielectric substrate, but the induced substrate charge is able to screen the Coulomb interaction, so that the net interelectron potential is, according to *Peeters et al.* [**90**],

$$V_C(r) = \frac{e^2}{4\pi\epsilon_0 r} - \frac{4\Lambda_s}{\sqrt{r^2 + (2d)^2}}. \tag{2.4}$$

An immediate conclusion, drawn from eq. (2.4), is that the (repulsive) interelectron interaction is weaker for TDES on thin helium films, supported by a dielectric substrate, than the interelectron interaction for TDES on bulk liquid helium.

2.2. Stability of the charged helium film surface

The maximum attainable electron density for a TDES on bulk liquid helium is $n_{sc} = 3.11 \times 10^{13} m^{-2}$, with higher electron densities leading to an instability of the liquid helium surface (see section 1.3). Two-dimensional electron systems of electron densities higher than n_{sc} can nevertheless be created on helium films that wet a dielectric substrate, because the van der Waals interaction between liquid helium and the substrate stabilizes the surface of liquid helium.

Quantitatively, the influence of the substrate should alter the dispersion relation of capillary waves. *Ikezi et al.* [**47**], using a continuous hydrodynamic approach, worked out the dispersion relation of capillary waves on the surface of

a helium film that has a thickness d and wets a substrate of dielectric constant ϵ_s. The dispersion relation is found to be

$$\rho_{He}\omega^2 = \left(\sigma_{He}k^3 + \left(\frac{3C}{d^4} + \rho_{He}g\right)k - \frac{(n_s e)^2}{2\epsilon_0}k^2 F(kd, \epsilon_s)\right)\tanh(kd), \quad (2.5)$$

where C is the van der Waals constant for the interaction between liquid helium and substrate, and the function $F(kd, \epsilon_s)$ is defined from

$$F(kd, \epsilon_s) = \frac{1 + \epsilon_s - (1 - \epsilon_s)e^{-2kd}}{1 + \epsilon_s + (1 - \epsilon_s)e^{-2kd}}. \quad (2.6)$$

Clearly, in the general case, eq. (2.5) is not a polynomial in k when $\omega = 0$ and it is not immediately obvious whether an instability occurs or not. But at the limit of thin films, which corresponds to the limit $kd \ll 1$, it is $F(kd, \epsilon_s) \longrightarrow \epsilon_s$. The condition $\omega = 0$ in eq. (2.5) leads then, in a manner analogous to that of section 1.3, to a critical saturated electron density

$$n_{sc}e = \left(16\sigma_{He}\frac{\epsilon_0^2}{\epsilon_s^2}\left(\rho_{He}g + \frac{3C}{d^4}\right)\right)^{1/4} \quad \text{(for thin film, } kd \ll 1\text{)}. \quad (2.7)$$

Furthermore, the critical wave vector k_{sc} for which $\omega = 0$ can be easily calculated to be

$$k_{sc} = \left(\frac{1}{\sigma_{He}}\left(\rho_{He}g + \frac{3C}{d^4}\right)\right)^{1/2} \quad \text{(for thin film, } kd \ll 1\text{)}. \quad (2.8)$$

Comparing the resulting critical saturated electron densities for the surface instability to occur, namely, eq. (1.22) for bulk liquid helium and eq. (2.7) for a thin helium film on a dielectric substrate, it is seen that n_{sc} will be generally higher in the case of a thin film, due to the van der Waals term $3C/d^4$.

Figure 2.1 shows the dependence of n_{sc} on the film thickness d for two commonly used substrates, silicon ($C = 3.59 \times 10^{-22}$J and $\epsilon_s = 11$) and glass ($C = 4 \times 10^{-22}$J and $\epsilon_s = 7.3$). Even for a film $d = 100$nm thick, it can be calculated, using the numerical data for silicon and glass, that $k_{sc}d \approx 10^{-3}$ and the thin film approximation $kd \ll 1$ is satisfied with good accuracy.

Metallic substrates are inherently unstable and they cannot be used with thin helium films, because electrons would very easily break through liquid helium. This can be concluded from eq. (2.7) and from the fact that $\epsilon_s \longrightarrow \infty$ for a metal, whence $n_{sc} = 0$.

Experimentally (e.g by *Etz et al.* [**35**]), it was demonstrated that much higher electron densities than the estimation by *Ikezi et al.* [**47**] were stable on helium films. *Hu et al.* [**46**] were led thus to question the continuous hydrodynamic approach followed by *Ikezi et al.* [**47**]. They used an expression derived by *Vil'k*

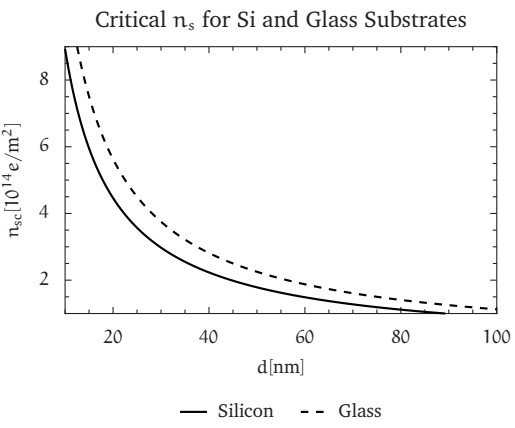

FIGURE 2.1. Critical saturated electron density n_{sc} as a function of helium film thickness d (from eq. 2.7) for silicon ($\epsilon = 11$ and $C = 3.59 \times 10^{-22}$J) and glass ($\epsilon = 7.3$ and $C = 4 \times 10^{-22}$J). See that n_{sc} is 10 times higher than the corresponding $n_{sc} = 3.11 \times 10^{13} m^{-2}$ for bulk liquid helium.

and Monarkha[1], for the ripplon-phonon coupled modes of an array of electrons and their images, to conclude that the helium film surface should be stable for any electron density.

The stability of the helium film surface for all electron densities is, according to *Hu et al.* [**46**], the result of the separation of a ground state TDES electron from the surface, due to quantum zero point motion. These authors show that this separation makes the charged surface of the helium film stable against perturbations for all electron densities.

Ultimately, for a helium film thickness $d \longrightarrow 0$, *Hu et al.* [**46**] find that electron density will be nevertheless constrained below a maximum value. This happens, because the electron wavefunction in the direction perpendicular to the helium surface will increasingly extend inside liquid helium. The probability that TDES electrons tunnel through the classically forbidden region $z < 0$ inside liquid helium will increase steadily, even though the potential there is infinite.

The prediction, made by *Hu et al.* [**46**], of quantum tunneling of electrons for $d \longrightarrow 0$ should be contrasted to the unnatural behavior predicted by eq. (2.7), namely that $n_{sc} \longrightarrow \infty$ for a helium film thickness approaching zero. Therefore, the foundations of the continuous hydrodynamic approach that led to eq. (2.7) fail for extremely thin ($d < 5$nm) films.

Experimentally, it is often the case that electrons break through for a film thickness $d > 5$nm. Electron breakthrough under these conditions should be rather attributed to substrate roughness. Indeed, the helium film wetting the peaks of a rough substrate will be thinner and electron tunneling will preferentially proceed from the rough spots of the substrate surface, even if the mean helium film thickness would not be enough for quantum electron tunneling to occur.

[1]Published in [Sov. J. Low Temp. Phys. **10**, 469 (1984)].

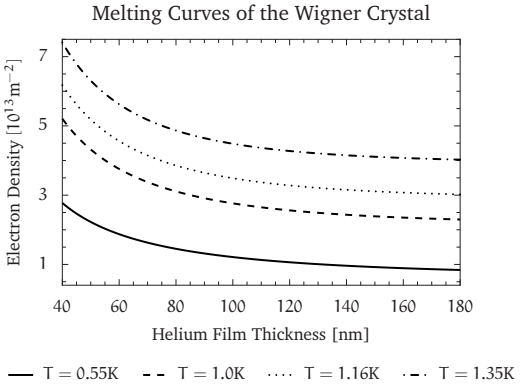

FIGURE 2.2. Melting curves of a TDES at various temperature T[K]. The liquid state at each T is below the melting curve (lower electron densities). The solid state is above the melting curve (higher electron densities). The melting curves were calculated, according to the approximate eq. (2.10) of *Saitoh* [**94**], for $\Gamma = 137$.

2.3. Phase transitions of TDES on helium films

The phase diagram of a TDES on a liquid helium film is theoretically studied in conjunction with the interplay between the thermal energy $k_B T$, the potential energy $e^2\sqrt{\pi n}/4\pi\epsilon_0$ and the Fermi energy $\pi\hbar^2 n/m$ of the TDES. Electron correlations are indicated by the plasma parameter Γ, defined in eq. (1.24), which is the ratio of the potential energy to the thermal energy. A similar, quantum plasma parameter Γ_q can be defined as the ratio of the potential energy to the Fermi energy,

$$\Gamma_q = \frac{me^2}{4\sqrt{\pi}\epsilon_0\hbar^2} n^{-1/2}. \tag{2.9}$$

In analogy with Γ, which is a measure of the relative strength between the potential energy of a TDES and the classical fluctuations, Γ_q is a similar measure, but for quantum fluctuations. Quantum fluctuations are the result of zero point motion and Pauli's exclusion principle for fermions, persisting even at the limit $T \longrightarrow 0$ where classical (thermal) fluctuations become zero.

The thermodynamics of TDES on liquid helium films that wet a dielectric substrate are altered when compared to TDES on bulk liquid helium for two reasons:

- Coulomb interactions are screened by the image charge of the dielectric substrate, being therefore weaker for TDES on helium films (cf. eq. 2.4). The plasma parameter is reduced in the case of TDES on helium films, and the liquid-to-solid transition, for a given electron density, takes place at a lower temperature compared to TDES on bulk liquid helium.
- No surface instability is associated with helium films that wet a dielectric substrate. This means that electron densities much higher than $3.11 \times 10^{13} m^{-2}$ can be achieved and an extended regime of the phase diagram becomes feasible.

Peeters [**89**] calculated the phase diagram of a TDES for both bulk liquid helium and helium films and verified that the parameter range (n, T) of the Wigner crystal state is contracted for helium films. *Saitoh* [**94**] used the results of *Peeters* [**89**] along with KTHNY-theory to derive an approximate expression, relating Γ with electron density n, temperature T and the helium film thickness d. If Γ is assigned the experimentally verified value $\Gamma = 137$, then T is the critical temperature T_c where the phase transition from liquid to solid occurs. More generally, one may write

$$k_B T = \frac{e^2 n^{1/2}}{4\sqrt{\pi}\epsilon_0 \Gamma}\left(1 - \frac{\epsilon_s - 1}{\epsilon_s + 1}\left(1 + \frac{4\pi n}{c_0^2 d^2}\right)^{-3/2}\right), \tag{2.10}$$

where ϵ_s is the dielectric constant of the substrate and $c_0 = 1.1016$.

In fig. 2.2, the melting curves $n(d)$ of the Wigner crystal are plotted for various temperatures, according to eq. (2.10). For a given melting curve, the liquid state of the TDES lies below the curve, whereas the solid state is correspondingly found above the curve (for higher electron densities). The critical electron density for Wigner crystallization is lowered for progressively thicker films, but it reaches a constant value as the bulk liquid helium limit is approached. Recalling that bulk liquid helium accepts TDES with an electron density less than $3.11 \times 10^{13} m^{-2}$, it is realized that a Wigner crystal on bulk liquid helium will be stable for $T < 1K$. However, on thin helium films it is possible to obtain a Wigner crystal even for temperatures $T \approx 1.5K$.

The much higher attainable electron densities on helium films allow one to probe higher values of the quantum plasma parameter Γ_q, where quantum fluctuations become increasingly important. For such high values of Γ_q the TDES will have already been solidified, passing through the Wigner phase transition. The Wigner crystal cannot remain stable for ever increasing electron densities; above a certain critical electron density, the repelling force, due to Pauli's exclusion principle will be so strong as to render the TDES into a degenerate electron gas (same as the free electron gas in the conduction band of metals and semiconductors). There must therefore exist a critical electron density where the TDES undergoes a transition from the solid to the gas state. If this phase transition obeys KTHNY-theory, the phase transition should occur for $\Gamma_q \approx 137$, whence the critical electron density is calculated from eq. (2.9) to be approximately $6 \times 10^{16} m^{-2}$. This phase transition has a purely quantum origin and relatively little is known theoretically for its properties.

Two-dimensional electron systems in semiconductors are a degenerate electron gas, because of their high electron density, whereas TDES on liquid helium can be a Wigner solid, because of their low electron density.

Decreasing TDES electron density in semiconductors is difficult, as it requires the fabrication of extremely clean samples. On the other hand, increasing TDES electron density on liquid helium is also difficult, because it requires the

fabrication of extremely smooth substrates. For this reason, the demonstration of either the quantum solid-to-gas or gas-to-solid phase transition of a TDES is—up to the time of writing—missing.

2.4. Influence of a dielectric substrate on electron mobility

Measurements of the electron mobility for TDES on helium films wetting many different dielectric substrates have been undertaken. *Andrei* [**9**] used a sapphire crystal, whereas *Kono et al.* [**57**] measured electron mobility on helium films adsorbed on a solid hydrogen substrate. *Jiang et al.* [**51**] carried out a more extensive study of the temperature dependence of electron mobility on helium films of various thicknesses that wet a glass substrate, whereas *Valkering et al.* [**110**] used a periodically structured silicon substrate.

A direct comparison of theory with the experimental results is not as straightforward, as in the case of TDES on bulk liquid helium. A general theoretical analysis is difficult because substrate roughness, which sensitively depends on the dielectric material and—more critically—on the history of each particular substrate, is not easy to capture in a theoretical formulation. For this reason, theoretical attempts on the quantitative prediction of TDES electron mobility on helium films have been concentrated on ideal substrates, in what *Krotscheck et al.* [**65**] term the 'generic' electron mobility. The unpredictable, history dependent nature of substrate roughness also inhibits the reproducibility of measurements and the comparison of experimental results. Nevertheless, two features of electron mobility of TDES on helium films that wet dielectric substrates, having a more general character, emerge:

- Electron mobility is significantly lower in the case of thin films, compared to bulk liquid helium.
- Electron mobility steadily decreases, as the thickness of the helium films decreases. However, for certain film thicknesses the decrease of electron mobility is large and abrupt. This phenomenon is referred to as the *mobility dip* and it was observed from *Andrei* [**9**] as well as *Kono et al.* [**57**].

The fact that electron mobility is generally lower for helium films in comparison to bulk liquid helium, is not unexpected and it can be explained by substrate roughness, which provides an additional scattering mechanism that is more effective when the thickness of the helium film decreases. Theoretical models simulate substrate roughness as a stochastic deviation of the substrate surface from a mean profile. For reasons of analytical tractability, the stochastic deviation in substrate roughness models is assumed to obey a normal distribution. Additional assumptions are usually made with regard to the variance of the resulting normal distribution (cf. *Ando et al.* [7], pp. 502–506).

Shikin [**98**] developed the models of substrate roughness further, by putting forward the *two-fraction model* for TDES on thin helium films supported by a rough dielectric substrate. In the two-fraction model, TDES electrons are divided into an immobile, pinned fraction n_{loc} and a corresponding mobile, agile fraction n_{fr} that mainly contributes to the conductivity of the TDES. The electron populations N_{loc} and N_{fr} are functions of the chemical potential and they can be determined in equilibrium from the condition $N_{loc} + N_{fr} = N$, where N is the total (fixed) number of TDES electrons.

Depending on the helium film thickness d, which is measured from the mean profile of the substrate, a specific number of rough spots higher than this film thickness will be exposed. The number of rough spots with height greater than d can be easily calculated, because rough spots have been assumed to be normally distributed. Pinned electrons reside on such rough spots and the probability that a TDES will be trapped there can be estimated after some simplifying assumptions for the potential of rough spots. Furthermore, *Shikin* [**98**] observed that when exposed rough spots are not distributed far apart[2], helium films suspended on nearby rough spots can be formed that would release electrons pinned on those spots. The potential on helium films suspended on rough spots can be calculated and it provides an estimation of the probability that a TDES will be free.

The two-fraction model has found successful applications, as it proved to explain important features of the mobility measurements *Klier et al.* [**56**] performed. Moreover, *Klier et al.* [**55**] were able to interpret the mobility measurements of *Mistura et al.* [**80**], while *Shikin et al.* [**99**] showed that the mobility dip can be understood in terms of the two-fraction model.

2.5. Dynamics of TDES in magnetic field

Each electron of a two-dimensional, nondegenerate system of noninteracting electrons, confined to move in xy-plane with a velocity $\boldsymbol{v} = (v_x, v_y, 0)$ when a homogeneous magnetic field $\mathbf{B} = (0, 0, B)$ is applied along the z-axis, experiences a Lorentz force $\mathbf{F} = e(\boldsymbol{v} \times \mathbf{B})$. This force is always perpendicular to the direction of velocity[3] and acts therefore as a centripetal force. Each electron will then perform a circular motion on the xy-plane with radius r_c (the nomenclature *cyclotron*, or occasionally *gyration* radius is used), given by

$$\frac{mv^2}{r_c} = evB \Longrightarrow \quad r_c = \frac{mv}{eB}. \tag{2.11}$$

[2]The meaning of "far apart" is made quantitatively precise in the two-fraction model and it relates to the thickness of the helium film and the magnitude of the holding field applied.

[3]As it can be easily seen from the dot product $\mathbf{F} \cdot \boldsymbol{v} = 0$, of $\mathbf{F} = eBv_y\mathbf{i} - eBv_x\mathbf{j}$ and $\boldsymbol{v} = v_x\mathbf{i} + v_y\mathbf{j}$.

A two-dimensional, nondegenerate system of noninteracting electrons has identical properties to that of a classical gas, and the magnitude of velocity v for each electron can be determined thermodynamically through the use of equipartition theorem. The available degrees of freedom are two, and each is assigned a mean kinetic energy equal to $k_B T/2$, whereby

$$\frac{1}{2}mv^2 = k_B T \Longrightarrow \quad v = \sqrt{\frac{2k_B T}{m}}. \tag{2.12}$$

Except for the cyclotron radius r_c, the cyclotron frequency $\omega_c = 2\pi/\mathcal{T}$, where $\mathcal{T} = 2\pi r_c/v$ is the period of circular motion, will prove important in the following. Elementary calculations furnish the expressions

$$r_c = \frac{\sqrt{2mk_B T}}{eB}, \quad \omega_c = \frac{eB}{m}. \tag{2.13}$$

Although r_c and ω_c, as stated in eq. (2.13) are always valid as definitions, their physical interpretation does not extend beyond the case of a classical electron gas without modifications. In the more general semiclassical model of electron dynamics, r_c retains its interpretation as cyclotron radius, only if m is no longer the free electron mass, but instead an appropriate effective electron mass.

2.5.1. Drude magnetoconductivity. As a first approach for the calculation of magnetoconductivity, pioneered by Drude, the electrons of a TDES are treated as classical point particles and their mutual Coulomb interactions are ignored.

Two-dimensional electron systems on liquid helium are nondegenerate, meaning that their statistical mechanics is indeed governed by the classical Maxwell-Boltzmann distribution, instead of the quantum Fermi-Dirac distribution. Coulomb interactions could have been ignored in principle, if they were insignificant compared to thermal motion, or if a screening mechanism rendered them unimportant as in the case of free electrons in metals. The plasma parameter $\Gamma = V/K$ is an indicator of the strength of interactions (enclosed in the potential energy V), relative to thermal motion (enclosed in the kinetic energy K). While it is $\Gamma \approx 1$ in the gas of free electrons in metals and $\Gamma \approx 0.02$ in semiconductors, for electrons on liquid helium Γ can easily exceed 100. This means that whatever screening mechanisms one might devise, Coulomb interactions cannot be ignored for TDES on liquid helium.

Nevertheless, as it will be explained in section 2.5.2, the combined effects of the quantization caused by the magnetic field (Landau levels) plus Coulomb interactions restore a Drude-like behavior of magnetoconductivity for high values of Γ and magnetic fields up to $B \approx 1T$[4]. Drude theory of magnetoconductivity is easy, intuitive as most classical theories, and it is in a surprisingly good agreement

[4]The review article of *M. Lea* in ref. [**10**] describes the theoretical predictions, their range of validity and the actual experimental observations.

with experimental results. At the same time, the physical foundations of Drude theory are plainly wrong, and its success almost the result of luck. This unusual combination of grace and faults should be interesting enough to justify a more detailed development of this theory.

The classical equation of motion for an electron moving with a velocity $\boldsymbol{v} = (v_x, v_y, 0)$, in the presence of a magnetic field $\mathbf{B} = (0, 0, B)$, an electric field $\mathbf{E} = (E_x, E_y, 0)$, and scatterers, is

$$m\mathbf{a} = -\frac{m\boldsymbol{v}}{\tau} - e\mathbf{E} - e(\boldsymbol{v} \times \mathbf{B}), \tag{2.14}$$

where a simple diffusion scattering was considered, with relaxation time τ.

The time dependence is determined by the driving electric field on the xy-plane, and it has the form $e^{i\omega t}$ for the commonly used AC-electric fields. The same time dependence will be exhibited by the velocity of electrons. If one substitutes $\mathbf{a} = \dot{\boldsymbol{v}}$, the vector equation (2.14) is written in component form as

$$im\omega \begin{pmatrix} v_x \\ v_y \\ v_z \end{pmatrix} = -\frac{m}{\tau} \begin{pmatrix} v_x \\ v_y \\ v_z \end{pmatrix} - e \begin{pmatrix} E_x \\ E_y \\ 0 \end{pmatrix} - eB \begin{pmatrix} v_y \\ v_x \\ 0 \end{pmatrix}, \tag{2.15}$$

from which it is evident that $v_z = 0$ and the problem is essentially two-dimensional. For this reason, z-components will be hereafter dropped.

The vector coefficients of eq. (2.15) can be rearranged, so that they involve only the cyclotron frequency $\omega_c = eB/m$ and electron mobility $\mu = e\tau/m$, as in

$$(1 - i\omega\tau) \begin{pmatrix} v_x \\ v_y \end{pmatrix} + \omega_c\tau \begin{pmatrix} -v_y \\ v_x \end{pmatrix} = -\mu \begin{pmatrix} E_x \\ E_y \end{pmatrix}. \tag{2.16}$$

The current density $\mathbf{j}$ is related to the mean velocity of electrons and the electric field, by means of the equations $\mathbf{j} = -ne\boldsymbol{v}$ and $\mathbf{j} = \boldsymbol{\sigma}\mathbf{E}$, where $\boldsymbol{\sigma}$ is the conductivity tensor. These equations can be written in component form as,

$$\begin{pmatrix} j_x \\ j_y \end{pmatrix} = -ne \begin{pmatrix} v_x \\ v_y \end{pmatrix} \quad \text{and} \quad \begin{pmatrix} j_x \\ j_y \end{pmatrix} = \begin{pmatrix} \sigma_{xx} & \sigma_{xy} \\ \sigma_{yx} & \sigma_{yy} \end{pmatrix} \begin{pmatrix} E_x \\ E_y \end{pmatrix}. \tag{2.17}$$

The substitution of $\boldsymbol{v}$ for $\mathbf{j}$ in eq. (2.16) and some algebra leads eventually to

$$\begin{pmatrix} j_x \\ j_y \end{pmatrix} = \frac{\sigma_0}{(1 - i\omega\tau)^2 + (\omega_c\tau)^2} \begin{pmatrix} 1 - i\omega\tau & \omega_c\tau \\ -\omega_c\tau & 1 - i\omega\tau \end{pmatrix} \begin{pmatrix} E_x \\ E_y \end{pmatrix}. \tag{2.18}$$

Here, $\sigma_0 = ne\mu$ is the DC-conductivity, and the components of the conductivity tensor have thus been determined.

In a lockin measurement with Sommer-Tanner or Corbino electrode geometry (see section 3.5.2), the $\sigma_{xx} = \sigma_{yy}$ component of the conductivity tensor is measured, or

$$\sigma_{xx} = \sigma_0 \frac{1 - i\omega\tau}{(1 - i\omega\tau)^2 + (\omega_c\tau)^2}. \tag{2.19}$$

The dependence of σ_{xx} on the magnetic field becomes apparent when one considers that $\omega_c\tau = \mu B$. Experimental data are usually reported in the form σ_0/σ_{xx}, whereby one has

$$\frac{\sigma_0}{\sigma_{xx}} = 1 - i\omega\tau + \frac{(\mu B)^2}{1 - i\omega\tau}. \tag{2.20}$$

Typical relaxation times for TDES on liquid helium lie in the range 10^{-7}s or lower, while typical cyclic frequencies ω of the AC-excitation generated by a lockin amplifier can be of order 10^5Hz at most. As a consequence, $\omega\tau \lesssim 10^{-2}$ and $1 - i\omega\tau \approx 1$, leading to the simpler approximate formula [**72**],

$$\frac{\sigma_0}{\sigma_{xx}} = 1 + \mu^2 B^2. \tag{2.21}$$

2.5.2. Landau level broadening and magnetoconductivity. The application of a magnetic field in the z-direction leads to the quantization of electron motion in the xy-plane. Electrons revolve in quantized circular orbits in the xy-plane, with their energy being an odd multiple of $\hbar\omega_c/2$ (Landau quantization, see appendix B).

Several important phenomena arise due to Landau quantization. The most prominent are the Shubnikov-de Haas oscillations, the primary experimental source of information on the shape of Fermi surface [**28**], and the (integer) quantum Hall effect [**109**], which provides the most accurate estimation of the hyperfine constant.

In the quantum limit, where $\hbar\omega_c \gg k_B T$, Landau levels indicate that the electron density of states $\mathcal{D}(E)$ obtains the form of Dirac δ-functions at positions E_ν,

$$\mathcal{D}(E, E_\nu) = \sum_\nu \delta(E - E_\nu). \tag{2.22}$$

The existence of scatterers changes the density of states, in that the δ-function maxima are no longer infinite and $\mathcal{D}$ is nonzero in a narrow interval $(E_\nu \pm \Delta E_\nu)$ around. In effect, δ-functions are replaced by gaussian-like, bell-shaped distributions. This amounts to the introduction of diffusion, and it is precisely the diffusive processes, which will eventually give rise to a finite value of magnetoresistance (otherwise magnetoresistance should be necessarily zero, or infinite [**82**]).

This can be understood by means of the following arguments: if $\mathcal{D}$ retains a δ-function form, then only perfectly elastic scattering *within* Landau levels and inelastic scattering with $\delta E = \nu\hbar\omega_c$ *across* Landau levels[5] are allowed.

The inelastic scattering of electrons with the associated huge energy changes of the order $\hbar\omega_c$ is practically impossible to take place and therefore it cannot contribute to conductivity. But the scattering of electrons with ripplons or helium gas atoms is not perfectly elastic, as it is instead associated with a negligibly small,

[5]The change of energy after scattering must be exactly equal to the energy difference between two distinct Landau levels.

but nonzero energy exchange. Abandoning δ-functions in favor of broadened Landau levels, makes inelastic scattering possible also within a Landau level, and leads to an intermediate—that is, finite—value of magnetoresistance.

2.5.3. Ando-Uemura transport theory. For TDES, these ideas have been incorporated in the Ando-Uemura[6] theory of transport [**8**], which is also discussed in the classic review article of *Ando et al.* [**7**].

Ando and Uemura distinguish short-range (Γ_s) from long-range (Γ_ℓ) scatterers in their calculation of the Landau level broadening Γ,

$$\Gamma_s^2 = \frac{2}{\pi}\hbar\omega_c\frac{\hbar}{\tau_0}, \quad \Gamma_\ell^2 = \langle(V(\mathbf{r}) - \langle V(\mathbf{r})\rangle)^2\rangle, \tag{2.23}$$

where τ_0 is the relaxation time at zero magnetic field assuming the same scatterers and $V(\mathbf{r})$ is the scattering potential of long-range scatterers.

A long and complicated formula for the main diagonal elements $\sigma_{xx} = \sigma_{yy}$ of the conductivity tensor, which we will not reproduce, can then be derived. A perturbation expansion of σ_{xx} in terms of the time constant $\omega_c\tau_0$ is possible, provided that $\omega_c\tau_0 < 1$, leading to

$$\begin{aligned}\sigma_{xx} = \frac{ne^2\tau_0}{m}\frac{1}{1+(\omega_c\tau_0)^2}\Bigg(1 - 2\frac{(\omega_c\tau_0)^2}{1+(\omega_c\tau_0)^2}\frac{2\pi^2 k_B T}{\hbar\omega_c} \\ \times \operatorname{csch}\left(\frac{2\pi^2 k_B T}{\hbar\omega_c}\right)\cos\left(\frac{2\pi\mu_p}{\hbar\omega_c}\right)\exp\left(-\frac{\pi}{\omega_c\tau_0}\right) + \cdots\Bigg).\end{aligned} \tag{2.24}$$

It should be noticed that μ_p in eq. (2.24) denotes the chemical potential and not electron mobility. A helpful visualization of σ_{xx} as it is calculated from the complicated eq. (2.24) for common parameters is depicted in fig. 2.3.

A simpler expression arises for Hall conductivity $\sigma_{xy} = -\sigma_{yx}$,

$$\sigma_{xy} = -\frac{ne}{B} + \Delta\sigma_{xy}. \tag{2.25}$$

In general, the expression for $\Delta\sigma_{xy}$ is rather involved and it will not be given here. However, the maximum of $\Delta\sigma_{xy}$ at zero temperature is reduced to the much simpler form

$$\lceil\Delta\sigma_{xy}\rceil = \frac{\Gamma}{\hbar\omega_c}\lceil\sigma_{xx}\rceil. \tag{2.26}$$

An important finding is that the maximum of σ_{xx} at zero temperature ($\lceil\sigma_{xx}\rceil$) is independent of the magnetic field and the nature of scatterers. It depends only on the fundamental constants e and $\hbar$, and it provides the context for understanding the integer quantum Hall effect [**109**],

$$\lceil\sigma_{xx}\rceil = \left(\nu + \frac{1}{2}\right)\frac{e^2}{\pi^2\hbar} \quad \nu = 0, 1, \ldots \tag{2.27}$$

[6] Ando and Uemura use the acronym SCBA (self-consistent Born approximation), which hints on the methodology they followed.

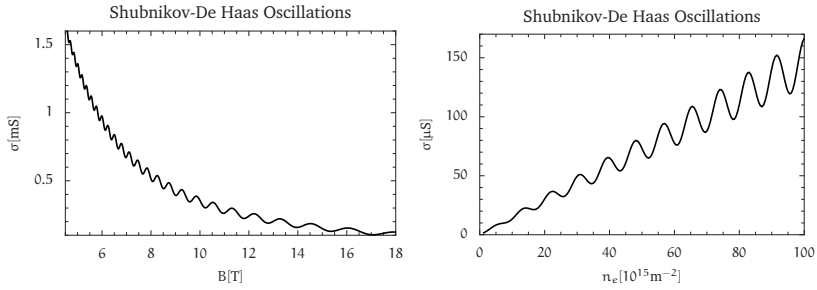

(A) Conductivity (σ) vs. magnetic field (B). (B) Conductivity (σ) vs. electron density (n_e).

FIGURE 2.3. Ando-Uemura theory predicts Shubnikov-de Haas-type oscillations (cf. eq. 2.24), which have been observed for TDES on heterostructures. Both plots were produced using the common parameters $\mu = 0.92 m^2/Vs$, $T = 1.2K$, but it is $n_e = 7.4 \times 10^{16} m^{-2}$ in (**A**), and $B = 18T$ in (**B**).

2.5.4. Coulomb liquid theory. Electrons on liquid helium can interact strongly with each other when their density is high enough. While free electrons in metals have a plasma parameter around 1 and TDES in semiconductors about 0.02, electrons on liquid helium exhibit plasma parameter values that easily exceed 100. Internal Coulomb forces cannot be ignored and they are strong enough, so that the application of the Fermi-liquid theory (not to mention Drude theory!) is not easily justified. The prominence of Coulomb interactions and the relative insignificance of Fermi repulsion (due to the Pauli exclusion principle) led to the characterization of TDES on liquid helium as a *Coulomb liquid*, in contrast to the *Fermi gas* (and, possibly, *Fermi liquid*) one would encounter in metals and semiconductors.

The importance of internal forces was recognized by *Dykman et al.* [**31, 32**], who showed that they give rise to a strong, fluctuating electric field $E_{||}$ that affects each electron. For strong magnetic fields, $E_{||}$ is almost uniform and it leads to a continuous correction $eE_{||}x_c$ of the discrete Landau spectrum for an electron whose center of circular orbit is at x_c.

If the coordinate frame is shifted, so that the center of circular orbit lies at rest, the energy spectrum retains its discrete Landau form. The continuous correction arises then from the scatterers, which fall with a high speed onto the circularly revolving electron about the fixed center. The technicalities of this coordinate shift, which simplifies the theoretical analysis considerably, along with the memory function methodology and a review of experimental results are presented in the review of *Monarkha et al.* [**82**].

The conductivity $\sigma = \sigma_{xx} + i\sigma_{xy}$ of the TDES can be generally written, in terms of the memory function formalism, as

$$\sigma_{xx} + i\sigma_{xy} = \frac{ie^2 n_s}{m(\omega - \omega_c + M(\omega))}, \tag{2.28}$$

where, except for obvious notation, $M(\omega)$ is the memory function, which encloses all information about scattering mechanisms.

More specifically, the scattering rate τ^{-1}, in the context of the memory function formalism, is given by the imaginary part of the memory function,

$$\tau^{-1}(\omega) = \mathrm{Im}\big(M(\omega)\big). \tag{2.29}$$

In the ideal case of no scattering, it is $\tau^{-1} \longrightarrow 0$, so that $M(\omega)$ is a real function. If, in addition, one assumes that the TDES is excited by a cyclic frequency $\omega = \omega_c$ (cyclotron resonance condition), then it is seen from eq. (2.28) that the $\sigma_{xx} = \sigma_{yy}$ components of the conductivity tensor become zero. This is expected, because the conductivity of a two-dimensional system should be zero in the absence of scattering (the nonzero value of conductivity arises due to diffusive scattering mechanisms). However, there will still exist a nonzero σ_{xy} component of the conductivity tensor, giving rise to a measurable Hall effect that could be used to trace the real part of the memory function[7]. Another physical interpretation of the real part of the memory function is that of a shift of the cyclotron resonance peak (section 2.5.6 elaborates on the cyclotron resonance technique). In the case of DC-conductivity, the real part of the memory function vanishes, $\mathrm{Re}\big(M(0)\big) = 0$.

For the scattering mechanisms encountered in TDES on liquid helium, the memory function can be written as

$$M(\omega) = \frac{1}{mN\hbar\omega}\big(G_{F^\dagger F}(0) - G_{F^\dagger F}(\omega)\big), \tag{2.30}$$

where N is the number of electrons and $G_{F^\dagger F}$ is the force-force Green function defined as

$$G_{F^\dagger F}(\omega) = -i\int dt\, e^{i\omega t}\theta(t)\langle[\hat{\mathcal{F}}^\dagger(t), \hat{\mathcal{F}}]\rangle \quad \text{for} \quad \mathrm{Im}(\omega) > 0. \tag{2.31}$$

In the former equation, $\theta(t)$ is the step function, being equal to 1 for $t \geqslant 0$ and 0 for $t < 0$, and the mean value of the commutator $[\hat{\mathcal{F}}^\dagger(t), \hat{\mathcal{F}}]$ is calculated from the definition of the force operator

$$\hat{\mathcal{F}} = \frac{m}{e\hbar} i\left[\hat{\mathcal{J}}, \hat{\mathcal{H}}\right], \tag{2.32}$$

where $\hat{\mathcal{H}}$ is the interaction hamiltonian and $\hat{\mathcal{J}} = \hat{\mathcal{J}}_x + i\hat{\mathcal{J}}_y$ is the current density operator, with magnitude $\mathcal{J} = -e\sum_e v_e$.

[7]Notice that in the absence of scattering, when $\omega = \omega_c$ the real part of the memory function is identical with the memory function itself, $\mathrm{Re}\big(M(\omega_c)\big) = M(\omega_c)$, because $\mathrm{Im}\big(M(\omega_c)\big) = 0$.

Obviously, the memory function depends on the possible interactions an electron of a TDES can have (these are enclosed in the interaction hamiltonian $\hat{\mathcal{H}}$) and the way these interactions are connected with electron kinetics (enclosed in the force operator $\hat{\mathcal{F}}$). *Monarkha et al.* [**82**] provide a detailed, analytical form of $\hat{\mathcal{H}}$ and $\hat{\mathcal{F}}$ and show that the scattering rate $\tau^{-1}(\omega)$ is ultimately connected to the dynamical structure factor $S(\mathbf{k},\omega)$ that is defined from

$$S(\mathbf{k},\omega) = \frac{1}{N}\int_{-\infty}^{+\infty} dt\, e^{i\omega t}\langle n_{\mathbf{k}}(t)\, n_{-\mathbf{k}}(0)\rangle, \tag{2.33}$$

where $n_{\mathbf{k}}(t) = \sum_{\mathbf{k}} \exp(-i\mathbf{k}\cdot\mathbf{r})$ is the Fourier transform of the electron density.

This means that the memory function (and the experimentally measured quantities that depend on it, like σ and τ^{-1}) can be determined from the easier to calculate dynamical structure factor $S(\mathbf{k},\omega)$. For example, in the simplest case of noninteracting two-dimensional electrons, $S(\mathbf{k},\omega)$ obtains the gaussian form

$$S(k,\omega) = \frac{1}{k}\left(\frac{2\pi m}{k_B T}\right)^{1/2} \exp\left(-\frac{(E_k - \hbar\omega)^2}{4E_k k_B T}\right), \tag{2.34}$$

where $E_k = \hbar^2 k^2/2m$. In the context of the memory function formalism, physical reasoning on the behavior of scattering time is reduced to the study of the dynamical structure factor $S(\mathbf{k},\omega)$. The gaussian form of $S(\mathbf{k},\omega)$, in the particular case of noninteracting electrons, is similar to the gaussian broadening of Landau levels that was postulated in the Ando-Uemura transport theory.

The presentation of further results from the Coulomb liquid theory must be suspended at this point, due to the inherent complexity of the subject and space considerations. However, more details can be found in the review article of *Monarkha et al.* [**82**] and the thesis of *Teske* [**104**].

2.5.5. Weak localization. Quantum objects exhibit a dual particle-wave nature, depending on the degree their wavefunction is localized or not in space. The consequences with regard to the quantum theory of scattering are profound when the wave-like character of one or both scatterers dominate, because then multiple scattering effects arise. Multiple scattering, refers to events whereby a scattered quantum wave is scattered elastically and repeatedly with other such quantum waves, or even with the initial incident quantum wave, producing constructive or destructive interference patterns.

Electrons of TDES typically collide with localized scatterers that are either periodically positioned (lattice ions), or disordered (impurities, gas atoms, ripplons, substrate surface anomalies). These scatterers may further be classified as fixed (lattice ions, impurities, substrate surface anomalies) and moving (gas atoms, ripplons). Multiple scattering of electrons becomes especially important

in the presence of periodic, immobile scatterers with high concentration[8] and weaker in the case of disordered, mobile scatterers with low concentration.

Ando-Uemura theory is based on the Born approximation and it therefore disregards effects due to multiple scattering[9]. Coulomb liquid theory at its fundamental level does not ignore multiple scattering, unless one decides (as in [**82**]) that this should be the case, in order to derive a tractable dynamical structure factor $S(\mathbf{k},\omega)$. *Altshuler et al.* [**4**] were the first to focus on how multiple scattering affects the transport properties of TDES in an environment with disordered scatterers, and they were able to derive the following exact formula for the magnetoresistance,

$$\sigma_{xx} = \frac{\sigma_0}{1+(\mu B)^2}\left(1-\frac{E_c}{k_B T}\right)e^{-E_c/k_B T} + \frac{\hbar e^2 n}{2\pi m\,(k_B T)^2} \times \int_{E_c}^{\infty} dE\, \frac{e^{-E/k_B T}}{1+(\mu B)^2}\left(\Psi\left(\frac{m\hbar}{4e\tau_0^2 EB}+\frac{1}{2}\right)-\Psi\left(\frac{m\hbar}{4e\tau_0\tau_\phi EB}+\frac{1}{2}\right)\right). \tag{2.35}$$

The digamma function is defined in terms of the gamma function as $\Psi(z) = \Gamma'(z)/\Gamma(z)$, while τ_0 and τ_ϕ are the relaxation and dephasing (or decoherence) time respectively.

The nomenclature is suggestive of the physical interpretation of τ_ϕ: on one hand, τ_ϕ is the mean time the phase of the electron wavefunction remains unchanged, while, on the other hand, it is a measure of how long quantum interference phenomena can last. From the fact that an electron evolves coherently in the time τ_0 between collisions, obviously τ_ϕ cannot be less than τ_0. Then, the lower limit of integration E_c, as calculated by *Stephen* [**102**], is always positive and well defined,

$$E_c = \frac{\hbar}{2\pi\tau_0}\ln\left(\frac{\tau_\phi}{\tau_0}\right) \quad \text{and} \quad \frac{E_c}{k_B T} \approx \frac{1.216\times 10^{-12}}{\tau_0 T}\ln\left(\frac{\tau_\phi}{\tau_0}\right). \tag{2.36}$$

Essentially, the lower limit of integration (E_c) indicates the interaction energies $E \leqslant E_c$ associated with multiple (coherent) scattering. Dephasing times τ_ϕ longer than an extremely short relaxation time τ_0 of the order of picoseconds, in an environment of very low temperatures T, make E_c comparable with the thermal energy $k_B T$, whereby coherent scattering dominates.

A celebrated macroscopic manifestation of quantum coherence in transport properties is the phenomenon of superconductivity, where conductivity

[8] This is the case for free electrons inside metals. Multiple scattering with lattice ions and the associated constructive or destructive interference is largely responsible for the formation of bands ($\sigma \longrightarrow \infty$) and gaps ($\sigma \longrightarrow 0$) respectively.

[9] The validity of Born approximation rests mildly on the weakness of the scattering potential, but strongly on the large value of the incident electron's wavenumber $k = \sqrt{2mE}/\hbar$. Since $k = 2\pi/\lambda$, the de Broglie wavelength λ will be small, or equivalently, the wave character will not be pronounced and the electron will indeed behave more like a particle.

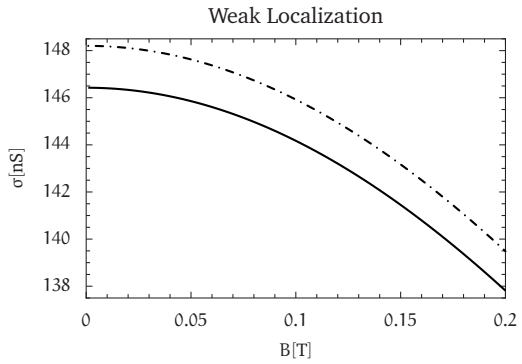

FIGURE 2.4. Conductivity σ vs. magnetic field B. Weak localization due to electron-vapor atom scattering leads to a lower σ (cf. eq. 2.35) in comparison to Drude's theory prediction (cf. eq. 2.21). For higher B, this difference disappears. The parameters used are as in *Karakurt et al.* [**52**].

becomes infinite when multiple scattering assumes a decisive role. Equation (2.35) nevertheless, suggests that in the absence of a magnetic field, $\sigma_{xx} \longrightarrow 0$ when $E_c \longrightarrow k_B T$ and quantum coherence appears to affect σ_{xx} in completely opposite ways in these two cases. This appears to be a contradiction, if it is not realized that quantum coherence can lead to either constructive or destructive interference. A periodic lattice, or otherwise ordered scatterers, favor constructive quantum interference, which results to superconductivity; the role of quantum coherence is reversed for disordered scatterers, as shown for the first time by *Anderson* [**6**], because they lead to destructive interference and the complete loss of conductivity.

At the limit $E_c \longrightarrow 0$, which is obtained when $\tau_\phi \approx \tau_0$, the first term of eq. (2.35) assumes the common Drude form and the integrand becomes zero, arriving at a magnetoconductivity as in eq. (2.21). In the intermediate range, except for the Drude term corrected for coherent phenomena, there is a second term which increases σ_{xx}. Basic properties of the digamma function can be used to show that this term disappears for $B = 0$ and $B \longrightarrow \infty$, and it is not negligible only in the range of weak magnetic fields (see fig. 2.4).

Therefore, the application of a weak magnetic field increases the conductivity of a TDES. This can happen only if the effects of quantum coherence (which decreases conductivity) are tempered. This magnetic field effect is known as "weak localization" and a demonstration of its physical content has been given by *Altshuler et al.* [**5**].

Altshuler et al. [**5**] consider the case of an electron which at time $t = 0$ is found at the position $\mathbf{r}$. Let the probability that the electron will return back to $\mathbf{r}$ after some time t—whereby the electron has zero drift, has not diffused at all, and is practically localized—be denoted $A(\mathbf{r}, t)$ (hereafter, the arguments $\mathbf{r}$ and t will be dropped for simplicity). There are infinite closed paths leading from $\mathbf{r}$ back to $\mathbf{r}$ after time t; let each path ξ be assigned a probability amplitude A_ξ. Any closed path ξ can be further assigned exactly two orientations, one clockwise,

denoted as α, and one counterclockwise, denoted as $\bar{\alpha}$. According to standard postulates of quantum mechanics, the probability $dP/d\mathbf{r}$ for an electron to be localized at $\mathbf{r}$ for time t, will be the square modulus of the sum of amplitudes $A_\xi = A_\alpha + A_{\bar{\alpha}}$ for all closed paths ξ from $\mathbf{r}$ back to $\mathbf{r}$, which, as already noted, can be decomposed in two paths α and $\bar{\alpha}$ with opposite orientations. Then, $dP/d\mathbf{r}$ can be expanded by means of the following mathematical operations:

$$\begin{aligned}
\frac{dP(\mathbf{r},t)}{d\mathbf{r}} &= \left|\sum_\xi A_\xi\right|^2 = \left|\sum_\alpha \left(A_\alpha + A_{\bar{\alpha}}\right)\right|^2 \\
&= \sum_{\alpha,\beta} \left(A_\alpha + A_{\bar{\alpha}}\right)\left(A_\beta^* + A_{\bar{\beta}}^*\right) \\
&= \sum_{\alpha=\beta} \left(A_\alpha + A_{\bar{\alpha}}\right)\left(A_\alpha^* + A_{\bar{\alpha}}^*\right) + \underbrace{\sum_{\alpha\neq\beta} \left(A_\alpha + A_{\bar{\alpha}}\right)\left(A_\beta^* + A_{\bar{\beta}}^*\right)}_{=0} \\
&= \sum_\alpha |A_\alpha|^2 + \sum_{\bar{\alpha}} |A_{\bar{\alpha}}|^2 + \sum_\alpha A_\alpha A_{\bar{\alpha}}^* + \sum_\alpha A_{\bar{\alpha}} A_\alpha^*.
\end{aligned} \tag{2.37}$$

In a disordered medium, genuinely different[10] paths ($\alpha \neq \beta$) are incoherent, meaning that their phases are randomly different, and this nullifies the sum underlined with the curly brace in eq. (2.37). This leaves only identical closed trajectories, differing only in the orientation α or $\bar{\alpha}$ they are traversed. But is this difference physically distinguishable?

If one imagines that all orientations are reversed, by turning all clockwise paths to counterclockwise and vice versa ($\alpha \leftrightsquigarrow \bar{\alpha}$ for all paths), one realizes that in effect the direction of time was reversed[11], so that $t \longrightarrow -t$. If time reversal leaves the hamiltonian invariant (as is normally the case), then the paths are physically identical and $A_\alpha = A_{\bar{\alpha}}$, otherwise the distinction has indeed a physical meaning and $A_\alpha \neq A_{\bar{\alpha}}$. The probability of electron localization in both cases will be,

$$\frac{dP(\mathbf{r},t)}{d\mathbf{r}} = \begin{cases} 2\sum_\xi |A_\xi|^2 & \text{if } A_\alpha = A_{\bar{\alpha}}, \\ \sum_\xi |A_\xi|^2 & \text{if } A_\alpha \neq A_{\bar{\alpha}}. \end{cases} \tag{2.38}$$

Equation (2.38) makes clear that the probability that an electron is localized is doubled when quantum coherence phenomena are taken into account. It remains to be shown that the case $A_\alpha \neq A_{\bar{\alpha}}$ is physically relevant.

Consider the hamiltonian of an electron in the presence of a magnetic field, eq. (B.1): the magnetic field is a polar vector and therefore it does not remain

[10] By this we mean those paths with different trajectories in space, regardless if their orientation is the same or not.

[11] The english language is very suggestive in this respect, as "*clock*wise" and "*counterclock*wise" already imply a connection between spatial and temporal orientations.

invariant under time reversal[12]. From $\mathbf{B} = \nabla \times \mathbf{A}$, this behavior is inherited by the vector potential $\mathbf{A}$, and the hamiltonian will *not* be invariant under time reversal. Clockwise and counterclockwise path orientations become physically distinguishable in the presence of a magnetic field ($A_\alpha \neq A_{\bar{\alpha}}$), quantum coherence is destroyed and the probability of localization is halved. It is exactly this "weak localization" inside a magnetic field which gives rise to the second term of eq. (2.35). One cannot hope to determine the contribution of weak localization quantitatively by means of the intuitive method outlined above. This is achieved with the help of the more rigorous methods of quantum field theory.

The first experimental demonstrations of weak localization were successful for TDES of thin metallic films (*Bergman* [**12**] reviews the relevant experiments and introduces weak localization theory). Weak localization in the case of electron-helium gas atom scattering was first observed for a TDES on solid hydrogen by *Adams et al.* [**2**], and later it was also reported for a TDES on liquid helium by *Karakurt et al.* [**52, 53**].

Dahm [**25**] argued that weak localization in the electron-ripplon scattering regime could also be observed in principle, but experimentally it was found difficult to unambiguously distinguish $e-e$ and electron-substrate roughness interactions from those of ripplons. Obstacles for the study of weak localization of TDES on liquid helium beyond the electron-gas atom scattering regime are mainly that:

- Ripplons are not fixed scatterers (their speed is though much less than that of electrons), meaning that coherent states last for a short time. Strong holding fields are needed to ensure a decent dephasing time, and these fields increase the electrostatic pressure electrons exert upon the surface of liquid helium to a degree that only liquid helium films can support.
- In liquid helium films, substrate roughness provides another uncontrollable source of scattering which reduces the dephasing time.
- Low electron densities are needed in order to dampen $e-e$ scattering. These densities are much below the saturated electron densities corresponding to the strong holding fields in use, and are associated with weak signals and reduced controllability.

The significance of weak localization experiments for TDES on liquid helium and elsewhere lies on the information they furnish about the dephasing time τ_ϕ, relative to other characteristic scattering times (for example $e-e$ interaction time τ_{ee} and electron-gas atom scattering time τ_{He}). This information can be used to test theories on scattering mechanisms, and elucidate their mechanics.

[12] This can be seen from Maxwell's equation $\nabla \times \mathbf{E} = -\partial_t \mathbf{B}$, by setting $t \longrightarrow -t$, whereby $\mathbf{B} \longrightarrow -\mathbf{B}$.

Karakurt et al. [**54**] studied the dependence of τ_ϕ on electron density, helium gas density and holding field, by assuming a Matthiessen rule $\tau_\phi^{-1} = \tau_{ee}^{-1} + \tau_{He}^{-1}$. The total dephasing time, due to helium gas atom scattering τ_{He}, can be further decomposed in a contribution due to scattering of electrons with helium gas atoms along the horizontal (τ_h) and vertical (τ_v) direction. Theoretically, it is expected that [**54, 102**],

$$\tau_h = \left(6\tau_0\tau_\lambda^2\right)^{1/3} \quad \text{where} \quad \tau_\lambda = \frac{\lambda}{\sqrt{2k_B T/m_{He}}}, \tag{2.39a}$$

$$\tau_v = \left(\frac{9}{2}\tau_0\tau_z^2\right)^{1/3} \quad \text{where} \quad \tau_z = \frac{76\times10^{-10}}{\sqrt{k_B T/m_{He}}}, \tag{2.39b}$$

$$\tau_{ee}^{-1} \propto \sqrt{\frac{n^{3/2}e^2}{2m\varepsilon}} \quad \text{with} \quad \varepsilon = \frac{\epsilon_{He}+1}{2}\epsilon_0. \tag{2.39c}$$

Here, λ denotes the de Broglie wavelength of the electron. *Karakurt et al.* [**54**] found a good agreement with their experimental data, and they were able to show that the interference of paths of duration t are damped by a 'squeezed' exponential factor $\exp\left(-(t/\tau_v)^3\right)$. Later, *Herman et al.* [**43, 44**] analyzed further this squeezed exponential damping behavior and provided a simple model as an explanation.

2.5.6. Cyclotron resonance. When an AC-electric field of the form $E_0 e^{i\omega t}$ is applied, in addition to a uniform magnetic field, a resonance will develop if ω happens to become equal to the cyclotron frequency ω_c of the TDES. The electron system will then absorb the offered electric energy at a maximum rate, or equivalently, the conductivity $\sigma(\omega)$ will obtain a maximum at $\omega = \omega_c$. But, if ω_c is identified, one can use its definition from eq. (2.13), in order to determine the effective electron mass m^*, and consequently electron mobility.

This "cyclotron resonance" technique was first developed and applied in the determination of electron and hole mobility in silicon and germanium crystals by *Dresselhaus et al.* [**30**], and it has found widespread applications ever since (in more complicated systems there might exist more than one cyclotron resonances, corresponding to 'heavy' or 'light' electrons and holes).

Cyclotron resonance for a TDES on liquid helium was exhibited by *Brown et al.* [**13**], in order to provide an independent verification that electrons were indeed bound on the surface of liquid helium as *Sommer et al.* [**101**] had proposed using the more conventional AC-technique, and not "flying around" as *Ostermeier et al.* [**87**] thought to have demonstrated in their experiments. *Brown et al.* [**13**] cleverly recognized and showed, that a two-dimensional bound state of electrons on xy-plane would change its cyclotron resonance frequency, if the magnetic

field in the z-direction were tilted by an angle ϕ. Had the electron system not been two-dimensional, no such dependence on ϕ would arise.

Except for the absolute position ω_c of the resonance peak, the width $\Delta\omega_c$ of the peak will be evidently associated with the broadening of Landau levels predicted by the Ando-Uemura theory, and the many-electron Coulomb effects predicted by the Dykman-Khazan theory. *Wilen et al.* [**115**] were thus led to measure the dependence of $\Delta\omega_c$ on saturated electron density n_s and to observe that $\Delta\omega_c$ increases with n_s, in contrast to the predictions of Dykman-Khazan theory which predicts exactly the opposite effect, namely the narrowing of resonance frequency width with increasing saturated electron density. Later measurements by *Teske et al.* [**105**] for a wider range of electron densities confirmed the observation of *Wilen et al.* [**115**], but also found that after a critical electron density $n_s > 10^{12}\mathrm{m}^{-2}$, the resonance frequency width $\Delta\omega_c$ increases with n_s, as Dykman-Khazan theory predicts. The theoretical explanation of this behavior was given by *Monarkha et al.* [**82**], who used the force-balance, and memory function formalism.

Experimental studies of cyclotron resonance were also performed for TDES on thin liquid helium films by *Würl* [**117**], where substrate roughness becomes a major uncontrollable scattering mechanism that interferes with electron motion. These experimental studies revealed that a fraction of electrons is strongly localized on surface roughness peaks and therefore does not participate in the dynamics of TDES. The two-fraction model was subsequently developed [**56**], which not only theoretically validates the picture of electrons 'pinned' on the top of surface roughness peaks, but also affords quantitative predictions on the relative percentage of free versus pinned electrons and is able to explain the experimental data *Würl* [**117**] collected.

In order to achieve cyclotron resonance experimentally, a resonance cavity is utilized, where only certain clearly identified modes ω of the electric field can be excited. The TDES is placed in the center of the cavity and magnetic field sweeps are performed, in order to identify the ω_c frequency which is equal to ω[13]. This is done by measuring the transmission and reflection coefficients of the TDES as a function of ω_c, with a network analyzer or a more conventional lockin technique, as is demonstrated in the theses of Würl [**117**], and *Teske* [**104**]. The basic model for the analysis of cyclotron resonance data, analogous to the transmission line or equivalent circuit models for the low-frequency measurements presented in section 3.6, is covered neatly by *Shikin* [**97**].

[13]That is, experimentally it is easier to keep the electric field constant and alter the magnetic field. The design of the resonance cavity is crucial, because it determines the quality and nature of the electric field modes excited.

2.6. Quantum computation with TDES on liquid helium

The research of TDES on the surface of liquid helium has been stimulated after *Platzman et al.* [**91**] suggested that they could be used to implement a quantum computer (for the principles of quantum computation see *Feynman* [**45**]). Quantum computation relies on the fundamental and little understood (cf. Schrödinger's cat paradox) superposition principle of coherent quantum states. Quantum computation attracts considerable interest, despite the fact that—with the exception of quantum cryptography—formiddable technological and theoretical barriers must be overcome before a reliable quantum computer can be constructed.

2.6.1. DiVincenzo criteria for quantum computation. Many systems with completely different physical properties have been proposed as candidates for quantum computation, making comparisons between them difficult without a general unifying framework that would define what the essential properties of a quantum computer should be. *DeVincenzo* [**29**], in the spirit of the celebrated von Neumann design of an electronic computer, classifies five properties that any candidate system for quantum computation must satisfy.

(1) **Scalable physical system with well characterized qubits:** Scalable means that the operation of the physical system should be easily extended, in principle, from a few qubits to several thousand (or million) of qubits. Well characterized qubits are those for which the hamiltonian (and energy eigenstates), the coupling between different states and the coupling to external fields are all known and controllable.

(2) **The ability to initialize the state of the qubits to a simple fiducial state, such as $|00\ldots\rangle$:** This arises from the need of registers that should be initialized to a known value before the start of a computation, and for quantum correction purposes.

(3) **Long relevant decoherence times, much longer than the gate operation time:** Decoherence time, is essentially the time the wavefunction of a quantum system evolves unitarily or, equivalently, the time between two successive "measurement" events that lead to the collapse of the wavefunction on one of its eigenstates.

The fact that this time should be longer than the gate operation time, means that computations carried out by the gates should most of the time happen in a coherent, 'quantum' state of the physical system. This is actually what distinguishes a quantum computation from an ordinary, classical computation. As a rule, decoherence time ought to be 10^4-10^5 times longer than the gate operation time, if fault-tolerant quantum computation is to be possible.

(4) **A universal set of quantum gates:** This means the ability to implement logical gates that would operate through sequences of unitary

transformations of the hamiltonian and allow universal computation, in the sense of a Turing machine.

(5) **A qubit-specific measurement capability:** This capability is of course necessary, if the result of a quantum computation is to be read out from the qubits.

2.6.2. Electrons on liquid helium as a quantum computer. Electrons on liquid helium could function as an analog quantum computer, as suggested for the first time by *Platzman et al.* [**91**], and laid out in more detail by *Dykman et al.* [**33**].

The two qubit states $|0\rangle$ and $|1\rangle$ were proposed to be the ground and first excited states of the TDES energy spectrum, respectively. These two states are separated by a transition frequency of 120GHz, as spectroscopic measurements by *Grimes et al.* [**38, 40**] demonstrated. This transition frequency is not fixed, but depends on the magnitude of the perpendicular holding electric field $E_\perp$ (Stark shift effect). The dependence on $E_\perp$ is appreciable and it alters the transition frequency at a rate approximately equal to 1GHz per 100V/m.

In view of the first DeVincenzo criterion, it is obvious that the proposed states $|0\rangle$ and $|1\rangle$ of a TDES are well characterized due to their huge frequency transition magnitude. Moreover, TDES on liquid helium are an easily scalable physical system, because electron density and electrode area can be easily varied. An electrode geometry, consisting of an arbitrarily large number of miniature (in the μm range) metallic electrodes, where each electrode confines a single electron of a TDES, would ultimately provide well characterized, scalable qubits equal to the number of TDES electrons (10^8 qubits for a moderate electron density of $10^{12}\mathrm{m}^{-2}$ on a total electrode area of $1\mathrm{mm}^2$).

Since electrons on liquid helium—unless excited by a strong external electric field—normally reside at the ground state, the ground state will also provide the fiducial state $|000\ldots\rangle$ required by the second DeVincenzo criterion.

Decoherence phenomena in TDES on liquid helium arise from electron interaction with helium gas atoms, ripplons and other electrons. Electron confinement should be sufficient as to eliminate $e-e$ interactions, while temperatures below 0.1K would do the same for electron-gas atom scattering. Then, the essential interaction that would influence decoherence time would be electron-ripplon scattering.

Dykman et al. [**33**] estimate that the decoherence rate for electron-ripplon scattering, associated with an electron transition from the ground state to the first excited state and conversely, is no less than $\tau_\phi^{-1} = 0.12\mathrm{MHz}$, or $\tau_\phi \approx 800\mathrm{ns}$. Electron-ripplon scattering within a TDES quantum state can be estimated by mobility measurements at low AC-excitation frequencies (e.g. *Mehrotra et al.* [**79**] and *Shirahama et al.* [**100**]) by means of the formula $\tau = em/\mu$, with obvious notation. It is found that the decoherence time is approximately 100ns at a

temperature of 10mK, and therefore it will be electron-ripplon scattering within a TDES quantum state, rather than across quantum states that will determine decoherence time.

According to the third DeVincenzo criterion, the gate operation time (or clock speed) should be much longer than the decoherence time. For TDES on liquid helium, the clock speed is estimated from the inverse of the Rabi frequency (Ω^{-1}), which gives the rate of change of the TDES wavefunction when an external resonant electric field with amplitude E_{RF} is applied. The Rabi frequency for electrons on liquid helium is given by

$$\Omega = \frac{1}{\hbar}|eE_{RF}\langle 1|z|0\rangle| \approx \frac{eE_{RF}a_0}{\hbar}, \tag{2.40}$$

where $a_0 = 74\text{Å}$ is the effective Bohr radius of TDES on liquid helium (see appendix A) and e the electron charge.

For a resonant field $E_{RF} = 1\text{kV/m}$, the clock speed is about 0.1ns, whereby decoherence time lasts 10^3 times longer than the clock speed. At least two orders of magnitude more can be won (making decoherence time 10^5 times greater than the clock speed), if a magnetic field with nonzero component along the z-direction is applied. This happens, because the magnetic field quantizes the electron energy spectrum (Landau quantization), reducing thus the electron-ripplon scattering rate drastically.

Decoherence phenomena would be experimentally observable as a broadening of the Rabi frequency Ω and the transition frequency f_{12}. Obviously, the more broadened these frequencies are, the more intense are thermal fluctuations, electron-ripplon scattering and other disturbances that destroy coherence.

Collin et al. [**22, 23**] measured the Rabi and the transition frequencies, together with the associated line widths, at various temperatures lower than 1.2K. They found that at 0.1K, which is the proposed working temperature of a future quantum computer with electrons on liquid helium, it is $\Delta\Omega/\Omega \approx 3.3 \times 10^{-3}$ and $\Delta f_{12}/f_{12} \approx 5 \times 10^{-6}$, even without using a magnetic field and confined electrons (which would thus reduce electron-ripplon scattering and $e-e$ interactions even further). These values corroborate the claims of *Dykman et al.* [**33**] and prove that coherent, well characterized qubits from TDES on liquid helium are feasible.

A quantum computer based on TDES on liquid helium would operate, as *Dahm et al.* [**26**] describe, with two logical quantum gates that support universal computation. These could be the SWAP gate, which interchanges the states of two qubits ($|0\rangle$ and $|1\rangle$ are transformed to $|1\rangle$ and $|0\rangle$), and the binary CNOT gate (conditional NOT gate), which gives $|0\rangle$ (true) or $|1\rangle$ (false), if the ordinary NOT operation between the two qubits agrees or not with a (conditional) third qubit.

Dahm et al. [**26**] imagine the operation of a SWAP gate as follows: at first, one begins with qubits $|0\rangle$ and $|1\rangle$ and applies the same holding electric field to

both qubits, so that the states $|01\rangle$ and $|10\rangle$ are degenerate. The system would then oscillate between the states $|01\rangle$ and $|10\rangle$, at a certain frequency defined by the interaction energy (Coulomb potential) between the qubits. If the holding electric field is applied for half cycle of this oscillation, the qubits will swap states.

The operation of the binary CNOT gate, according to *Dahm et al.* [**26**], could proceed as follows: two qubits are brought into the states $|0\rangle$ and $|1\rangle$ and an AC-electric field whose frequency is equal to the transition frequency from $|0\rangle$ to $|1\rangle$, is applied to one of the states. A transition will or will not occur, depending on whether the AC-electric field was applied on the state $|0\rangle$ or $|1\rangle$, respectively. Then, in the same way, an AC-electric field is applied on the third control qubit and—depending on the final state of the control qubit—one sees whether the condition is satisfied or not. Therefore, the demand of a universal set of quantum gates, which is imposed by the fourth DeVincenzo criterion, is satisfied.

Qubits can be read out, as *Dahm et al.* [**26**] and *Dykman et al.* [**33**] propose, by applying a negative DC-electric field at the electrodes. If the magnitude of the electric field is selected such that electrons in the first excited state could escape, these electrons could have been collected by a complementary electrode structure placed on top of the TDES. The absence of electrons at specific electrodes would of course indicate that these electrons were at the ground state.

Lea et al. [**70**], on the other hand, point out the technical complexity of such a complementary electrode structure and propose the use of miniature single-electron transistors (SET) that would function both as confining electrodes and as elements for the read out process. *Papageorgiou et al.* [**88**] constructed and successfully tested a single-electron electrostatic trap, where electrons are detected with a SET.

Part II

Localization

CHAPTER 3

Measurement and Data Analysis Methods

3.1. Experimental apparatus and operation

Experimenting with TDES on liquid helium requires temperatures below 2K. Depending on the TDES features to be probed (e.g. quasi zero-dimensional localization, weak localization), magnetic fields up to several tesla might be additionally required. All measurements concerning quasi zero-dimensional localization were thus performed in a large dilution refrigerator[1] with a 7T magnet. The full power of the dilution refrigerator (nominal base temperature of 15mK) was almost never needed and the dilution refrigerator was mainly used as an extremely efficient ^{3}He-cryostat of great cooling power (temperatures of approximately 500mK were reached by circulating exclusively ^{3}He).

Closing and cooling the cryostat down to its operating temperature was a relatively time consuming process, lasting no less than three days (with the same amount of time needed for warming up). Three more days were needed for the helium gas to condense into the relatively voluminous experimental cell, until the level of liquid helium inside the cell reached the bottom plate.

Two features of this particular dilution refrigerator, namely its large liquid helium consumption and its proneness to vibrations, were especially disturbing for experiments. Both features resulted from a design error in the size of outflow space that led to turbulence in the flow of the helium gas that was evaporating from the dewar of liquid helium. The turbulent flow increased the consumption of liquid helium to an astounding 2lt per hour, meaning that an almost daily transfer of liquid helium was necessary (liquid nitrogen was transferred every second day). Furthermore, the turbulent flow caused vibrations of the cryostat, which would render any TDES unstable and destroy it within minutes after it were created.

The primary source that relayed vibrations to the experimental cell was found to be the relatively flexible plastic rod of the cryostat's insert, which extended from the still to the mixing chamber. For this reason, the experimental cell was

[1] The dilution refrigerator used was a specially modified MNK-126 series model produced by Leiden Cryogenics. The company site at `www.leidencryogenics.com` contains much useful technical information, while chapter 11 of the book (in German) of *Enss and Hunklinger* [**34**] explains the physical principles behind the operation of a dilution refrigerator.

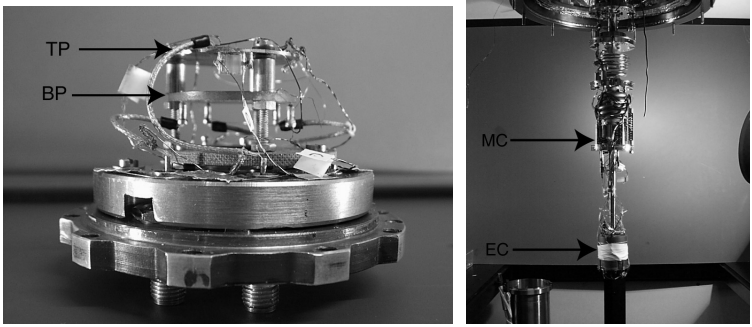

(A) The experimental cell (B) The dilution refrigerator

FIGURE 3.1. Picture of the bottom part of the experimental cell and the lower part (insert) of the dilution refrigerator used in the zero-dimensional localization experiments. The bottom plate (BP), containing the electrodes and the guard ring, and the top plate (TP) are visible in (A). The top part of the experimental cell (EC) and the mixing chamber (MC) of the dilution refrigerator are visible in (B).

held stable by means of three plastic, thermally insulating screws 60° degrees apart from each other, which were screwed in from the enclosing copper pot. Moreover, an automated filling system was also installed, so that the tubes for liquid helium transfer were removed only when a fresh full dewar had to be connected to the cryostat.

The bottom part of the experimental cell is shown in fig. 3.1A. A brass cylinder is screwed above the copper deck, in order to reduce the cell volume that must be filled with liquid helium. Three brass screws support the bottom plate, which contains the guard ring and the electrode structure (the bottom plate's design is shown in fig. 3.7). The substrate is placed on the electrode structure and it is kept in place by making use of a small amount of apiezon grease.

Approximately 6mm above the bottom plate, the copper top plate is mounted. Three tiny holes are bored in the top plate, in order to accommodate an equal number of miniature incandescent lamps (filaments) whose protecting glass bulb has been carefully broken. The filaments are glued in the holes with a glue specially made to be resistant at low temperatures. These filaments are the source of free electrons, by means of thermionic emission (see section 3.3). It is essential to ensure that absolutely no electrical contact exists between any of the various constituents of the experimental cell described so far (top plate, guard, filaments, electrodes).

The bottom deck has four special SUHNER vacuum plugs for coaxial cables, and a 10-pin plug in the center. The three electrodes and the top plate are normally connected with coaxial cables to the SUHNER plugs, whereas the filaments (two cables for each filament are required) and the guard ring are connected with copper or brass cables to the 10-pin plug.

The top deck of the experimental cell is permanently mounted at the bottom of the cryostat's insert (see fig. 3.1B). A helium level meter (see section 3.2), requiring four electrical connections, is mounted inside the top deck. The electrical connections are led out of the experimental cell by a 4-pin plug on the top of this deck.

After making sure that no electrical connection persists among any two elements of the experimental cell and no filaments were broken, or wet by glue, the experimental cell can be hermetically sealed. To this purpose, the rims of the decks should be at first cleaned with ethanol. Then, an indium cable about 1mm thick that is cleaned with ethanol and rubbed with a small amount of low-temperature glue is adjusted tightly around the rim of the bottom deck. The one free end of the indium cable (which has now been turned into a ring) is pressed on the other free end. The bottom deck is subsequently positioned below the top deck, which bears copper screws, and it is gently pushed up, so that the copper screws of the top deck enter the holes of the bottom deck. Two steel half-rings are worn on the rim of the bottom deck and the nuts are then gently screwed in (the half-rings ensure that the pressure of the nuts is distributed uniformly around the rim) such that at any time no nut is pressing the bottom deck more than any other.

After this procedure is completed, the cryostat cables are connected with the respective plugs at the bottom deck and a check of the electrical contacts is performed. If everything is in order, the experimental cell is pumped by a leak detector and a leak test is performed, by spraying helium gas around the rim connecting the two decks and on the plugs and capillaries. Only when no leak is detected (the leak detector should indicate a steady helium gas concentration less than 10^{-9} even when spraying with helium gas) can the cryostat be sealed, closed and be prepared for cooling down.

The minimum of required measuring devices for experiments with TDES on liquid helium are a sensitive lockin amplifier (for the AC-measurement, see section 3.5), an RCL-meter (for measuring the capacitance of the level meter, see section 3.2), two voltage sources (for setting the guard and bottom plate voltage independently), a pulse generator (for pulsing the filaments) and an oscilloscope (to visualize the filament response to the pulse). An accurate bridge for measuring the resistance of the sensor (e.g. RuO_2 resistor) used for the determination of temperature is also needed, had it not been provided with the cryostat.

3.2. Determination of liquid helium layer thickness

The accurate knowledge of where the position of the surface of liquid helium is in the experimental cell, is obviously critical for the analysis of transport measurements. But as in such experiments direct visual contact inside the experimental cell is impossible and, even if it can be established, it is deadened by the fact that superfluid helium is colorless, completely calm, with an almost invisible surface[2], other indirect methods must be developed.

3.2.1. Measurement of bulk liquid helium level. The position of the surface of bulk liquid helium inside the experimental cell is determined by measuring the capacitance of a cylindrical capacitor (the *level meter*) mounted vertically inside the cell, as it is progressively filled with liquid helium. Since liquid helium is a dielectric ($\epsilon_{He} = 1.057$), the capacitance $C(L)$ of a level meter of length L full with liquid helium will be greater than the capacitance $C(0)$ of the empty level meter; more precisely, it will be $C(L) = \epsilon_{He} C(0)$. For a level meter partially filled up to an intermediate height $0 < l < L$, the length ratio is equal to the ratio of the respective capacitance differences and a simple relation emerges:

$$\frac{l}{L} = \frac{C(l) - C(0)}{C(L) - C(0)}. \tag{3.1}$$

From the fact that $C(L) - C(0) = (\epsilon_{He} - 1)C(0)$ and after numerically substituting ϵ_{He} in eq. (3.1), an estimation for the precision of the capacitive method is obtained,

$$\frac{l}{L} = 17.54386 \left(\frac{C(l)}{C(0)} - 1 \right). \tag{3.2}$$

The house-made level meters consisted of two hollow, steel, cylindrical tubes with radii $r_o = 3\text{mm}$ and $r_i = 2.5\text{mm}$, having a length of $L = 41.5\text{mm}$. The r_i-tube was positioned inside the hollow of the r_o-tube and two insulating pertinax bucklers were adjusted on the respective edges of the tubes, in order to stabilize the structure and ensure that the tubes have no electrical connection with one another. A brass rod with a diameter of 2mm was subsequently inserted in the hollow of the inner tube through small holes in the center of the bucklers, again with no contact to either tube. The construction was equipped with electrical contacts by soldering the cores of a pair of coaxial cables one on each steel tube and the shields of both cables on the brass rod. The level meter is mounted in the cell exclusively from the brass rod, which is then at the common ground voltage of the cell (each steel tube must remain electrically insulated from anything else). In this way, a four-point capacitance measurement from a RCL-meter becomes possible.

[2]The index of refraction of liquid ^{4}He is 1.026, similar to that of the air. For a comparison, pure water, whose surface is also not easily discernible, has a refractive index of 1.333.

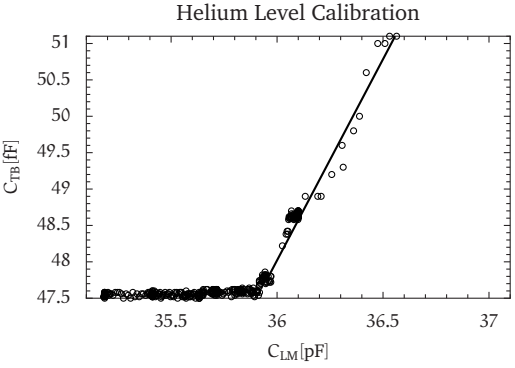

FIGURE 3.2. Top-bottom plate capacitance C_{TB} as a function of level meter capacitance C_{LM}. Notice that C_{TB} varies within a range of just 4fF, with the effect that its measurement is not free of fluctuations and inaccuracies.

Regarding the physical dimensions of the level meter, it should be noted that the space between the steel tubes should not be so narrow as to permit capillary effects and, in order for liquid helium to enter easily, the outer tube should have a slit of about 0.5mm.

From electromagnetic theory, the capacitance of a cylindrical capacitor L length units long, with outer and inner radii r_o and r_i respectively, is known to be

$$C = \frac{2\pi\epsilon_0 L}{\ln(r_o/r_i)}. \tag{3.3}$$

After substituting the numerical values for the level meter used in the experiments in eq. (3.3), the expected capacitance of the completely empty level meter is calculated as $C(0) = 12.6571$pF. Inspection of fig. 3.2 reveals that the experimentally observed capacitance is almost three times larger, more precisely $C(0) = 35.114$pF. In fig. 3.2, the rise of liquid helium inside the experimental cell, captured by bigger values of C_{LM}, initially leaves C_{TB} unaltered, because the level of helium is still below the bottom plate. As soon as liquid helium floods the bottom plate and starts filling the space between the top and bottom plates, C_{TB} increases along with C_{LM}, until the top plate is reached, where C_{TB} assumes its maximum constant value.

There are various reasons for the discrepancy between the theoretical and experimental capacitance of the level meter, the most important of which is the stray capacitance of the coaxial cables that connect the level meter with the measuring devices. Stray capacitance is generally larger for longer cables and depends strongly on their quality: the use of exactly the same type of level meter in a smaller glass cryostat, where the cable length was approximately 3m instead of the approximately 6m of the dilution refrigerator's setup, reduced $C(0)$ to 26pF (almost 30%). Except for stray capacitance, the *measured* capacitance—in contrast to the theoretically calculated, which is a purely geometric property of the capacitor—will depend on the details of the four-point measurement

such as excitation voltage and frequency. Better resolution, which means a larger magnitude of $C(0)$, is achieved for higher frequencies and excitation voltages. Nevertheless, excitation voltage should not be set at too high a value (2V were used), because this would have adverse effects in the temperature of the experimental cell. These effects are of course more pronounced for temperatures in the millikelvin range. Similarly, the excitation frequency (85kHz were used) should be different from the excitation frequency of the lockin amplifier, in order to avoid cross talk that would influence the quality of measurements. This is especially true in the case of level meter calibration, where two RCL-meters measure the capacitance of the level meter and the top-bottom plate configuration. Regular oscillations of the measured capacitances are observed when the excitation frequency is the same for both RCL-bridges.

It is usually straightforward to measure capacitance with an accuracy of $\pm 10^{-3}$pF. Then, eq. (3.2) suggests that the resulting accuracy in the determination of the height of liquid helium surface is ± 0.7mm. In experiments that involve bulk liquid helium, it is not expected that electron properties would be sensitive to the thickness of helium layer. The only experimental constraint is actually the magnitude of the measured signal. Bigger measured signals are preferred, because they allow a better resolution of transport properties. This means that the TDES should be as close to the measuring electrodes as possible, in a range beginning from roughly 0.2mm and up to 2mm. Therefore, the relatively large uncertainty in the determination of liquid helium thickness is not physically critical—in the sense that it would not invalidate data analysis and theoretical argumentation—but it is, nevertheless, experimentally important: after the choice of bulk liquid helium level of, for example, (1.2 ± 0.7)mm has been made, careful and time consuming fine tuning is often needed, so that the measured signal obtains its optimized maximum magnitude.

3.2.2. Uncharged liquid helium film thickness. As liquid helium films are characterized by a thickness from 5Å up to hundreds of μm, a range of values three to seven orders of magnitude smaller than the measurement error of the helium layer thickness with a level meter, some further properties of liquid helium must be exploited, if the capacitive method is to determine the liquid helium thickness in the film range accurately.

Superfluid helium is a universal wetting agent[3] and it will creep over every available surface inside the experimental cell, forming a film whose thickness depends on gravity and the affinity force that binds liquid helium with the surface. In order to make the last statement mathematically precise, assume that a dielectric wall (of dielectric constant ϵ) is raised vertically with respect to the

[3]It was believed for a long time that no exceptions exist for this property, but in 1991 it was theoretically proposed [**17**] and shortly thereafter experimentally demonstrated [**84**] that surfaces of some alkali atoms (Cs, Rb) are not wet by superfluid helium.

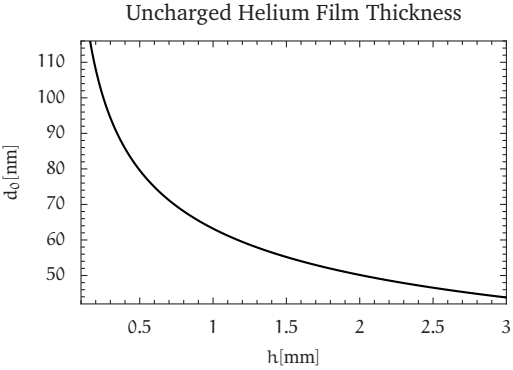

FIGURE 3.3. Thickness d_0 of a horizontal liquid helium film as a function of the distance h from bulk liquid helium below. Changes of the bulk liquid helium level in the mm-range (measurable with a level meter) translate to changes of film thickness in the nm-range. This is essentially a plot of eq. (3.5) for silicon ($C_3 = 26$K).

surface of bulk liquid helium (the contact angle is 90°). Liquid helium will creep up the wall up to the height h, where gravitational potential becomes equal to the attracting part of the Lennard-Jones potential that describes the interaction between the helium atoms and surface atoms. If liquid helium density and the acceleration of gravity are denoted with ρ and g respectively, the equilibrium condition can be written as[4]

$$\rho g h = \frac{C_3}{d_0^3}, \tag{3.4}$$

where d_0 is the thickness of the resulting helium film at that particular height h, and C_3 is the Lennard-Jones coefficient, which encloses the details of surface-helium atom interaction.

Solving for the thickness $d_0(h)$ of the uncharged liquid helium film that forms on the horizontal plane h length units above the surface of bulk liquid helium, one obtains

$$d_0(h) = \left(\frac{C_3}{\rho g h}\right)^{1/3}. \tag{3.5}$$

The *ab initio* calculation of Lennard-Jones coefficient C_3 in the general case (cf. the short review of *Babb* [**11**] and references therein) follows from

$$C_3 = \frac{1}{4\pi}\int_0^\infty d\omega\, \alpha(i\omega)\frac{\epsilon(i\omega)-1}{\epsilon(i\omega)+1}, \tag{3.6}$$

where $\epsilon(i\omega)$ is the dielectric function and $\alpha(i\omega)$ the dynamic electric dipole polarizability function of the interaction between helium atoms and the material of the surface in question. Usually, ϵ is considered constant and information on α relies on a blend of theory and experiments (for liquid helium on silicon this information can be found in [**86**]). For silicon, it is $C_3 = 26$K and to substitute

[4]Notice that the common "6–12" form for the exponents of the Lennard-Jones potential describe interactions between point-like particles. Here, the interaction involves a particle and a two-dimensional wall with the effect that it becomes generally stronger. The exponents are thus lowered, so that the Lennard-Jones potential becomes a "3–6" potential in this case.

this value into eq. (3.5), one must multiply with Boltzmann's constant, $k_B = 1.38 \times 10^{-23} JK^{-1}$. The resulting thickness of the liquid helium film on silicon as a function of the distance from bulk helium is depicted in fig. 3.3.

The influence of retardation (or Casimir-Polder effect [**15**]) was ignored in the preceding discussion. It contributes a potential term with the asymptotic form ('large' values of r)

$$V(r) = -\frac{3\hbar c\alpha(0)}{8\pi r^4}, \tag{3.7}$$

where $\alpha(0)$ is the static electric dipole polarizability, which for helium, as theoretical studies and various experiments validate [77], is numerically equal to $\alpha(0) = 1.383 a.u.$

The absolute value of eq. (3.7) would have to be added as a second term in the right-hand side of equilibrium eq. (3.4), but it can be safely ignored for r that make it much smaller than C_3/d_0^3. This is indeed the case for helium films with thickness 0.9nm to 100nm over a silicon substrate.

The error $\delta d_0(h)$ in the estimation of the film thickness as a function of the level meter error $\delta\epsilon$ is derived from eq. (3.5) by differentiation. Its absolute value reads

$$\delta d(h) = \frac{7}{3}\left(\frac{C_3}{\rho g}\right)^{1/3} h^{-4/3}\delta\epsilon, \tag{3.8}$$

which, as a direct numerical application shows, results in an estimated film thickness (65 ± 15)nm, or a relative error of 20% for a bulk level (1 ± 0.7)mm below a helium film on a silicon substrate.

In contrast to experiments on TDES over bulk liquid helium, where transport properties are not sensitive to errors in the estimation of bulk thickness (as long as its lower thickness bound does not happen to fall below the substrate), transport properties of TDES on liquid helium films depend critically on film thickness and a 20% measurement error is unacceptable. Fortunately, an electron sheet above a helium film possesses an 'electric' weight, in a sense that will be made precise in the following section, and the decisive factor that affects film thickness becomes the TDES density, rendering the contribution of level meter error to film thickness estimation irrelevant.

3.2.3. Charged liquid helium film thickness. Electrons on a liquid helium film exert an electrostatic pressure on the film and they eventually alter its thickness according to

$$d(n_s, h) = d_0(h)\left(1 + \frac{(n_s e)^2}{8\epsilon_0 \rho g h}\right)^{-1/3}. \tag{3.9}$$

In analogy with a heavy body, a dense TDES squeezes helium away from the film and reduces its thickness. For high enough saturated electron densities n_s, this effect becomes dominant and almost diminishes initial differences in

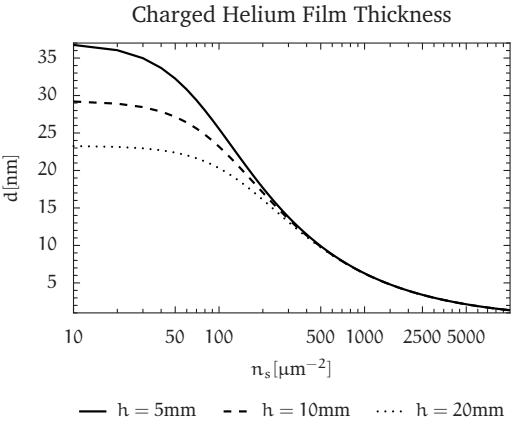

FIGURE 3.4. Thickness d of three horizontal charged liquid helium films as a function of the saturated electron density n_s. The films are h above bulk helium. For high n_s, charged film thicknesses become identical, regardless of the initially different d_0. This is a consequence of eq. (3.9).

$d_0(h)$, as experimental results of *Etz et al.* [**35**] and the theoretical plot, shown in fig. 3.4, of $d = d(n_s)$ for various initial $d_0(h)$, demonstrate.

The electrostatic pressure depends positively on the saturated electron density n_s. In turn, saturated electron density is controlled experimentally by the value of holding field voltage V_{TB}. The high electron densities that can be supported over liquid helium films make it ultimately possible to control helium film thickness through V_{TB}. In this way, inaccuracies arising from errors in the precise position of bulk liquid helium surface are avoided. A natural question that arises in this case, is the extent to which n_s can be reliably controlled and estimated. But before this question is analyzed in section 3.4, it is more appropriate to divert into the details of the process of pulsing electrons on the liquid helium surface.

3.3. Charging the liquid helium surface with electrons

Electrons are brought on the surface of liquid helium by thermionic emission of a tungsten filament placed on the top plate. The filament is procured from a common miniature incandescent lamp with operational data $V = 1.2V$ and $I = 50mA$ (at 20°C) whose glass bulb is carefully broken. The incandescent lamp is electrically connected to a pulse generator that delivers voltage pulses with well defined peak, form, duration and period. A quantitative sense of the amount of electrons released from the filament, as a function of the experimentally accessible control variables (voltage and pulse duration), is important and it is the subject of the following paragraphs. The present discussion is complementary to the relevant experimental data presented in the thesis of *Würl* [**117**], which cover various properties of the filaments that were also used in the experiments of the present work. All physical properties of tungsten referred in this section were recovered from the monograph of *Lassner and Schubert* [**68**].

PROPERTIES OF TUNGSTEN (W)

Atomic Weight[g/mol]	Density[g/cm] (20°C)	Specific Heat[J/g K]	Melting Point[K]
183.84	19.25	0.13	3695

3.3.1. Thermionic current–voltage filament characteristic. The voltage V applied on the filament sets the electron gas inside it in motion and increases its energy. The electron gas inside tungsten is degenerate and it behaves therefore as an ideal fermion gas contained in a volume sl, where s is the cross section and l the length of the filament. In thermodynamic terms, the electron gas undergoes an isochoric heating, where the offered electric energy $Q = V^2/R$ is fully transformed into thermal energy according to $Q = nC_v(T - T_0)$, with obvious notation.

Tungsten's resistivity ρ does not remain constant during heating but changes with temperature T in accordance with the empirical formula

$$\rho(T) = 0.48\left(1 + 4.8297 \times 10^{-3}T + 1.663 \times 10^{-6}T^2\right) \quad [\Omega\ \mathrm{cm}]. \tag{3.10}$$

The filament is a thin thread of circular cross section with radius r and length $l = \kappa r$, where κ is a dimensionless proportionality factor. Resistance R is generally associated with resistivity through the formula $R = \rho l/s$ that, by making use of the filament's geometry, reduces to $R = \rho\kappa/\pi r$. Taking into account the filament's operational data and eq. (3.10), one calculates that $\pi r/\kappa \approx 0.052$cm even without exact knowledge of the radius or the proportionality factor *per se*. The final temperature T of the filament, after a voltage V has been applied at its ends, will be then implicitly calculated from

$$\frac{\pi r V^2}{\kappa n C_v} = \int_{T_0}^{T} \rho(\tau)\mathrm{d}\tau. \tag{3.11}$$

Obviously, the initial temperature T_0 will be the temperature of the cell at the time of pulsing, whereas the molar quantity n of tungsten can be found from $n = \rho\pi\kappa r^3/183.84$, where ρ[g cm^{-3}] is tungsten's density. Here, an exact value of either r or κ is needed and, if factory data are missing, it is easier and better to measure the length of the filament, unless a microscope is available for the measurement of its diameter. Estimated values are $r \approx 16.5\mu$m and $\kappa = 1000$ and the molar quantity is thus calculated to be $n \approx 1.48 \times 10^{-6}$mol.

Thermionic emission is described by an Arrhenius-type law, known in this context as Richardson-Dushman equation, giving the thermionic current density j as a function of temperature. For tungsten, Richardson-Dushman equation

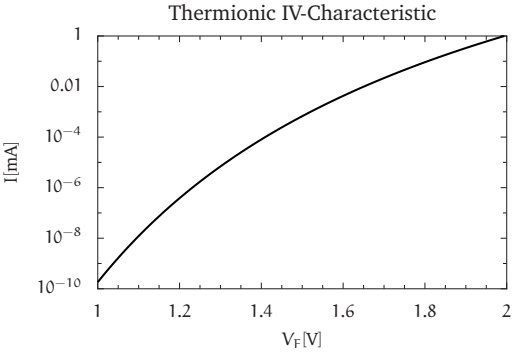

FIGURE 3.5. Thermionic current I emitted by a tungsten filament with radius $r = 16.5\mu m$ and proportionality factor $\kappa = 1000$ as a function of the voltage V_F applied on its pins. The applied voltage from the pulse generator is in reality higher than V_F.

obtains the empirical form

$$j = 60.2T^2 \exp\left(-\frac{52230}{T}\right) \quad \left[\mathrm{A\,cm^{-2}}\right]. \tag{3.12}$$

The thermionic current I emitted from the filament will obviously be $I = 2\pi\kappa r^2 j$ (see fig. 3.5), and the total thermionic charge q will be the product $q = It$, where t is the pulse duration. A numerical application shows that a 50ms pulse at 1.5V produces an electron density of $620e/\mu m^2$ on an electrode area of $1cm^2$, in the ideal case where no electrons are lost. Comparing with fig. 3.4, it is clear that this density is already high enough to overshadow uncertainties in the measurement of the thickness of the uncharged liquid helium layer.

Voltage V will not exactly coincide with the amplitude of the applied pulse. It will be generally smaller, because the resistance of the cables that connect the filament with the pulse meter has been ignored[5].

3.3.2. Experimental details of pulsing. Thermionic electrons that overcome the surface barrier imposed by the filament do not rest on the surface, as the theoretical Richardson-Dushman framework would suggest. They behave instead as a classical Maxwell-Boltzmann-distributed gas with temperature equal to that of the operating filament [**36**] and this immediately implies that their average speed $\overline{v}[\mathrm{m\,s^{-1}}]$ will be given by $\overline{v} \approx 0.618 \times 10^4 \sqrt{T}$.

Average speeds for typical temperatures up to 2K have a magnitude of hundred kilometers per hour. Clearly, if no diffusive medium or counteracting voltage is present, thermionic electrons will either be absorbed from surrounding conducting surfaces or reach and break through the surface of liquid helium due to their high speed.

A simple preventive measure is to pulse the filament only at temperatures where the vapor pressure of helium gas is high enough, so that collisions between

[5]Thin copper cables are normally used for electric connection, with a resistance of about 50Ω at room temperature. One finds that the pulse amplitude should be between 1.5 and 2.0 volt.

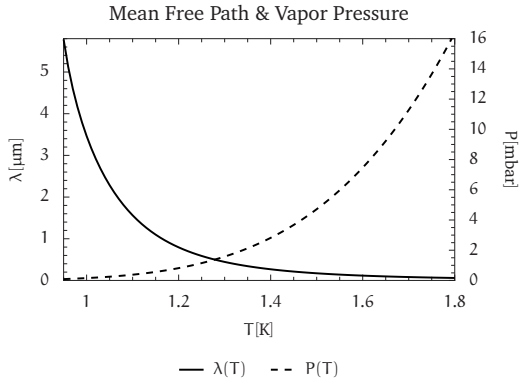

FIGURE 3.6. Vapor pressure P of helium and mean free path λ of an electron within helium gas, as a function of temperature T. Vapor pressure increases exponentially with temperature, hence the mean free path decreases exponentially when the temperature increases.

gas helium atoms and electrons effectively break the latter down. Inspection of fig. 3.6 reveals that pulsing should not be attempted at temperatures lower than 1.1K in general.

Indeed, the average distance x traveled by electrons within helium gas after n collisions is $x = \sqrt{n}\lambda$, if this motion is regarded a random walk. Then, the time t to cover the distance x is simply $t = x^2 (\bar{v}\lambda)^{-1}$. For a cell temperature of $T = 1.164$K, this means that electrons need a time of approximately 0.15ms to advance 1mm, or equivalently that their speed has been reduced four orders of magnitude, down to the very acceptable 6.67m/s.

If no other electric field is present, the electron gas will expand in space, diffusing within the helium gas, until it reaches metallic or otherwise conducting surfaces, where it will be absorbed. Since the top plate is the nearest conducting surface, it has to be set at a sufficient negative potential with respect to ground, or equivalently, the bottom plate has to be set at a positive potential. Practically, it is also prudent to set the filament at an offset negative voltage, so that thermionic electrons will not remain at the filament's surface, or even be re-absorbed by it.

The microscopic dynamics of the thermionic electron gas is certainly very complicated and the potential configuration in the area between the top and the bottom plate proves to be critically important. The absolute potential values of the top and bottom plates do not in an obvious way provide a hint on the dynamic lines of the static electric field in the enclosed area, nor does their ratio. For this reason, potential profiles for the configuration at hand must be furnished, by numerically solving the Laplace equation for the boundary conditions (voltage configuration) one is interested in.

Nevertheless, extensive experimentation, detailed theoretical profiles, or better a combination of the two is in most cases sufficient to allow for the saturated electron density to be reached after two or three pulses and for the electrons to reach the surface of liquid helium softly enough that no danger of electron breakthrough arises.

3.4. Determination of saturated electron density

Consider a TDES on liquid helium for a given holding field $E_\perp$ between the top and the bottom plate. The TDES is a negative charge distribution that induces an electric field E in the opposite direction of $E_\perp$. Hence, provided that the holding field remains constant, additional electrons that will join the TDES after a pulse will further increase E, making the approach of more electrons increasingly difficult.

Saturated electron density n_s is defined as the TDES density for which E exactly counter-balances $E_\perp$, leaving the space *above* and *below* the TDES[6] free of any electric field. After this point, pulsing has no effect on the electron density.

It is the complete screening, or "no field" property that makes the determination of n_s possible. More specifically, the systems TDES-top plate and TDES-bottom plate form two plane capacitors whose plates lie at a distance L apart, their surface area being A. An elementary application of electromagnetic theory provides the following expression for the capacitance of a plane capacitor:

$$C = \epsilon_0 \epsilon \frac{A}{L}. \tag{3.13}$$

From the definition of capacitance and saturated electron density, it is $Q = CV$ and $n_s e = Q/A$, respectively, whereby by making use of eq. (3.13) and the fact that $V = V_{TB}$, saturated electron density n_s results in

$$n_s = \frac{V_{TB}\epsilon_0 \epsilon}{eL}, \tag{3.14}$$

where L is the distance of TDES from the bottom plate and ϵ the dielectric constant of the medium found in the space separating them. In order to derive the quotient ϵ/L, one must analyze what media are present in this space.

If one starts descending from the TDES down to the bottom plate, four more plane capacitors connected in series can be identified. These capacitors can be characterized by the medium that fills the space between the plates.

Vacuum: "Plates" of this capacitor are the TDES and the surface of the liquid helium film. The dielectric constant of vacuum is unity[7], whereas the distance L_{vac} between the plates is found by *Hu et al.* [**46**] to vary approximately as $L_{vac} \approx 2 + 0.1 L_{He}$, where L_{He}[nm] is the thickness of the thin helium film.

Helium film: The dielectric constant of helium is ϵ_{He} and the thickness of helium film is L_{He}.

---

[6] Of course, an accurate description is *above* and up to the top plate, and *below* and down to the bottom plate respectively. We shall avoid using this longer expression, but always imply it in the analysis of this section.

[7] The dielectric constant of vacuum is actually $\epsilon_0 \cdot 1$ but in eq. (3.14) ϵ_0 has been already drawn out as a common factor. In the same manner, the dielectric constant of liquid helium is $\epsilon_0 \epsilon_{He}$.

Insulating oxide layer: The surface of a metallic or semiconducting substrate, like silicon, always reacts with atmospheric oxygen and an oxide layer (rust) is grown on the surface of the substrate. Good substrate preparation reduces but does not diminish this layer, which in the case of SiO_2 has a thickness $L_{SiO_2} \approx 200\text{nm}$ and a dielectric constant $\epsilon_{SiO_2} = 4.5$.

Substrate: The substrate is made of silicon with a dielectric constant $\epsilon_{Si} = 11$, having a thickness of $L_{Si} = 0.5\text{mm}$.

For serially connected capacitors, the total inverse capacitance for TDES-bottom plate is the sum of the inverse component capacitances

$$\frac{1}{C} = \frac{1}{C_{vac}} + \frac{1}{C_{He}} + \frac{1}{C_{SiO_2}} + \frac{1}{C_{Si}}, \tag{3.15}$$

where the various subscripted Cs on the right hand side can be substituted according to eq. (3.13), respecting the fact that ϵ and L should also bear the appropriate subscript. C on the left-hand side is substituted without subscripts. Then, the quotient ϵ/L (or actually its inverse) is obtained,

$$\frac{L}{\epsilon} = L_{vac} + \frac{L_{He}}{\epsilon_{He}} + \frac{L_{SiO_2}}{\epsilon_{SiO_2}} + \frac{L_{Si}}{\epsilon_{Si}}. \tag{3.16}$$

Saturated electron density n_s can now be readily calculated from eq. (3.14), substituting ϵ/L from the previous equation. Notice that $L/\epsilon \approx L_{Si}/\epsilon_{Si}$, because the thickness L_{Si} of a substrate is normally several orders of magnitude greater than L_{He} and L_{SiO_2}.

3.5. The AC-technique

A major difficulty in the experimental study of TDES on liquid helium—in contrast to electron systems in heterostructures—is that it is impossible to measure their electric properties by making physical contact through wires or otherwise. Metallic electrodes in proper arrangement, placed under the part of the helium surface to be charged with electrons, are used instead. The electrode sides not facing the helium surface are connected with coaxial cables that lead outside the cryostat.

One of the electrodes (the *driving electrode*) is then set to an AC-voltage excitation and, as a consequence, the potential on the helium surface over the electrode alternates. This causes electrons to be alternatively drawn in and out of that part of the helium surface, and charge density fluctuations (an AC-current) develop on the electron sheet. A second electrode (the *pickup electrode*) responds to those fluctuations and collects the AC-current that flows through the electron system. In an effort to reduce the cross talk between driving and pickup electrodes, a third electrode is usually placed between them.

Obviously, the measuring process just described (AC-technique) depends critically on the alternating voltage excitation, because otherwise no charge fluctuations will be induced and the electron system will remain inert.

3.5.1. Signal detection with a lockin amplifier. A lockin amplifier was used in the experiments of this thesis as source and detector of AC-voltage or current excitations. As a source, the lockin amplifier delivers an AC-excitation with well defined amplitude, phase and frequency to the driving electrode, whereas as a detector it measures the AC-response at the *same* frequency (but eventually different amplitude and phase) from the pickup electrode.

In an ideal setting, any differences in the amplitude and phase of the response would have been caused exclusively from the TDES, and it is then only a matter of theoretical ingenuity to extract information about the state of the electron system.

The lockin amplifier can measure either the AC-voltage at the pickup electrode, or the AC-current that flows through the driving and pickup electrodes. There exist two modes of operation, affecting the way voltage (or current) is displayed and stored:

RTheta-Mode: The amplitude R and phase θ of the signal (current or voltage) $Re^{i\theta}$ is measured.

XY-Mode: The in-phase X and out-of-phase Y component of the signal (current or voltage) $X+iY$ is measured.

The difference between the two modes lies in the coordinate representation, which is polar in (R,θ)-mode and cartesian in the (X,Y)-mode, not in their information content. Therefore, these modes are completely equivalent and one can shift mode by means of the transformation equations

$$\begin{cases} X = R\cos\theta, \\ Y = R\sin\theta. \end{cases} \tag{3.17}$$

The lockin amplifier is characterized by an impedance Z_0 due to the resistance R_0 and capacitance C_0 of its internal circuitry. Impedance Z_0 depends also on the cyclic frequency ω of the AC-excitation and it is calculated from

$$Z_0 = \frac{R_0}{1+(\omega R_0 C_0)^2} + \frac{i}{\omega C_0}. \tag{3.18}$$

Ohm's law, applied for the measuring circuit of the lockin amplifier, states that

$$V_{ex} = IZ_0. \tag{3.19}$$

A current I flows through the bipolar element whose unknown impedance Z is to be measured. Ohm's law, applied for this element, states that

$$Y = \frac{I}{V}, \tag{3.20}$$

where Y is the admittance[8] of the element. By definition, admittance is written in terms of conductance G and capacitance C as

$$Y = G + i\omega C. \tag{3.21}$$

3.5.1.1. *Current mode.* Assume that the lockin amplifier is set in XY-mode, measuring the current $I = X + iY$. Then, the voltage in eq. (3.20) is actually the excitation voltage V_{ex} and by replacing Y with the right-hand side of eq. (3.21), one arrives at the expression

$$X + iY = V_{ex} G_x + i V_{ex} \omega C_x, \tag{3.22}$$

whereby the conductance G_x and capacitance C_x of the unknown bipolar element that is connected to the lockin amplifier are readily obtained as

$$G_x = \frac{X}{V_{ex}}, \quad \omega C_x = \frac{Y}{V_{ex}}. \tag{3.23}$$

It should be noticed that the resistance and capacitance of the lockin amplifier (R_0, C_0) do not enter into the expressions for G_x and C_x. This is due to the fact that one *common* current flows through the whole circuit, and this is the biggest advantage of operating the lockin amplifier in current mode instead of voltage mode.

3.5.1.2. *Voltage mode.* If the lockin measures voltage $V = X + iY$ instead of current, the electric current I is substituted from eq. (3.19) to eq. (3.20) to obtain

$$V = \frac{V_{ex}}{Z_0 Y}. \tag{3.24}$$

Replacing Z_0 and Y from eqs. (3.18) and (3.21) respectively into eq. (3.24) and after some algebra, one arrives at the expression

$$V = \underbrace{\left(\frac{V_{ex} R_0}{1 + (\omega R_0 C_0)^2} G_x - \frac{V_{ex}}{C_0} C_x \right)}_{X-\text{component}} + i \underbrace{\left(\frac{V_{ex}}{\omega C_0} G_x + \frac{\omega R_0 V_{ex}}{1 + (\omega R_0 C_0)^2} C_x \right)}_{Y-\text{component}}.$$

[8] Admittance is defined as the inverse of impedance and, likewise, conductance is the inverse of resistance.

A 2×2 system of equations results whose solution, in terms of the unknown conductance G_x and capacitance C_x, is

$$G_x = \frac{\omega C_0\left(1+(\omega R_0 C_0)^2\right)}{V_{ex}\left(1+3(\omega R_0 C_0)^2+(\omega R_0 C_0)^4\right)}\left(Y+\omega R_0 C_0 X+(\omega R_0 C_0)^2 Y\right), \tag{3.25a}$$

$$\omega C_x = \frac{-\omega C_0\left(1+(\omega R_0 C_0)^2\right)}{V_{ex}\left(1+3(\omega R_0 C_0)^2+(\omega R_0 C_0)^4\right)}\left(X-\omega R_0 C_0 Y+(\omega R_0 C_0)^2 X\right). \tag{3.25b}$$

The resulting expressions in the case where the lockin amplifier measures voltage, eqs. (3.25a) and (3.25b), are clearly much more complicated than the corresponding expression for current, eq. (3.23), to the extent that one wonders why would someone want to set the lockin amplifier in voltage mode.

An answer is that many older lockin amplifiers do not come with the facility for current measurement. This is the case for the models EG&G-5510 and Ithaco-5219, which were used in some of our experiments.

However, the most important reason is that normally a *coupling circuit* is used for measuring the conductance of a TDES. In this case, the resulting expressions for the admittance and capacitance are of comparable complexity both for the current and for the voltage mode and the advantage of current mode is lost (see section 3.5.3).

3.5.2. Electrode geometries. A simple electrode geometry that was used already since the earliest transport measurements [**101**] is the rectangular or Sommer-Tanner arrangement, show in fig. 3.7B. It comprises of three consecutive rectangular electrodes and it proves advantageous in localization experiments, because a preferred direction of current flow from driving to pickup electrode can immediately be defined. On the other hand, a preferred direction also implies a lack of symmetry, a fact that complicates the analysis significantly and is the main disadvantage of this arrangement.

A highly symmetrical electrode geometry is the Corbino arrangement (fig. 3.7A), where the electrodes are three concentric rings. The azimuthal symmetry is valuable when a magnetic field is present and it reduces the complexity of data analysis. Corbino geometry is used extensively in experiments on weak electron localization and for studying the properties of edge magnetoplasmons (see the relevant chapters in [**10**].

3.5.3. Coupling circuit. The application of a holding field that would push the electrons toward the helium surface is imperative in experiments. Such a field can be produced either by applying a negative DC-voltage on the top plate, while keeping the bottom plate grounded, or by applying a positive DC-voltage

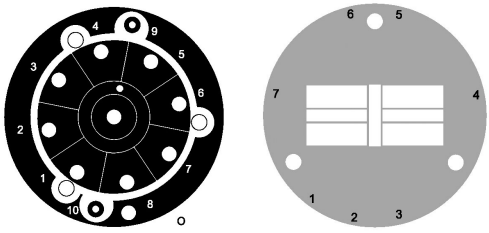

(A) Corbino (B) Sommer-Tanner

FIGURE 3.7. Sketch of a Corbino-type (A) and Sommer-Tanner-type (B) electrode geometries. White circles indicate conducting contact areas, where cables can be soldered. In (A), the outer ring is divided into 8 independent subelectrodes. In (B), the driving and response electrodes are divided into 3 independent subelectrodes. This is done for better flexibility in measurements.

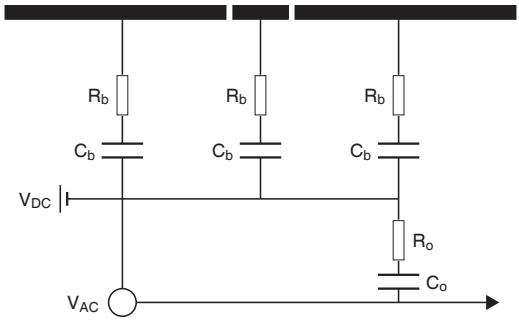

FIGURE 3.8. Sketch of the three electrodes (top), the coupling circuit and the lockin amplifier. The coupling circuit consists of three resistors (R_b) and three capacitors (C_b), connected to a voltage source that sets the electrodes on a positive offset DC-voltage V_{DC}. The AC-voltage excitation V_{AC} of the lockin amplifier is superimposed on V_{DC} without being affected thereby.

on the bottom plate, keeping the top plate grounded. It proves experimentally convenient to use the second possibility.

However, the bottom plate is also used for the application and detection of an AC-voltage excitation via the lockin amplifier. A proper electric circuit must then be designed that would allow an AC-excitation voltage to pass through the electrodes and at the same time set its offset from the ground of the lockin amplifier. A circuit with that function is depicted in fig. 3.8 and it will be referred in the following as the "coupling circuit".

Each of the three electrodes (or, for that matter, the coaxial cables that lead to them) is connected with a resistor R_b. The free ends of the resistors are joined together. An offset DC-voltage can thereby be created, if the active pole of a bipolar voltage source is connected to the resistors' common end (the neutral pole must be at the same ground with the lockin).

Moreover, each electrode is connected with a capacitor C_b. The free end of the capacitor on the response electrode is plugged in the excitation output of the lockin amplifier, whereas the respective capacitor of the detecting electrode will ultimately lead to one of the lockin channels. Since capacitors are interrupts in DC-voltage or current, the AC- and DC- components do not interfere with each other and only the AC-component will be measured by the lockin amplifier.

If the helium surface is not yet charged with electrons, AC-current will pass through a $(C_b - 2R_b - C_b)$ circuit and it will be measured as background current. Ideally, this current should be zero, or much smaller than the current expected to flow though surface electrons, because otherwise a weak electron signal might not be accurately resolved or even distinguished.

The demand of a background current close to zero must mean a very high impedance of the open coupling circuit that, in turn, suggests a high resistance R_b and a low capacitance C_b. Resistance R_b and capacitance C_b should be also higher than the resistance R_e and capacitance C_e of the electron layer, usually of the order of $10^8\,\Omega$ and 10^{-13}F respectively.

Following a procedure completely analogous to the procedure that led into eq. (3.23), it is found out that in the presence of a coupling circuit the conductance G_x and the capacitance C_x of a TDES will be given by

$$G_x = (\omega C_b)^2 \frac{V_{ex}X - R_b X^2 - R_b Y^2}{(V_{ex}\omega C_b - \omega R_b C_b X - Y)^2 + (X - \omega R_b C_b Y)^2}, \tag{3.26a}$$

$$\omega C_x = \omega^2 C_b \frac{V_{ex}\omega C_b Y - X^2 - Y^2}{(V_{ex}\omega C_b - \omega R_b C_b X - Y)^2 + (X - \omega R_b C_b Y)^2}. \tag{3.26b}$$

In voltage mode, the expressions for G_x and C_x in the presence of coupling circuit, are derived from the respective expressions eq. (3.25a) and eq. (3.25b), by making the substitutions

$$R \longrightarrow R_0 + R_b, \quad \frac{1}{C} \longrightarrow \frac{1}{C_0} + \frac{2}{C_b} \tag{3.27}$$

It should be noticed that the simplicity of the current mode expressions for G_x and C_x, exhibited in eq. (3.23), disappears when a coupling circuit is present. Therefore, a coupling circuit makes both modes of operation similarly complex for the purposes of data analysis.

3.5.4. Temporal resolution. The time constant $\tau_e = R_e C_e$ of TDES on liquid helium is expected to be about 10^{-5}s, a time that can be seen as the maximum temporal resolution of the system. Phenomena that last less than

some τ_e cannot be observed by measurements of R_e or C_e, being therefore even in principle inaccessible for experiments of this kind.

Ultimately, it will be the time constant $\tau = RC$ of the employed coupling circuit that will determine the experimental temporal resolution. Earlier, the conditions $R \gg R_e$ and $C \ll C_e$ were imposed and this, in turn, means that the coupling circuit's time constant τ will be generally greater than τ_e. The time constant of the lockin amplifier should reflect these considerations and be set at a value higher than, or comparable with τ.

3.6. Dynamics of a TDES under an AC-excitation

In section 3.5.1, beginning from macroscopically measurable quantities, formulas were derived that provide the conductance G_x and the capacitance C_x of TDES on liquid helium. Here, beginning from the microscopic properties of TDES, models are developed that relate the basic transport properties of TDES on liquid helium with the G_x and C_x.

There are two ways to model a TDES and their degree of sophistication varies according to application and accuracy demands. In the *equivalent circuit model* the TDES is emulated by an equivalent RC (seldom, also RCL) circuit. This elementary approach fails to provide intrinsic properties of the TDES (e.g. its conductivity), because it completely ignores the geometrical features of the TDES. In the *transmission line model* things are improved, because the distributed character and the particular geometry of a TDES are taken into account. The conductivity and all related transport properties can then be determined.

Both models were used in early mobility measurements of two-dimensional electrons on bulk liquid helium performed by *Sommer et al.* [**101**]. Even for the favorable environment that bulk liquid helium presents for transport measurements, a difference of approximately 14% resulted for the calculated electron mobilities. The equivalent circuit model is developed in section 3.6.1, following the remarks of *Sommer et al.* [**101**].

Mehrotra et al. [**79**] sketch briefly a general transmission line model, in their effort to calculate electron mobility in conditions of intense electron-ripplon scattering on bulk liquid helium. An extensive analysis, however, is provided by *Lea et al.* [**71**] and *Mehrotra et al.* [**78**] from a slightly different perspective, as *Lea et al.* [**71**] derive a formula for the total current that flows through a TDES (ideal for current measurements), whereas *Mehrotra et al.* [**78**] are interested in the total admittance of a TDES (more suitable for voltage measurements). The physically more illuminating derivation of *Lea et al.* [**71**] will be followed in section 3.6.2.

3.6.1. Equivalent circuit model. The part of the electron sheet above the driving or the response electrode, together with the electrode itself, can be thought of as the two plates of a plane capacitor filled partially with a weak

dielectric (liquid helium) and having a certain capacitance. Accordingly, the electron sheet above the middle electrode can be considered an insulator with a certain resistance.

The electric properties of a TDES above helium can thus be simulated by an equivalent circuit (*C-R-C*) of two capacitors connected in series with a resistor. After an elementary circuit analysis, the impedance Z and admittance Y of the TDES equivalent circuit are found to be

$$Z = R - \frac{2i}{\omega C} \implies \quad Y = \frac{(\omega C)^2 R}{4 + (\omega RC)^2} + i\frac{2\omega C}{4 + (\omega RC)^2}. \tag{3.28}$$

From the definition of admittance in eq. (3.21), the conductance G_x and capacitance C_x of the TDES, as a function of the resistance R and capacitance C of the TDES equivalent circuit will be

$$G_x = \frac{\omega^2 RC^2}{4 + (\omega RC)^2}, \quad \omega C_x = \frac{2\omega C}{4 + (\omega RC)^2}. \tag{3.29}$$

These expressions form a 2×2 system of equations that can be solved with respect to the unknowns R and C, finding out that

$$R = \frac{G_x}{G_x^2 + (\omega C_x)^2}, \quad \omega C = \frac{2\left(G_x^2 + (\omega C_x)^2\right)}{\omega C_x}. \tag{3.30}$$

If the lockin amplifier operates in XY-mode and measures current, the conductance G_x and capacitance C_x, are given by eq. (3.23). A substitution in eq. (3.30) leads to the following expressions for the resistance and capacitance of the TDES as a function of measured quantities (X, Y) and the experimentally controlled parameters V_{ex} and ω:

$$R(X,Y) = \frac{X}{X^2 + Y^2} V_{ex}, \quad C(X,Y) = \frac{X^2 + Y^2}{Y} \frac{1}{\omega V_{ex}}. \tag{3.31}$$

Similar but more complicated formulas hold when voltage is measured, whereby the conductance G_x and capacitance C_x are substituted from eqs. (3.25a)-(3.25b) respectively. The extent of algebraic expressions is somewhat reduced by setting $\xi = \omega R_0 C_0$, to finally obtain

$$R(X,Y) = \frac{V_{ex}}{\omega C_0} \frac{\left(\xi^2 Y + \xi X + Y\right)\left(1 + 3\xi^2 + \xi^4\right)}{1 + \xi^2} \times \left(\left(1 - 2\xi + 4\xi^2 - 2\xi^3 + \xi^4\right) X^2 + 2\xi\left(1 + \xi^2\right) XY + \left(1 + \xi^2\right)^2 Y^2 \right), \tag{3.32a}$$

$$C(X,Y) = \frac{2C_0}{V_{ex}} \frac{1+\xi^2}{1-\xi+4\xi^2-3\xi^3+4\xi^4-\xi^5+\xi^6} \times \frac{\left(\xi^4-2\xi^3+4\xi^2-2\xi+1\right)X^2+2\xi\left(1+\xi^2\right)XY+\left(1+\xi^2\right)^2Y^2}{X}. \quad (3.32b)$$

Usually, more important are physical quantities that are independent of the geometrical details (like shape and size) of a system, as for example the resistivity ρ or the conductivity $\sigma = 1/\rho$. The effects of geometry cannot be deduced solely by the model and as a consequence the resistivity will be $\rho = \kappa R$, where κ is an unknown geometrical factor. In the simpler case of a metal conductor the geometrical factor is of course $\kappa = l/s$, where l is its length and s its cross section.

3.6.2. Transmission line model. The physical picture used to justify the equivalent circuit model is oversimplified, because it was not clearly explained why the resistance and capacitance were assumed to be lumped above each electrode. A more accurate way for modeling the electron gas would be to consider it a two-dimensional transmission line with distributed capacitance and resistance, since every section of the electron layer exhibits to a greater or lesser extent a mixed capacitive-resistive character.

If current density is denoted by $\mathbf{j}$, the potential distribution in the area of the TDES by v and the conductivity by σ, these three quantities according to electromagnetic theory are interrelated by

$$\mathbf{j} = \sigma \nabla v. \quad (3.33)$$

Substituting $\mathbf{j}$ from eq. (3.33) into the continuity equation

$$\nabla \cdot \mathbf{j} = -\frac{\partial q}{\partial t}, \quad (3.34)$$

the differential equation

$$\nabla^2 v(x,y,t) = -\rho \frac{\partial}{\partial t} q(x,y,t) \quad (3.35)$$

is obtained, where $\rho = 1/\sigma$. This differential equation determines the potential distribution $v(x,y,t)$, if the charge density $q(x,y,t)$ is known.

The driving voltage is of the form $V_{ex}e^{i\omega t}$ and it is expected that this harmonic time evolution will be retained (accompanied perhaps by a phase shift ϕ) by the potential distribution. This observation allows the separation of time evolution from the spatial potential distribution $u(x,y)$ and limits the range of possible $v(x,y,t)$ to functions of the form

$$v(x,y,t) = u(x,y)e^{i(\omega t+\phi)}. \quad (3.36)$$

Assuming that saturated electron density has been reached, so that electrons completely screen the holding field, the capacitance C per unit area of the idealized electron layer-electrode plane capacitor will be given by the right-hand side of eq. (3.13) divided by the area A.

By definition, it is $q = Cv$ whence, after replacing $v = q/C$ into eq. (3.36), differentiating the resulting expression with respect to time and substituting the derivative into the continuity equation (3.34), one finally arrives at

$$\frac{\partial}{\partial t} q(x,y,t) = i\omega C u(x,y) e^{i(\omega t+\phi)} \Longrightarrow \tag{3.37}$$

$$\nabla^2 u(x,y) = -i\omega C \rho u(x,y). \tag{3.38}$$

In the absence of a magnetic field, charge motion along y-direction will not take place, meaning that the potential there remains constant. The dimensionality of the problem is thus further reduced to one-dimensional. One is led in this case at the harmonic oscillator differential equation

$$u''(x) + i\frac{\omega C}{\sigma} u(x) = 0, \tag{3.39}$$

whose general solution is given by

$$u(x) = K_1 \exp\left((1+i)\frac{x}{\delta}\right) + K_2 \exp\left(-(1+i)\frac{x}{\delta}\right), \tag{3.40}$$

where $\delta = (2\sigma/\omega C)^{1/2}$. The *skin depth* δ is a measure of the damping experienced by an electric field wave (a charge density fluctuation) as it propagates through the electron sheet. As seen by its definition in eq. (3.40) and the form of differential equation (3.39), the role of skin depth is analogous to that of the spring constant (in mechanical oscillations) or the time constant (in electrical oscillations).

In the presence of magnetic field, charge motion takes place in both directions. The general solution for each direction will preserve the form of eq. (3.40). Moreover, it should be kept in mind that the use of a rectangular electrode geometry means that net charge fluctuations along only one direction are measurable. If a homogeneous constant magnetic field with nonzero component along the z-direction is applied, electrons describe circular orbits, but the net oscillation of the centers of circular orbits that excitation voltage induces will be only along one direction (which could be arbitrarily taken to be the x-direction).

In order to fully determine the potential distribution $v(x,y)$, suitable boundary conditions have to be imposed. *Lea et al.* [**71**] demand that current must not flow beyond the perimeter of the electrodes. Assuming that there are three electrodes, extending $\mathfrak{L}$ length units along the x-direction and $\mathfrak{W}$ length units along y-direction in total, and that both driving and response electrodes have the same length l, the boundary conditions read

$$\nabla v(0,y) = \nabla v(\mathfrak{L},y) = 0. \tag{3.41}$$

From the boundary conditions and after integrating on the whole electrode area, *Lea et al.* [**71**] derive the expression for the total current I_{ac},

$$I_{ac} = \sigma \iint dx\,dy\ \nabla v(x,y) \Longrightarrow \tag{3.42}$$

$$I_{ac} = (1+i)V_{ex}\frac{\omega C}{2}\mathfrak{W}\delta\frac{\sinh\big((1+i)l/\delta\big)^2}{\sinh\big((1+i)\mathfrak{L}/\delta\big)}. \tag{3.43}$$

The total current I_{ac} is a complex number and eq. (3.42) will eventually break up to one equation for the real part and another one for the imaginary part. From the fact that in the end two equations are obtained for essentially one unknown (the conductivity σ, enclosed in δ), one might argue that an unnatural redundancy of the experimental data appears, for it seems that only the real or, equivalently, the imaginary component of the total current suffice to determine the conductivity. However, this is not true, because equations that contain transcendental functions (like hyperbolic sines) accept generally more than one root as a solution and, in order to find the single conductivity compatible with experimental data, both equations must be taken into account.

A somehow unfortunate feature of eq. (3.42) is that its output are experimental data computed out of conductivity values as input, while our requirement would be an inverted formula that would evaluate conductivity out of experimental data. But conductivity is buried inside the hyperbolic sines, the equation cannot be inverted and an analytic expression for conductivity as a function of the current amplitude I_{ac} and phase ϕ, as in the equivalent circuit model, does not exist. Equation (3.42) can be solved only numerically for σ and a correct procedure for determining the conductivity must address several subtleties that might otherwise lead to false results.

The same behavior is exhibited by the expression for the admittance Y that *Mehrotra et al.* [**78**] derive. These authors consider a configuration with three electrodes, where the i-th electrode has a length l_i, finding out that

$$Y = \frac{1}{(1+\xi)^2}\left(\frac{i\omega C}{R+i\omega L}\right)^{1/2}\frac{\sinh(\gamma l_1)\sinh(\gamma l_3)}{\sinh\big(\gamma(l_1+l_2+l_3)\big)}, \tag{3.44}$$

where

$$\gamma = \sqrt{i\omega RC - \omega^2 LC}. \tag{3.45}$$

A commonly used limit is to consider a thin substrate, whereby the ratio ξ, of the capacitance between the electron sheet and the top plate to the capacitance between the electron sheet and the electrodes, tends to zero. Moreover, freely moving electrons of a TDES make the inductance per unit length (L) negligible.

After these approximations have been made, the admittance depends only on the resistance R per unit length and the capacitance C per unit length. In conditions of saturated electron density, C will be given by the right-hand side of eq. (3.13) divided by the total electrode length. Again, as in eq. (3.42) for the

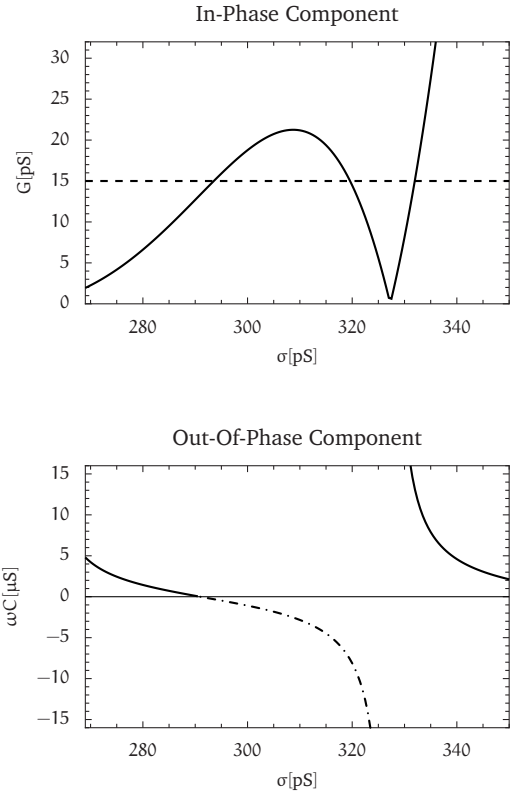

FIGURE 3.9. The in-phase component (G) and out-of-phase component (ωC) as calculated from eq. (3.42) for excitation frequency $f_{ex} = 65\text{kHz}$, excitation voltage $V_{ex} = 10\text{mV}$, total electrode length $\mathfrak{L} = 10\text{mm}$, electrode width $\mathfrak{W} = 10\text{mm}$ and a common length $\mathfrak{l} = 4\text{mm}$ for the driving and response electrodes. There exists a forbidden range of conductivities, where $\omega C < 0$ (dot-dashed curve). The ambiguity with respect to the three σ compatible with a single value of G (dashed line) is thus resolved. Notice that ωC is six orders of magnitude greater than G, justifying the term "capacitive coupling" of TDES with the electrodes.

total current, two equations (one for the real part and one for the imaginary part of Y) are obtained for only one unknown, the resistance R per unit length.

In contrast to the expression of *Lea et al.* [**71**], an extrinsic property of the TDES—namely, the resistance or conductance—is calculated from eq. (3.44). For this reason, *Mehrotra et al.* [**78**] term Y the *equivalent* admittance, and their model can be seen as a blend of the primitive equivalent circuit model with the more accurate transmission line model. Therefore, the analysis of experimental data presented in this thesis relied on eq. (3.42) exclusively.

As a first step for the analysis, one could plot the real and imaginary part of the right-hand side of eq. (3.42) within a plausible range of σ. The experimentally measured real or imaginary current component will then correspond to a straight line parallel to the conductivity axis, while the point where the experimental line intersects with the theoretical curve will provide the conductivity.

In fig. 3.9, the real (in-phase component) and imaginary (out-of-phase component) parts of the total current are depicted against conductivity, for the parameter values encountered in the measurement depicted in fig. 3.10.

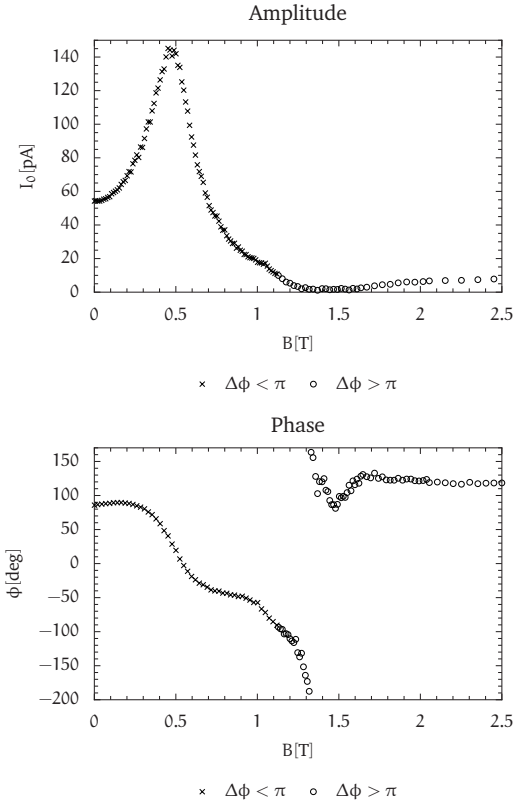

FIGURE 3.10. Measured AC-current amplitude (I_0) and phase (ϕ) plotted against the magnetic field (B) at T = 1.09K in conditions of saturated electron density $n_s = 1.47 \times 10^{14} m^{-2}$ on the nanotower structure (depicted in fig. 4.1). Bulk helium surface lies 0.5mm below the TDES. The other parameters are as in fig. 3.9. Notice the very strong phase change. The circle-point part of the phase curve and the discontinuity at B ≈ 1.34T indicate that $\Delta\phi > 180°$.

The dashed line in the upper plot of fig. 3.9 indicates that three potential conductivity values are compatible with the measured value G = 15pS of the in-phase component. This unnatural multiplicity of conductivity values is resolved, when the out-of-phase component ωC for the same parameter values, depicted in the bottom plot of fig. 3.9, is considered. Two candidate conductivity values can then be rejected, on the physical grounds that they result in a negative ($\omega C < 0$) out-of-phase component. A unique conductivity value is compatible with both measured components, as one would demand from a correct physical model.

3.6.3. From the transmission line to the equivalent circuit model. The analysis so far has demonstrated that the transmission line model is more accurate in capturing the physical properties of electrons on helium, because it takes into account the electrode dimension and the distributed capacitive-resistive nature of the system. On the other hand, the equivalent circuit model is much simpler and its numerical application would have been preferable, if it could be ascertained that the results would not be far from reality. Thus, it is useful to

derive the equivalent circuit from the transmission line model and illuminate the conditions for which such a derivation is possible, that is, when could TDES be approximated as a system with lumped capacitance and resistance.

Starting point of the derivation is the right-hand side of eq. (3.42), which is expanded in a Taylor series with respect to $1/\delta$, keeping terms up to order $O(1/\delta)^4$. A much simpler approximate expression for the total current I_{ac} emerges,

$$I_{ac} \approx V_{ex}\omega C l^2 \frac{\mathfrak{W}}{\mathfrak{L}} \left(i + \frac{1}{3\delta^2}(\mathfrak{L}^2 - 2l^2) \right) \tag{3.46}$$

The approximation will hold true for large skin depths δ, or equivalently for $\omega C\rho \ll 1$. This is the condition that must be met for the electron system to be considered lumped, fulfilled for a weak capacitive coupling (small ωC) and an environment of bulk liquid helium in low temperatures (small ρ).

If the measured AC-current is written as $I_{ac} = X + iY$, it immediately follows by solving equation eq. (3.46) for $\rho = 1/\sigma$ that

$$\rho \approx \frac{6\mathfrak{W}l^2}{(\mathfrak{L}^2 - 2l^2)\mathfrak{L}} \frac{X}{Y^2} V_{ex} \tag{3.47}$$

This expression for ρ is almost identical to eq. (3.31), which gives the resistance in the context of the equivalent circuit model. It has the added advantage that the geometrical factor κ is explicitly given in terms of the total electrode width $\mathfrak{W}$ and length $\mathfrak{L}$ as well as the length l of the driving electrode (assumed to be equal to the response electrode). Equation (3.47) will become identical with the first equation of (3.31) when $X^2 + Y^2 \approx Y^2$, that is, when the dissipative (resistive) character of the system is weak compared to its capacitive character.

CHAPTER 4

Theory of Quasi Zero-Dimensional Localization

4.1. Periodic surfaces for quasi zero-dimensional localization

A substrate surface that is not flat, but instead exhibits ridges and troughs, will constrain a sufficiently thin liquid helium film to follow its morphology. Consequently, the surface of the helium film will not be flat and it is not immediately obvious whether electron potential will retain the simple form of eq. (1.2), which was derived for the flat surface of bulk liquid helium.

Topologically, there will always exist a properly small scale where a globally curved surface can be considered flat[1]. Then, the electron potential of eq. (1.2) will remain valid for areas small enough—with respect to the global curvature of the film surface—to be regarded as locally flat. If one imagines all these locally flat surfaces joined together, one finds that transverse electron motion remains quantized and lateral electron motion free as for the surface of bulk liquid helium. The mean distance from the film surface of the various quantum states must be constant throughout and equal to the respective distance for bulk liquid helium. This means that the global, lateral motion of electrons should follow the curvature of the helium film, which in turn is determined from the morphology of the substrate.

The free lateral electron motion on structured substrates will be constrained in practice due to substrate roughness. Indeed, the helium film should be in principle thicker in troughs and thinner on ridges (detailed film profiles are derived in section 4.2), meaning that electron breakthrough and the associated pinning of electrons on ridges is more likely. Nevertheless, it should be kept in mind that for a sufficiently thick film on the ridges of a perfectly fabricated structured substrate, there is absolutely no reason to expect that electron motion is constrained due to the ridges, because, in a sense, electrons are able to 'surf' the curved helium film surface.

Unconstrained electron motion on curved helium films takes place in the absence of external fields. If TDES are subject to external fields, like a holding

[1]It took some centuries for humans to realize the truth of this 'simple' statement for the planet they inhabit.

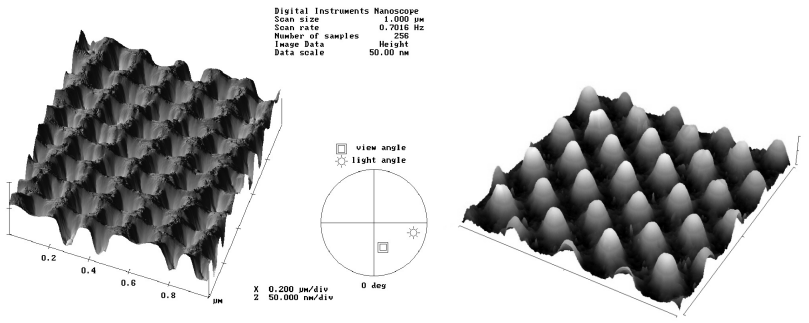

(A) Nanohole structure (B) Nanotower structure

FIGURE 4.1. AFM-images of periodic structures suitable for quasi zero-dimensional localization of TDES on liquid helium. The nanohole structure shown in (A) exhibits troughs 50nm deep and 100nm wide, while the nanotower structure shown in (B) exhibits ridges 100nm high, 600nm apart. Topologically, these two periodic structures are distinguished from the fact that the nanotower has isolated areas of higher elevation (ridges), while the nanohole has isolated areas of lower elevation (troughs). Both structures were fabricated at PAUL SCHERRER INSTITUTE (Switzerland), by means of nanolithography on the surface of a square silicon substrate 0.5mm thick and 1cm wide.

field $E_\perp$ and a magnetic field $\mathbf{B} = (0, 0, B)$, electron motion in the x- and y-direction will be affected (see sections 4.4 and 4.5), although these fields have *no* components in coordinates x and y.

The fact that $E_\perp$ and B have no x and y components means that their influence is apparent only for an external observer who has the privilege of an extra dimension, not for electrons themselves. A partial analogy can be drawn with gravitation as arising from the curvature of spacetime, a proposal made in the context of general relativity theory. Indeed, the dynamic properties of TDES, with the exception of Coulomb interactions, are modified not due to intrinsic interactions within the domain where electrons move, but due to the combined extrinsic effects caused by the presence of external fields, namely, curvature (due to the electric field) and anisotropy (due to the magnetic field).

The need for periodic structures at the mesoscopic scale arises naturally, if one examines the physical parameters that influence the localization process. A promising procedure for electron localization appears to be the use of a magnetic field along the z-direction, whereby "localization" means that electrons occupy at most the area of a circular disk with (cyclotron) radius that can be made extremely small. This area will be of course $\mathfrak{A} = \pi r_c^2$, where r_c denotes the cyclotron radius; from the definition of cyclotron radius, eq. (2.13), one obtains

the following useful numerical estimates for $\mathfrak{A}$ and r_c:

$$\mathfrak{A} = 6154\frac{T}{B^2} \quad [nm^2], \quad r_c = 31.29\frac{\sqrt{T}}{B} \quad [nm]. \tag{4.1}$$

Experiments with TDES on liquid helium usually take place in the temperature range from 0.1K to 1.6K, whereas magnetic fields above 10T are not easy to generate. The experimental apparatus at hand could generate magnetic fields up to 7T nominally, but it was felt that this maximum should be lowered to 3T as a safety precaution against a possible quench. Hence, it is seen from eq. (4.1) that localization radii will be some tens of nanometers, and the design of periodic surfaces at the mesoscopic scale (cf. fig. 4.1) reflects that fact.

The design of periodic surfaces should be guided by a tradeoff between the need for a small trough radius on one hand, and the need for a large helium film depression in the troughs on the other hand. Periodic surfaces with small trough radii are usable only when they are wet by very thin helium films, which prove difficult to work with and are prone to electron breakthrough. For example, electron localization on the nanohole structure (trough radius 100nm) obviously cannot be expected for helium film thickness near, or above 100nm. However, a helium film thickness around 65nm, while already somewhat thick for the nanohole structure, was found to be acceptable for the nanotower structure (trough radius 400nm). For this reason, experimental results on electron localization are reported for the nanotower structure exclusively.

4.2. Profile of a deformed liquid helium film

The thickness of a liquid helium film on a periodically structured substrate is determined from the capillary action of bulk liquid helium whose surface lies at a specified level below the substrate. In order to follow the morphology of the periodic surface, the film must be thin enough. Clearly, knowledge of the film profile beyond the qualitative level is needed, as this (and the magnitude of the magnetic field) is the most critical factor that affects electron localization. The physics of capillary phenomena are covered in the classic *Landau and Lifshitz* [**67**], pp. 38-250.

An important distinction can be drawn between the nanohole and the nanotower structure, with respect to the dynamics of capillary action before the film reaches equilibrium.

The lower elevations of the nanotower structure are not isolated, and capillary action can proceed from lower elevations up to the ridges, until a suspended helium film is formed.

Observe that this is not the case for the nanohole structure, as the troughs (areas of low elevation) are now isolated from each other, so that wetting proceeds from areas of higher elevation to those of lower elevation. Even with an initially very thin film of uniform thickness everywhere on the surface of the

nanohole structure, liquid helium will be constantly flowing inside the troughs and accumulate in there, as this is energetically favorable. Ultimately, a thick film will be formed in the troughs, which could almost cover them completely. Deep troughs would not alter the situation; they would just delay the inevitable, because the decisive point is that the equilibrium wants the troughs filled up to the top with liquid helium. A concave helium film profile in the area of the troughs, if it exists at all, would depend more on the area of a trough than on its depth.

An upper bound can be calculated for the time t it would take for a trough to be completely filled up with liquid helium. For this purpose, estimates for the flow speed v of liquid helium, the volume of the troughs $\mathfrak{V}$, and the film thickness d_{top} on the ridges are needed. Superfluid liquid helium moves along surfaces with a speed that is experimentally found to be around $v = 30\text{m/s}$ (the theoretical upper bound is the roton critical speed $v_c = 60\text{m/s}$). An overestimate of the volume of a trough in the nanohole structure is $\mathfrak{V} = 2\delta_0 b^2$, if the trough is assumed, for simplicity, to be a square prism with base side $b = 100\text{nm}$ and height $2\delta_0 = 50\text{nm}$. The volume of liquid helium, falling in the trough from each one of its four sides after time t, will be simply $(vt)d_{top}b$, and the trough will have been filled up with liquid helium after

$$4d_{top}vtb = 2\delta_0 b^2 \Longrightarrow \quad t = \frac{b\delta_0}{2d_{top}v} \approx 17\text{ns}, \tag{4.2}$$

if the thinnest theoretically possible film, whose thickness is $d_{top} = 5\text{nm}$, is assumed to wet the ridges[2]. Of course, thicker films decrease the filling time even further. Even a rough overestimation of the filling time shows that the troughs of the nanohole structure get filled with liquid helium almost instantly, and more generally that the wetting equilibrium[3] for superfluid liquid helium is reached very quickly.

4.2.1. Uncharged liquid helium film. If the profile of the liquid helium surface is denoted with $d(x)$, its shape in equilibrium will be determined from the Young-Laplace equation, which in this context takes the form

$$\sigma_{He}\frac{d''(x)}{(1+d'(x)^2)^{3/2}} = \rho_{He}gh + \left(\rho_{He}gd(x) - \frac{C_3}{d(x)^3}\right). \tag{4.3}$$

Parameters that appear in this equation are the surface tension $\sigma_{He} = 3.75\times10^{-4}\text{J/m}^2$ (the numerical value is taken from the experiment of *Vicente et al.* [**111**]) and density $\rho_{He} = 134\text{kg/m}^3$ of liquid helium, and the van der Waals constant $C_3 = 3.59\times10^{-22}\text{J}$. The van der Waals constant is a measure of the

[2]Superfluidity is destroyed for films thinner than 5nm and wetting would not proceed in this case.

[3]By this it is meant that no large scale motion of the liquid takes place, so that its macroscopic kinetic energy is zero.

strength of the interaction between liquid helium and the silicon substrate. The necessity for the particular form of Young-Laplace equation can be motivated from an interpretation of its individual terms.

- $d''(x)/\left(1+d'(x)^2\right)^{3/2}$ has dimensions of inverse length, expressing the curvature of the surface with profile $d(x)$. This term can be thus set equal to $1/R$, where R denotes the radius of curvature.
- $\rho_{He} g h$ is the gravitational potential energy density [J m^{-3}] of a liquid helium layer at a height h above the surface of bulk liquid helium. Here, it is reminded that the surface of bulk helium lies below the substrate and the helium film on the substrate is formed by a wetting process, whereby liquid helium creeps over any free surface. If, as is natural, the surface of bulk liquid helium is selected as the zero of gravitational potential energy, any level higher than that has a positive potential energy.
- $\rho_{He} g d(x)$ is the gravitational potential energy density of a liquid helium layer placed at the top of a helium film with thickness $d(x)$. Equivalently, this term gives the gravitational potential energy density of a helium film with thickness $d(x)$.
- $C_3/d(x)^3$ is the potential energy density due to van der Waals interaction between a liquid helium layer and the substrate at a distance $d(x)$ apart. An equivalent formulation is that this term gives the van der Waals potential energy density between the substrate and a helium film with thickness $d(x)$.

Therefore, Young-Laplace equation is nothing more than an application of the energy conservation principle, as the net surplus or deficit of the potential energy densities in the right-hand side—being generally nonzero except for the case of a plane surface—is set equal to the energy density due to the deformation of the surface[4].

Although the focus was more on the liquid helium film that wets the substrate, Young-Laplace equation is valid everywhere along the surface of a simply connected body of liquid. Obviously, the sum of all potential energy densities for the bulk liquid is zero and this must also be the case for films formed by the same body of liquid, for otherwise energy was created or lost. If, therefore, the sum of potential energy densities for a film is nonzero, the film deforms accordingly so that its total potential energy density becomes zero as in bulk liquid.

By convention, the starting point of the radius of curvature is taken outside the liquid, with the effect that a surface with a concave profile ($d''(x) > 0$) is associated with positive energy, while a convex profile ($d''(x) < 0$) is associated with negative energy.

[4]The physical dimension of surface tension is [J m^{-2}], and as a consequence σ_{He}/R is an energy density, which can be rightly called "deformation energy density".

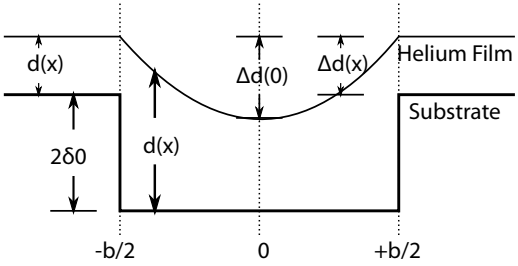

FIGURE 4.2. Schematic profile of the "nanotower" substrate and a charged liquid helium film, which exhibits a parabolic depression in the area of the trough. Symbols are defined in the text.

A natural length l_{He} is implicit in the Young-Laplace equation, in the sense that capillary effects dominate for length scales smaller than l_{He} and conversely; this length is known as the *capillary length* and for liquid helium it is equal to

$$l_{He} = \sqrt{\frac{\sigma_{He}}{\rho_{He} g}} \approx 0.534\text{mm}. \tag{4.4}$$

It might be easier to derive the signs with which the various potential energy densities enter into the right-hand side of Young-Laplace equation, by thinking in terms of the work bulk liquid helium expends upon the formation of a film on the substrate (work expended and potential energy acquired have opposite signs).

Each liquid helium layer must be lifted above the surface of bulk liquid helium with an energy cost of $-\rho_{He} g h$, and then be piled up on the already existing layers with an associated energy cost of $-\rho_{He} g d(x)$. After a certain thickness, any additional layers placed at the top of the film would squeeze out layers at the bottom due to their weight, unless the substrate—via van der Waals attraction—stabilizes the lower layers, by expending a work $-C_3/d(x)^3$. For liquid helium, the work expended by the substrate provides a relief equal to $+C_3/d(x)^3$.

The profile $\delta(x)$ of a periodically structured substrate can be modelled by setting a mean height h, as in equation

$$\delta(x) = \begin{cases} h + \delta_0 & 0 \leqslant x \leqslant a, \\ h - \delta_0 & a < x < a + b. \end{cases} \tag{4.5}$$

Ridges deviate from h by an amount $+\delta_0$ upwards and troughs by an amount $-\delta_0$ downwards. Ridges and troughs are allowed different extents a and b horizontally, so that the period is equal to $a + b$ (see fig. 4.2).

Young-Laplace equation is highly nonlinear; for this reason, the film profile is almost always determined after appropriate simplifications. For $0 \leqslant x \leqslant a$, the helium film is formed $h + \delta_0$ above bulk helium surface and the planar surface leads to a plane helium film profile with constant thickness d_{top}, whence $d''(x) = 0$, meaning that the left-hand side of Young-Laplace equation is equal to zero. By definition, the thickness of a film is extremely small, with the effect

that the van der Waals term C_3/d_{top}^3 becomes much larger in comparison to $\rho_{He} g d_{top}$, which can therefore be dropped out completely. One arrives then at a formula for the thickness d_{top} of a liquid helium film in the region $0 \leqslant x \leqslant a$ of the form

$$d_{top}^3 = \frac{C_3}{\rho_{He} g\,(h+\delta_0)} \approx \frac{C_3}{\rho_{He} g h}, \quad (h \gg \delta_0). \tag{4.6}$$

For $a \leqslant x \leqslant a+b$, the profile cannot be expected to be a straight line in general, except for the limiting cases $b \gg 2\delta_0$ or $2\delta_0 \gg b$. However, the film is much thicker in this region, making the van der Waals term C_3/d_{top}^3 negligible when compared to $\rho_{He} g d(x)$. The term $\rho_{He} g d(x)$ can be also dropped out, because it is much smaller than $\rho_{He} g h$ (h is approximately 10^{-3}m, while $d(x)$ approximately 10^{-7}m.

Observing the definition of capillary length in eq. (4.4) and the approximations described in the previous paragraph, one is led to the following differential equation for the helium film profile $d(x)$ in the region $a \leqslant x \leqslant a+b$:

$$\frac{d''(x)}{(1+d'(x)^2)^{3/2}} = \frac{1}{R}, \quad R \equiv \frac{l_{He}^2}{h}. \tag{4.7}$$

The differential equation (4.7) is analytically tractable and its general solution is a parabola of the form

$$d(x) = K_1 \pm \sqrt{\left|x^2 + 2K_2 R x + R^2\left(K_2^2 - 1\right)\right|}, \tag{4.8}$$

where K_1 and K_2 are integration constants that will be determined from the boundary conditions.

The two boundary conditions, in a shifted coordinate frame with origin at $c = a + b/2$, demand that the helium film thickness at $\pm b/2$ should be equal to $d_{top} + 2\delta_0$, whence one immediately obtains

$$d\left(\pm\frac{b}{2}\right) = d_{top} + 2\delta_0 \Longrightarrow \quad K_1 = d_{top} + 2\delta_0 + \sqrt{R^2 - \frac{b^2}{4}}, \quad K_2 = 0. \tag{4.9}$$

Physical considerations suggest that the film profile should additionally be concave, a requirement satisfied only by the solution of eq. (4.8) with the negative sign in front of the root. A shift back to the original reference frame with origin at $x = 0$ furnishes the final expression for the thickness $d(x)$ of the helium film in the whole range $0 \leqslant x \leqslant a+b$, that is,

$$d(x) = \begin{cases} d_{top} & 0 \leqslant x < a, \\ K_1 - \sqrt{R^2 - (x-c)^2} & a \leqslant x \leqslant a+b. \end{cases} \tag{4.10}$$

At the point $c = a + b/2$ one observes the maximal depression Δx of the film surface that will obviously be the helium film thickness $d(c)$ there minus

the helium film thickness at a 'flat' area, for example $d(a)$. Use of the solution in eq. (4.10) and a subsequent Taylor expansion up to $\mathcal{O}(1)$ terms result in

$$\Delta d = \left(\sqrt{1 - \left(\frac{b}{2R} \right)^2} - 1 \right) R \Longrightarrow \quad \Delta d \approx -\frac{b^2}{8R}. \tag{4.11}$$

Such an approximation is valid if $b/2R \ll 1$, a requirement that is fulfilled with great accuracy. A numerical estimation of the maximal depression for realistic mesoscopic structures is very illuminating: the nanotower structure has $b \approx 800\text{nm}$, and for bulk liquid helium found $h = 0.5\text{mm}$ below the substrate, the radius of curvature is calculated to be $R = 0.57\text{mm}$, giving a maximum deformation of -1.4Å (the minus sign indicates that the deformation is actually a depression). This deformation is comparable with the size of the hydrogen atom and it cannot have any observable effect. Nevertheless, TDES on liquid helium films, depending on their density, tend to magnify small deformations and appreciable deformations even on mesoscopic structures become possible.

4.2.2. Charged liquid helium film. In the discussion of Young-Laplace equation (4.3) it was noted that it is essentially an application of the energy conservation principle on the liquid film in equilibrium.

Any mechanical system admits in general a treatment not only in terms of energy, but also in terms of force (for extended bodies, as opposed to point particles, the treatment is in terms of energy density and force density, with the latter being more commonly known as pressure). This can be seen from the fact that the physical dimension of pressure (force per area, $[\text{N m}^{-2}]$) is the same as that of potential energy density (energy per volume, $[\text{J m}^{-3}]$).

Then, the physical content of Young-Laplace equation can be restated as a pressure equilibrium, in that the pressure exerted on the surface of a film at a height h above the surface of bulk liquid helium should be the sum of the hydrostatic pressure of a column of the liquid with height h, plus the hydrostatic pressure due to the film itself (whose thickness is d), plus the pressure the substrate exerts on the film (by van der Waals interaction).

A static electric field exerts a pressure on a dielectric material. In the general case of an anisotropic and inhomogeneous dielectric material, the pressure from the electric field is different for each of the nine possible coordinate pairs in space that exhaust the ways a material can be stretched or twisted[5], and the stress tensor (a 3×3 matrix) is defined, whose components p_{ij} are the pressures along the respective coordinate pairs. Isotropic and linear dielectric materials make the stress tensor symmetric ($p_{ij} = p_{ji}$), with its components having the form

[5]For a cartesian coordinate frame these pairs are xx, yy, zz, which describe stretching, and xy, yx, xz, zx, yz, zy, which describe twisting along the corresponding direction.

(cf. *Landau and Lifshitz* [**66**], p. 61)

$$p_{ij} = -p_0(\rho, T)\delta_{ij} - \frac{\epsilon_0 E^2}{2}\left(\epsilon - \rho\left(\frac{\partial \epsilon}{\partial \rho}\right)_T\right)\delta_{ij} + \epsilon_0 \epsilon E_i E_j, \tag{4.12}$$

where indices i and j are a short-hand of cartesian coordinates x, y, z. In the formula above, $\mathbf{E}$ denotes the electric field (a subscript is used for a particular component), ρ and ϵ are the density and dielectric constant of the material, and $p_0(\rho, T)$ is the pressure without electric field at the same conditions of temperature and density. Finally, δ_{ij} is the Kronecker delta and ϵ_0 is the dielectric constant of vacuum.

Liquid helium is a homogeneous (ρ is constant) dielectric, with a dielectric constant $\epsilon_{He} = 1.057$. Above the free surface of liquid helium only helium vapor can coexist. The vapor pressure of helium gas is rather low, especially when compared with the pressure arising from electric fields; therefore, $p_0(\rho, T) \approx 0$. A holding field $\mathbf{E} = (0, 0, E)$ simplifies the stress tensor considerably, because then only p_{zz} remains different from zero.

As a consequence, a holding field $\mathbf{E}$ (regardless of whether it is positive or negative) is pressing the liquid helium surface along the z-direction and this pressure must be inserted into the Young-Laplace equation as an additional term. A trivial calculation of p_{zz} from eq. (4.12) leads to the electrostatic pressure p_{el} due to a two-dimensional electron sheet, which turns out to be

$$p_{el} = \frac{\epsilon_0 \epsilon}{2} E^2, \quad \text{where} \quad E = \frac{n_s e}{2\epsilon_0} \tag{4.13}$$

is the electric field of a two-dimensional distribution of charges characterized by a saturated electron density n_s. Saturated electron density, in turn, directly depends on the holding field, which is set by controlling the voltage difference between the top and bottom plate (cf. eq. 3.14).

The Young-Laplace equation for a liquid helium film of thickness $d(x)$ at a height h above bulk liquid helium surface, in the presence of a TDES with saturated electron density n_s, becomes accordingly

$$\sigma_{He} \frac{d''(x)}{(1 + d'(x)^2)^{3/2}} = \rho_{He} g h + \frac{\epsilon}{8\epsilon_0} (n_s e)^2 + \left(\rho_{He} g d(x) - \frac{C_3}{d(x)^3}\right). \tag{4.14}$$

In the region $a \leqslant x \leqslant a + b$, the thick film limit is reached, where the hydrostatic pressure of the film itself and the pressure due to van der Waals interaction with the substrate (the two terms in the parentheses at the right-hand side) can be neglected when compared with the hydrostatic pressure $\rho_{He} g h$ and the electrostatic pressure. After minor manipulations, one arrives at the

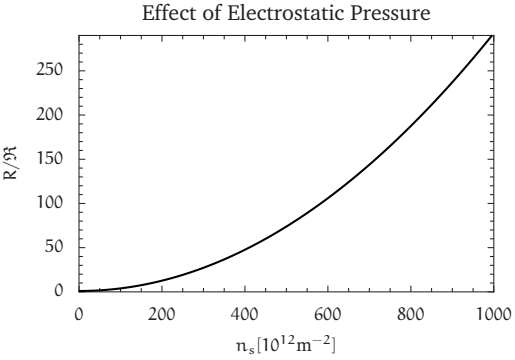

FIGURE 4.3. Values of the dimensionless ratio $R/\Re$ (cf. eq. 4.15), as a function of saturated electron density n_s, for a liquid helium film $h = 0.5$mm above the surface of bulk liquid helium. The ratio of maximum depression for a charged versus an uncharged surface is the same as $R/\Re$.

differential equation

$$\frac{d''(x)}{(1+d'(x)^2)^{3/2}} = \underbrace{\frac{1}{R}\left(1+\frac{\epsilon}{8\epsilon_0}\frac{(n_s e)^2}{\rho_{He} g h}\right)}_{\equiv 1/\Re}. \tag{4.15}$$

This equation has the same form—and consequently the same solutions—as the differential equation (4.7) for the uncharged film, provided that $1/R$ is replaced with $1/\Re$, which is generally larger (making $\Re$ smaller than R). The radius of curvature for a charged surface decreases, and this means that the charged surface is in essence more 'concave' than the uncharged one. In particular, the maximum depression $\Delta d \approx -b^2/8\Re$ at the troughs of the charged surface is larger than that of the uncharged.

Employing approximations similar to those that led to eq. (4.6) and considering the definitions of R and $\Re$, it is found that the thickness of a charged helium film at the ridges of a periodically structured substrate is

$$d_{top}^3 = \frac{C_3}{\sigma_{He}}\frac{1}{\Re}. \tag{4.16}$$

It is immediately obvious that the film thickness at the ridges of the charged surface increases, when compared with the respective thickness of the uncharged surface there.

4.2.3. Two-dimensional profile. Results for one-dimensional profiles retain their relevance in two dimensions only when symmetry is present. Both the nanohole and the nanotower structure exhibit cylindrical symmetry around the z-axis that passes through the center of a trough, and this coordinate frame will be adopted in the following analysis.

Maximum depression of the film surface, eq. (4.11), occurs at the point $(x, y) = (c, c)$, where it is convenient to set the zero level ($z = 0$) as well. The deepest point of a trough becomes the origin in the new coordinate frame. The

helium film profile will be symmetric for x and y around the origin of the new coordinate frame and it will be given by

$$\Delta d(x,y) = -\left(\sqrt{1-\left(\frac{x}{R}\right)^2-\left(\frac{y}{R}\right)^2}-\sqrt{1-\left(\frac{b}{2R}\right)^2}\right)R. \tag{4.17}$$

This profile defines a parabolic well, extending from $x,y=-b/2$ up to $x,y=+b/2$, whose maximum depth is $\Delta d(0)$. The parabolic form can be shown explicitly after a Taylor expansion around $(x,y)=0$, leading to

$$\Delta d(x,y) \approx \Delta d(0)\left(1+\frac{x^2+y^2}{2R\Delta d(0)}\right), \quad \text{for} \quad x,y \ll R. \tag{4.18}$$

Observe that the Taylor expansion is valid for $x,y \ll R$, making it therefore an extremely good approximation not only for x and y very near the origin, but also for the whole range $-b/2 \leqslant x,y \leqslant +b/2$ of the parabolic well, since it is $b \ll R$.

4.3. Statistical mechanics of a TDES on a deformed film

It can be claimed intuitively that electrons of a TDES are localized in the troughs of periodically structured substrates, when a thin liquid film wets the substrate and external holding electric and magnetic fields are present. However, a theoretical demonstration of localization under these conditions would not only validate intuition, but also provide detailed quantitative results on the proportion of electrons that are localized in specific conditions of temperature, film thickness, field magnitude and whatever other factors prove to be essential for this phenomenon.

A single electron is described by a hamiltonian whose eigenvalues define the spectrum of energies this electron can have. Each energy level defines a number of quantum states (from one to infinite, depending on the degeneracy of energy levels) and in a multielectron system each quantum state can be occupied by at most two electrons. The probability that an energy level is occupied in a multielectron system is given by the Fermi-Dirac distribution.

The considerations of the previous paragraph suggest a methodology for the study of electron localization, which can be outlined in the following manner: electrons in the area of ridges and electrons in the area of troughs can be considered as two systems of N noninteracting particles at the same conditions of temperature and area. The two systems are not isolated, so that particles are allowed to change system, meaning that while the number of particles in each system is not conserved, the sum of particles of both systems is indeed conserved. Statistical equilibrium among the two systems would soon set in, and this equilibrium would determine the partial fractions of particles that reside on the ridges and in the troughs. In order to determine this equilibrium, one must:

(1) Set up the single-electron hamiltonian for each system and find the respective energy spectra, together with the degree of degeneracy of energy levels (the number of distinct quantum states corresponding to each energy level). Then, the density of states $\mathcal{D}(E)$, giving the number of quantum states for an energy E, can be defined for each of the two systems.

(2) The number of particles N, with eigenenergies in the range (E_0, E_1) whose corresponding indices are (ν_0, ν_1), in a system with density of states $\mathcal{D}(E)$, is

$$N(\mu, T) = \sum_{\nu=\nu_0}^{\nu_1} \frac{\mathcal{D}(E_\nu)}{e^{\beta(E_\nu - \mu)} + 1}, \quad \text{or} \quad N(\mu, T) = \int_{E_0}^{E_1} \frac{\mathcal{D}(E)dE}{e^{\beta(E-\mu)} + 1}, \tag{4.19}$$

where μ is the chemical potential and $\beta = 1/k_B T$ is the inverse thermal energy at temperature T. Summation over distinct eigenenergies may be replaced by integration at the limit of large $\nu_1 - \nu_0$ (Thomas-Fermi approximation). Each system is characterized by a particular range of energies, so that the summation indices ν_0 and ν_1, as well as the integration limits E_0 and E_1, are generally fixed. As a consequence, N is a function of temperature and chemical potential only.

(3) If the total number of particles is N, statistical equilibrium at temperature T for the two systems with number of particles N_1 and N_2 is equivalent to the demand that

$$N_1(\mu_0, T) + N_2(\mu_0, T) = N, \tag{4.20}$$

from which the only unknown, the equilibrium chemical potential μ_0, can be found.

(4) The partial fraction of particles that reside in the i-th system in equilibrium will obviously be given then by $N_i(\mu_0, T)/N$.

This four-step plan for the study of electron localization underlies the investigations presented in sections 4.4 and 4.5.

Single-electron hamiltonians imply that Coulomb interactions among electrons are completely ignored. An excuse for this radical simplification of the problem's physics is that any serious treatment that includes electron interactions must necessarily employ the toolbox of quantum field theory[6], leading to a radical complication of the problem's mathematics.

Another excuse with more physical content is that in a setting where one electron occupies each trough, Coulomb interactions among localized electrons should not be large. Even when many electrons are localized inside the same

[6] An exception is the *constant interaction model* [**60**], where the potential term of the Coulomb interaction among electrons of a quantum dot is assumed to be constant. A constant Coulomb interaction is certainly preferable than no interaction at all, but still an idealization. Moreover, the estimation of a reasonable constant interaction potential quickly becomes very complex.

trough, a simple Drude-like model would prove useful, if discrepancies between the model and the experimental data could demarcate effects due to Coulomb interactions. In any case, before elaborating, it is always useful to examine how much can be explained by simple means, but no simpler.

4.4. Localization with a holding field

Assume that an electron resides above a flat helium film and a holding field $E_\perp$ is present. Then, the potential will contain a term $-eE_\perp z$, where z is the distance of the electron from the helium film surface, and a term $-\Lambda_s/d$, where d is the thickness of the helium film and Λ_s has been defined in eq. (2.1).

If one imagines that the film surface is deformed such that troughs develop, whose depression is measured by $\Delta d(x,y) \leqslant 0$ as defined in eq. (4.18), the influence of the substrate in the area of a trough will be given by $-\Lambda_s/\big(z+d(x,y)\big)$, with $d(x,y)$ defined in eq. (4.10) and there will also exist an additional potential term $eE_\perp \Delta d(x,y) < 0$. This additional potential term reflects the fact that a depression is an area of lower potential energy when a holding field 'pushes' electrons towards the bottom plate. The total potential of this setting would then be written down as

$$V(x,y,z) = -\frac{\Lambda}{z} - eE_\perp z - \frac{\Lambda_s}{z+d(x,y)} + eE_\perp \Delta d(x,y). \tag{4.21}$$

Observe that for a flat substrate it is $\Delta d(x,y) = 0$ and $d(x,y) = d$ and eq. (4.21) is reduced in a form similar to the potential of eq. (2.2).

At the limit of thick films ($z \ll d$) a Taylor expansion of $\big(z+d(x,y)\big)^{-1}$ up to first order terms leads to

$$V(x,y,z) = \underbrace{-\frac{\Lambda}{z} - \left(eE_\perp + \frac{\Lambda_s}{d^2}\right) z}_{V(z)} + \underbrace{eE_\perp \Delta d(x,y) - \frac{\Lambda_s}{d(x,y)}}_{V(x,y)}. \tag{4.22}$$

From eq. (4.22) it is seen that the potential is separable into a component $V(z)$ for transverse and a component $V(x,y)$ for lateral electron motion. Film thickness $d(x,y)$ can be substituted by either a constant value in Λ_s/d^2, or the whole contribution Λ_s/d^2 can be dropped out completely, because it is much smaller than the already small perturbation coefficient $eE_\perp$. Then, Schrödinger equation can be solved separately for $V(z)$ and $V(x,y)$, yielding the common Stark-shifted surface states of TDES on liquid helium in the z-direction, as it was intuitively claimed in the beginning of this chapter.

Electron dynamics in the (x,y) plane will be determined from the $V(x,y)$ part of eq. (4.22). Substitution of $\Delta d(x,y)$ as approximated in eq. (4.18) into $V(x,y)$ and the additional approximation

$$d(x)^{-1} \approx \frac{1}{\mathfrak{R}}\left(\frac{K_1}{\mathfrak{R}} - 1\right)^{-1} - \left(\frac{K_1}{\mathfrak{R}} - 1\right)^{-2} \frac{1}{2\mathfrak{R}} \left(\frac{x}{\mathfrak{R}}\right)^2, \tag{4.23}$$

which can be expressed as

$$d(x)^{-1} \approx \frac{8\mathfrak{R}}{b^2} - \frac{32\mathfrak{R}}{b^4}x^2, \tag{4.24}$$

after making use of $K_1/\mathfrak{R} - 1 \approx -b^2/8\mathfrak{R}^2$, accompanied by algebraic manipulations that will not be reproduced, leads ultimately to the harmonic oscillator potential

$$V(x,y) = \frac{\Lambda_s}{d_{top}+2\delta_0} - \frac{m\omega_E^2 b^2}{8} + \frac{m\omega_E^2}{2}\left(x^2+y^2\right) \quad \text{(trough)}, \tag{4.25}$$

where

$$\omega_E = \sqrt{\omega_s^2+\omega_e^2}, \quad \omega_s^2 = \frac{64\Lambda_s\mathfrak{R}}{mb^4} \quad \text{and} \quad \omega_e^2 = \frac{eE_\perp}{m\mathfrak{R}}. \tag{4.26}$$

On a ridge, $\Delta d(x,y) = 0$ and the film thickness equals the constant value d_{top}. Consequently, the potential on the ridges will be just the constant $-\Lambda_s/d_{top}$. A redefinition of the potential by adding Λ_s/d_{top} on both ridges and troughs leads to zero potential on a ridge and $V(x,y)$ as in eq. (4.25) in a trough.

From eq. (4.25) it is evident that a parabolic potential well of depth $\Lambda_s/(d_{top}+\delta_0) - m\omega_E^2 b^2/8$ is formed. Except for the dimension of the trough, which is reflected in the diameter b, the depth of the parabolic well is determined by the thickness d_{top} of the helium film on the ridges and the cyclic frequency ω_E. In turn, ω_E is the sum of a term ω_s that depends on the nature of the substrate and a term ω_e that depends on the applied holding field[7].

It is seen from eqs. (4.25) and (4.26) that an increasing holding field $E_\perp$ deepens the potential well and therefore enhances electron localization in the troughs. For the same holding field and electron density, stronger dielectric substrates (larger Λ_s) increase the depth of the potential well, because electrons interact stronger with the substrate.

Substitution of numerical values for the physical quantities in eq. (4.26) reveals that ω_s is several orders of magnitude larger than ω_e. As a result, electron localization in the troughs of helium films that wet periodically structured substrates is determined almost exclusively from the interaction of electrons with the dielectric substrate.

The hamiltonian for an electron in a trough can be written down as

$$\hat{\mathcal{H}} = \frac{\hat{p}^2}{2m} + \frac{m\omega_E^2}{2}\left(\hat{x}^2+\hat{y}^2\right) + \frac{\Lambda_s}{d_{top}+2\delta_0} - \frac{m\omega_E^2 b^2}{8}. \tag{4.27}$$

This is the hamiltonian of a two-dimensional harmonic oscillator shifted by a constant energy. The energy shift will be carried over in the energy spectrum,

[7] If it is assumed that electron density corresponds to the saturated electron density, the radius of curvature $\mathfrak{R}$ of the charged surface, which is present in both ω_s and ω_e, will be a function of the holding field as well.

which will be given by

$$E_\nu = (2\nu+1)\hbar\omega_E + \frac{\Lambda_s}{d_{top}+2\delta_0} - \frac{m\omega_E^2 b^2}{8}, \quad \nu = 0,1,\ldots \tag{4.28}$$

From the form of eigenenergies it is seen that the discrete density of states, taking into account the two possible orientations of electron spin, is simply $\mathcal{D}(E_\nu) = 2(2\nu+1)$. The density of states in the continuous limit of the Thomas-Fermi approximation is easily found to be $\mathcal{D}(E)dE = (1/\hbar\omega_E)dE$, where again electron spin states were taken into account.

If the number of electrons localized in the troughs is denoted with N_{loc}, and the potential in the troughs spans the energy range from $-V_0$ (bottom of the potential well) up to 0, one can write, in accordance with eq. (4.19),

$$N_{loc}(\mu,\beta) = \frac{1}{\hbar\omega_E}\int_{-V_0}^{0} \frac{dE}{e^{\beta(E-\mu)}+1}, \tag{4.29}$$

where

$$V_0 = \frac{m\omega_E^2 b^2}{8} - \frac{\Lambda_s}{d_{top}+2\delta_0} - \hbar\omega_E > 0. \tag{4.30}$$

It is important to note that the lower integration limit $(-V_0)$ does not coincide with the bottom of the potential well, $\Lambda_s/(d_{top}+2\delta_0) - m\omega_E^2 b^2/8$, but it is higher by the amount $\hbar\omega_E$, which is the energy due to the zero-point motion of the quantum harmonic oscillator with two degrees of freedom. For very weak dielectric substrates and holding fields, the cyclic frequency ω_E might not be high enough to make $V_0 > 0$, whereby the potential well is so shallow that no electrons would be localized in the troughs anyway. In this case, $N_{loc} = 0$ and eq. (4.29) is no longer valid.

Realistic dielectric substrates (e.g silicon, with $\epsilon_s = 11$) are always associated with sufficiently deep parabolic wells, where the Hartree-Fock continuum approximation is well justified. As an example, one can calculate that the potential well of a trough with diameter $b = 800$nm of a suspended helium film that wets a silicon substrate and is formed 0.5mm above bulk liquid helium, can contain a total of 4525 quanta $\hbar\omega_E$.

Holding fields for which eq. (4.29) can be applied, being thus capable of causing electron localization in the troughs, should be stronger than the critical field $E_\perp^{(c)}$. The critical field is determined from the condition $V_0 = 0$, which leads to a critical ω_E calculated from eq. (4.29). Substitution of the critical ω_E in the relevant expression of eq. (4.26) yields the critical holding field

$$E_\perp^{(c)} = \frac{16\hbar^2\mathfrak{R}}{emb^4}\left(1+\sqrt{1+\frac{mb^2\Lambda_s}{2\hbar^2 d_{top}}}\right)^2 - \frac{64\Lambda_s\mathfrak{R}^2}{eb^4}. \tag{4.31}$$

Except for the limiting cases of a weak dielectric substrate ($\Lambda_s \approx 0$) or extremely high electron densities that would make $\mathfrak{R}$ small enough, a potential well can be formed for any (positive) holding field.

The integration in the expression for N_{loc}, eq. (4.29), can be carried analytically, furnishing the final expression for the number of localized electrons in the presence of holding field,

$$N_{loc}(\mu,\beta) = \frac{1}{\hbar\omega_E\beta}\ln\left(\frac{1+e^{\beta(\mu+V_0)}}{1+e^{\beta\mu}}\right). \tag{4.32}$$

For progressively deeper potential wells ($V_0 \longrightarrow \infty$), the number of localized electrons is independent of temperature and it behaves asymptotically as $N_{loc} \sim \omega_E$. At the limit of high ($\beta \longrightarrow 0$) and low ($\beta \longrightarrow \infty$) temperatures indeterminate forms arise that can be easily dealt with an application of L' Hôpital rule[8], finding that for high temperatures it is $N_{loc} \sim 0$, whereas for low temperatures it is $N_{loc} \sim \omega_E$.

As electrons on the ridges are free (the potential there is almost zero), both their hamiltonian and their energy spectrum should be those of an electron on the surface of bulk helium.

The density of states of an electron, moving with two degrees of freedom in the Thomas-Fermi approximation, is $\mathcal{D}(E)dE = (m/\pi\hbar^2)dE$, if the two possible spin states are taken into account. The number $N_{fr}(\mu,\beta)$ of free electrons, according to eq. (4.19), will be then

$$N_{fr}(\mu,\beta) = \frac{mb^2}{4\hbar^2}\int_0^{1/\beta}\frac{dE}{e^{\beta(E-\mu)}+1} = \frac{mb^2}{4\hbar^2\beta}\left(1+\ln\left(\frac{1+e^{\beta\mu}}{e+e^{\beta\mu}}\right)\right). \tag{4.33}$$

At the limit of low temperatures ($\beta \longrightarrow \infty$) the number of free electrons tends asymptotically to zero as $N_{fr} \sim 1/\beta$. The limit of high temperatures ($\beta \longrightarrow 0$) has the asymptotic form $e^{\beta\mu}/\beta$, which is an indeterminate form $0/0$, since μ tends to $-\infty$ at high temperatures. The indeterminacy is removed, if one recalls that the dependence of chemical potential on temperature is logarithmic at the high-temperature limit, so that $\mu \sim \ln\beta$. This implies that $N_{fr} \sim e^{\beta\ln\beta}/\beta$, which tends to infinity at the limit of high temperatures, as one would intuitively expect.

A trough extends in an area $\pi b^2/4$, and in equilibrium the total number of electrons at this area will be $n_s\pi b^2/4$, where n_s is the saturated electron density. Of these electrons, N_{loc} are localized and N_{fr} free. In equilibrium, according to eq. (4.20), it will be

$$N_{loc}(\mu,\beta) + N_{fr}(\mu,\beta) = \frac{\pi b^2}{4}n_s. \tag{4.34}$$

[8]The asymptotic expression derived from L' Hôpital rule contains combinations of $\beta\mu$ whose asymptotic properties, as known from statistical mechanics, are $\beta\mu \longrightarrow -\infty$ for $\beta \longrightarrow 0$, and $\beta\mu \longrightarrow 0$ for $\beta \longrightarrow \infty$. The chemical potential for $T = 0$ is the Fermi energy.

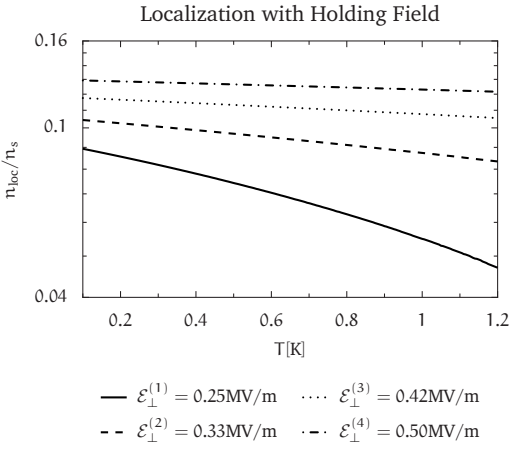

FIGURE 4.4. Partial fraction n_{loc}/n_s of localized electrons, as a function of temperature T at the limit $\Lambda_s \to 0$ (no interaction with the substrate). Saturated electron densities (in m^{-2}) of $\mathcal{E}_\perp^{(i)}$ are 1.21×10^{15}, 1.82×10^{15}, 2.43×10^{15}, 3.04×10^{15} and 3.65×10^{15} for $i = 1,2,3,4$ respectively. Only $\approx 12\%$ of electrons are localized at best. Scale of the y-axis is logarithmic.

The only unknown parameter in eq. (4.34) is the chemical potential, whose value μ_0 in equilibrium can then be determined. Inspection of the equilibrium equation (4.34) suggests that an analytic expression for μ_0 is not possible, and numerical methods, like Newton's method, should be employed instead. Provided that μ_0 has been determined, the partial fraction of free electrons in equilibrium for a given temperature and holding electric field is

$$\frac{n_{fr}}{n_s} = \frac{m}{\pi\hbar^2\beta n_s}\left(1 + \ln\left(\frac{1+e^{\beta\mu_0}}{e+e^{\beta\mu_0}}\right)\right), \tag{4.35}$$

while the partial fraction of localized electrons at the same conditions of temperature and holding electric field will be

$$\frac{n_{loc}}{n_s} = \frac{4}{\pi\hbar\omega_E\beta n_s b^2}\ln\left(\frac{1+e^{\beta(\mu_0+V_0)}}{1+e^{\beta\mu_0}}\right). \tag{4.36}$$

The numerical solution of eq. (4.34) for realistic dielectric substrates (e.g silicon, or silicon oxide) indicates complete electron localization in the troughs, due to the very strong interaction of electrons with the substrate.

At the limit $\Lambda_s \longrightarrow 0$, which corresponds to weak dielectric substrates, or no substrate at all, it turns out that a significantly smaller fraction of electrons is localized in the troughs. Fig. 4.4 depicts the behavior of n_{loc}/n_s with respect to temperature and magnitude of holding field, as derived from the numerical solution of eq. (4.34) for $\Lambda_s \longrightarrow 0$. Stronger fields (higher electron densities) are able to localize a larger fraction of electrons. Across the various holding fields, lower temperatures are generally associated with more localized electrons.

A striking feature of fig. 4.4 is that extremely strong holding fields are required for an appreciable fraction of localized electrons in the case of weak dielectric substrates. Holding field magnitudes in the order of 10^6V/m imply

that voltages in the kV range must be applied between the bottom and the top plate. In practice, this means that in the case where no dielectric substrate is present, electrons on deformed films should be in principle free as they cannot be localized by means of a holding field alone.

On the other hand, dielectric substrates like silicon interact so strongly with TDES on deformed films that most, if not all electrons, should be already localized in the troughs even for the weakest holding fields.

4.5. Localization with a holding field and a magnetic field

An electron inside a trough of a helium film that wets a periodically structured substrate, in the presence of a holding field and a magnetic field $\mathbf{B} = (0, 0, B)$, is characterized by the hamiltonian

$$\hat{\mathcal{H}} = \frac{\hat{\mathbf{p}}^2}{2m} + \frac{m\Omega^2}{2}\left(\hat{x}^2 + \hat{y}^2\right) + \frac{\omega_c}{2}\hat{\mathcal{L}}_z + \frac{\Lambda_s}{d_{top} + 2\delta_0} - \frac{m\omega_E^2 b^2}{8}, \tag{4.37}$$

where

$$\Omega = \sqrt{\omega_E^2 + \frac{\omega_c^2}{4}}, \quad \omega_c = \frac{eB}{m}, \tag{4.38}$$

ω_E has been defined in eq. (4.26) and $\hat{\mathcal{L}}_z$ is the operator of the z-component of angular momentum. The classical picture of electron motion implied by the hamiltonian of eq. (4.37) is that of revolutions in circular orbits with cyclic frequency Ω. The hamiltonian of eq. (4.37) is obtained from the more general form of the hamiltonian in eq. (B.1), the potential of eq. (4.25) and the selection of the symmetric gauge $\mathbf{A} = -\mathbf{r} \times \mathbf{B}/2$ for the vector potential $\mathbf{A}$.

Apart from the shift $\Lambda_s/(d_{top} + 2\delta_0) - m\omega_E^2 b^2/8$, the hamiltonian of eq. (4.37) is identical to the analytically solvable Darwin-Fock hamiltonian[9]. Therefore, the eigenenergies of $\hat{\mathcal{H}}$ in eq. (4.37) will be given by

$$E_{\nu,l} = (2\nu + |l| + 1)\hbar\Omega - \frac{l}{2}\hbar\omega_E + \frac{\Lambda_s}{d_{top} + 2\delta_0} - \frac{m\omega_E^2 b^2}{8}, \tag{4.39}$$

where the indices take values $\nu = 0, 1, \ldots$ and $l = 0, \pm 1, \ldots$.

Instead of the precise form of the *Darwin-Fock* wavefunctions, which will not be reproduced here, we will make use of the *magnetic length* λ_B, defined by

$$\lambda_B = \left(\frac{\hbar}{m\Omega}\right)^{1/2}. \tag{4.40}$$

The magnetic length characterizes the spatial extent of Darwin-Fock wavefunctions, in the sense that quantum objects described by the *Darwin-Fock* wavefunctions and are some λ_B apart can be regarded as distinct, particle-like entities.

[9]The Darwin-Fock hamiltonian was introduced and solved by *Fock* in [Z. Phys. **47**, 446 (1928)] and independently by *Darwin* in [Proc. Camb. Phil. Soc. **27**, 86 (1930)].

For all measurements presented in this thesis, the magnetic length was never larger than 5nm.

On the ridges, the potential $V(x,y)$ is zero, and electron motion there is described by a hamiltonian identical with that of eq. (B.2). As a result, electron motion on the ridges will correspond to circular motion with cyclic frequency ω_c (Landau oscillations) and an energy spectrum given by

$$E_\nu = (2\nu+1)\hbar\omega_c. \tag{4.41}$$

Cyclotron radius r_c has been defined in eq. (2.13) as the mean classical radius at temperature T of the circular orbit an electron describes, under the influence of a magnetic field along the z-direction. More generally, the cyclotron radius R_c can be similarly defined as the mean classical radius at temperature T of the circular orbit an electron describes, under the influence of both a holding field and a magnetic field along the z-direction. It is not difficult to show that the equation that relates R_c and Ω is

$$R_c = \frac{1}{\Omega}\left(\frac{2k_BT}{m}\right)^{1/2}. \tag{4.42}$$

The ground Darwin-Fock state ($\nu = 0$ and $l = 0$) exhibits the lowest cyclotron frequency, equal to Ω, while excited states ($\nu = 1,2,\ldots$ and $l = 0$) are associated with progressively higher cyclotron frequencies (3Ω, $5\Omega,\ldots$). An inversely proportional relation, eq. (4.42), connects cyclotron frequency to cyclotron radius, meaning that the ground Darwin-Fock state exhibits the largest cyclotron radius, which becomes progressively smaller for excited states.

Localization of electrons inside the troughs of a periodic substrate is expected for $R_c \leqslant b/2$, where it is reminded that b is the diameter of a trough (for the nanotower surface $b \approx 800$nm). Electron localization will be complete, if the cyclotron radius of the ground Darwin-Fock state is less than or equal to $b/2$. This condition, along with eq. (4.42) and the definitions of ω_c and ω_E in eqs. (2.13) and (4.25) respectively, leads after some algebra to a condition for the onset of complete electron localization, of the form

$$\frac{8mk_BT}{e^2b^2} \leqslant \frac{64m\Lambda_s\mathfrak{R}}{e^2b^4} + \frac{mE_\perp}{e\mathfrak{R}}. \tag{4.43}$$

Physical factors that induce complete electron localization are those that either minimize the left-hand side, or maximize the right-hand side of eq. (4.43). For example, an increasing temperature T, a larger trough radius b, stronger holding fields $E_\perp$ and increasing electron densities (enclosed in the radius of curvature $\mathfrak{R}$) all induce complete electron localization. But when dielectric substrates are present, whose influence is enclosed in Λ_s, the term $64m\Lambda_s\mathfrak{R}/e^2b^4$ is so large that complete electron localization happens for any magnetic field regardless of its magnitude.

By definition, in complete localization electrons cannot be free and the (dynamic) equilibrium equation (4.20) at any instance of time will involve two systems; electrons instantly localized in a trough and electrons instantly localized on a ridge. Taking electron spin into account, the discrete density of states of the system "electron in a trough" is $\mathcal{D}_t(E_{\nu,l}) = 2(2\nu + |l| + 1)$ and the continuous, Hartree-Fock density of states is equal to $\mathcal{D}_t(E) = 1/2\hbar\Omega$. Again taking electron spin into account, the discrete density of states of the system "electron on a ridge" is $\mathcal{D}_r(E_\nu) = 2(2\nu+1)$ and the Hartree-Fock density of states is $\mathcal{D}_r(E) = 1/2\hbar\omega_c$. Noting that the area of a trough (which contains the majority of electrons and is much larger than the area of a ridge) is approximately $s = \pi b^2/4$, the sum of partial fractions from the ground state ($\nu = 0$ and $l = 0$) upwards leads to the equilibrium equation

$$\sum_{\nu=0}^{\infty} \frac{\mathcal{D}_r(E_\nu)}{e^{\beta(E_\nu-\mu)}+1} + \sum_{\nu,l=0}^{\infty} \frac{\mathcal{D}_t(E_{\nu,l})}{e^{\beta(E_{\nu,l}-\mu)}+1} = \frac{\pi b^2}{4} n_s, \tag{4.44}$$

from where the equilibrium chemical potential $\mu_0(T, B, E_\perp)$ can be determined.

Except for temperature T, magnetic field B and holding field $E_\perp$, the equilibrium chemical potential depends also on experimental parameters like the dielectric constant Λ_s of the substrate and the diameter b of a trough, which cannot be changed in the course of a measurement.

For numerically solving eq. (4.44), the infinite summation must be truncated into a summation that involves a finite number of states. The resulting finite series converges to a progressively more accurate value of μ_0 when more excited states are included. It was found by numerical experimentation that the inclusion of excited states up to $\nu = 40$ was always sufficient for numerical convergence.

Provided that the equilibrium chemical potential μ_0 is known, the partial fractions of electrons occupying the state with energy $E_{\nu,l}$ inside a trough will then be given by

$$\frac{n_{\nu,l}}{n_s} = \frac{\mathcal{D}(E_{\nu,l})}{e^{\beta(E_{\nu,l}-\mu_0)}+1}. \tag{4.45}$$

An identical equation holds for the partial fraction of electrons that belong to the state with energy E_ν on a ridge, as it suffices to substitute $E_{\nu,l}$ in eq. (4.45) with E_ν as given in eq. (4.41).

The partial fractions of electrons in the troughs and electrons on the ridges remain constant when the physical quantities that affect electron potential do not change. One would expect then, that the measured conductivity should be a constant nonzero value, reflecting the random fluctuations of electron motion due to temperature and Coulomb interactions.

However, when the magnetic field is not kept constant the partial fractions of electrons in the troughs and on the ridges readjust to a new equilibrium, following the changes of B. This readjustment means that electrons should be

diffusively drawn in and out of the ridges as the magnetic field changes, whence a contribution to the admittance of the TDES should emerge.

In the ideal case where localized electrons on either the ridges or the troughs do not conduct at all, a nonzero admittance can only be attributed to electrons that diffuse from the ridges to the troughs and vice versa. If only the magnetic field changes, this *flow admittance* $Y = I/V$ of the TDES can be restated as

$$Y = \frac{1}{V}\left|\frac{dn}{dB}\right| \cdot \left|\frac{dB}{dt}\right|, \tag{4.46}$$

where n is the electron charge (in Cb) on the ridges, or in the troughs. The absolute value of the derivatives was used, because flow admittance should be positive irrespective of the sign of the rate of change of the charge.

Physically, flow admittance arises because a voltage difference V emerges between a trough and a peak and it is measurable because the diffusive motion of electrons from the troughs to the peaks except for the z-component, which cannot be measured with the experimental apparatus used, contains also a xy-component, which can be measured because peaks and troughs are obviously at different locations in the xy plane.

For simplicity, V in eq. (4.46) can be considered to be the voltage difference between a ridge and the bottom of a trough. The potential on a ridge has been defined to be zero, whereas the bottom of a trough has a potential energy $\Lambda_s/d_{top} - m\omega_E b^2/8$, meaning that the voltage difference is

$$V = \frac{\Lambda_s}{e(d_{top} + 2\delta_0)} - \frac{m\omega_E b^2}{8e}. \tag{4.47}$$

The electron charge density (in Cb/m^2) inside a single trough is the sum of $n_{\nu,l}$ as given in eq. (4.45) over all states multiplied by the electron charge e. A single trough has an area of approximately $\pi b^2/4$ and the nanotower substrate, whose area is $\mathfrak{A} = 1cm^2$, contains $4\mathfrak{A}/\pi b^2$ troughs. Therefore, the electron charge n in the troughs of the nanotower substrate will be

$$n = e\mathfrak{A}n_s \sum_{\nu,l} \frac{\mathcal{D}(E_{\nu,l})}{e^{\beta(E_{\nu,l}-\mu_0)}+1}, \tag{4.48}$$

with a similar equation holding for the electron charge on the ridges.

If a measurement of the admittance of a saturated TDES on the nanotower substrate is performed such that the temperature T and the holding field $E_\perp$ are kept constant while the magnetic field B is changed at a constant rate, then the experimental data (values of Y under these conditions) can be compared with the flow admittance that is calculated from eq. (4.46). Of course, in realistic experimental conditions, it should be expected that the measured admittance be generally larger than the flow admittance. However, the measured admittance should approach the theoretically calculated flow admittance in the limit of high magnetic fields, low temperatures and low electron densities. Indeed, for high

magnetic fields and low temperatures it is reasonable to expect that electron localization in both peaks and troughs would be strong and therefore that diffusive processes there would be weak, meaning that there is very little—if at all–conduction from electrons. Low electron densities have the same effect, as they ensure that Coulomb interactions among electrons are minimal and do not disturb their localization.

To our knowledge, neither the physical motivation nor any mathematical definition of the flow admittance appears in the relevant literature. This can be understood if one recalls that flow admittance is zero either for TDES on flat films when B changes (because then $n'(B) = 0$) or TDES on deformed films when B is constant or zero (because then $B'(t) = 0$). Indeed, flow admittance is peculiar to TDES only on deformed films and only when the magnetic field is altered.

CHAPTER 5

Experiments on Quasi Zero-Dimensional Localization

5.1. General considerations

Quasi zero dimensional localization was investigated experimentally in TDES on liquid helium films that wet the nanotower periodic structure, depicted in fig. 4.1.

Two dimensional electron systems of various electron densities held at various temperatures underwent a magnetic field sweep at a constant rate while the admittance $Y = I/V$ (with obvious notation) was measured by means of a Sommer-Tanner electrode geometry (see fig. 3.7). Temperature and electron density were kept constant throughout the magnetic field sweep.

The conductivity of TDES on liquid helium in the presence of a magnetic field depends on temperature, electron density and the magnitude of the magnetic field. Temperature dependence of conductivity reflects the strength of the various scattering mechanisms (ripplons, helium gas atoms, substrate), while electron density affects conductivity by means of the Wigner phase transition, as discussed in the relevant sections of chapters 1 and 2. The application of a magnetic field $B \lesssim 1.5\text{T}$ leads to a resistance $R(B) = R(0)\left(1 + \mu^2 B^2\right)$, where $R(0)$ is the resistance in zero magnetic field and μ is electron mobility (see section 2.5.1). A plot of $R(B)$ as a function of B^2 should then be a straight line whose slope is $\mu^2 R(0)$, as shown in fig. 5.1 which depicts a measurement of the resistance of a TDES on bulk liquid helium above the nanotower substrate. It should be noted that for stronger magnetic fields or higher electron densities deviations from this simple Drude behavior occur, which are reviewed both theoretically and experimentally by *Monarkha et al.* [**82**].

The use of suitable periodically structured dielectric substrates wet by helium films, in order to achieve electron localization of TDES, was explored extensively by *Kovdrya* and coworkers in the one dimensional case [**62, 63, 85**] and *Valkering et al.* [**110**] in the zero dimensional case.

Valkering et al. [**110**] measured the admittance of a TDES on a thick helium film with estimated thickness $0.4\mu\text{m}$ that wet a two dimensional grating similar to the nanotower substrate, as a function of a magnetic field perpendicular to

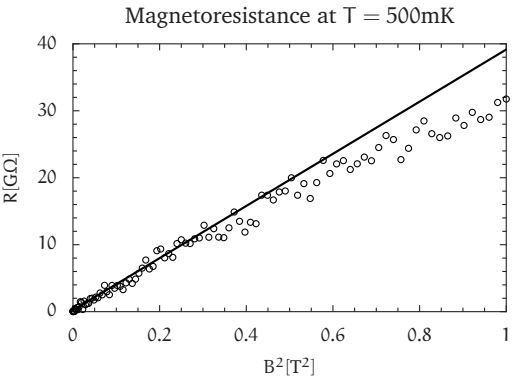

FIGURE 5.1. Resistance R of a TDES on bulk liquid helium as a function of the square of the magnetic field, B^2, measured at a temperature $T = 500mK$. A linear Drude behavior is observed for weak B, with zero field resistance $R(0) = 9.45 \times 10^7 \Omega$ and electron mobility $\mu = 1020 m^2/Vs$.

the surface of liquid helium. A linear Drude behavior with respect to B^2 could be established, but the resulting electron mobility was one order of magnitude lower than for a comparable TDES on bulk liquid helium at the same temperature. To our knowledge, the ideas and results of *Valkering et al.* [**110**] were not expanded further and we could not find other instances in the literature where zero dimensional electron localization with periodically structured substrates is attempted.

The application of a magnetic field perpendicular to the surface of liquid helium forces electrons to revolve along circular orbits whose classical radius r_c, defined in eq. (4.42), becomes smaller for increasing magnetic field magnitudes. If the nanotower substrate is wet with a sufficiently thin helium film, the surface of liquid helium will follow the curvature of the substrate, developing thus troughs and ridges. As the magnitude of the magnetic field increases, the radii of electron orbits will become equal or smaller than the radii of the troughs and electrons will be trapped in there, revolving around the 'walls' of the troughs.

Conductivity in the presence of a magnetic field is largely determined from the diffusive motion of the centers of the circular electron orbits, which is much less pronounced for trapped electrons. As a result, in the ideal case of very low temperatures, it should be expected that the conductivity (or equivalently, admittance[1]) would abruptly decrease when the magnetic field makes r_c equal to the trough radius and this abrupt decrease would signal the onset of zero dimensional localization.

For higher temperatures, the thermal energy might be enough to permit electrons (especially those belonging to the ground Landau state) to be drawn in and out of the troughs, but this effect should progressively diminish as r_c decreases further and electrons are drawn towards the bottom of the trough. This means

[1]A direct equivalence exists between conductivity and admittance for TDES with the same geometry and in the following, depending on the context, they will be referred to as equivalent.

that the abrupt decrease of conductivity at lower temperatures would be softened at higher temperatures and would resemble an activation-type Arrhenius law.

This simple qualitative picture of electron localization must be amended in view of the experimental results to be presented and the model that was developed in chapter 4.

According to the theoretical results of chapter 4, the interaction of electrons with the dielectric substrate is so strong that most electrons are localized in the troughs under the influence of the holding field even before a magnetic field is applied. The conductivity of a TDES under these conditions should be close to zero, with any nonzero conductivity arising due to thermally induced fluctuations in the motion of localized electrons plus the conductivity due to the small fraction of free electrons.

If, in addition, a magnetic field is applied, the density of states is altered and the partial fractions of free (delocalized) versus trapped (localized) electrons are altered as well. This means that as the magnetic field changes, electrons localized in the troughs move diffusively to the ridges, in order to account for the alteration of the partial fractions, so that in the end a diffusive current associated with a nonzero admittance develops.

From the definition $Y = I/V$ of admittance, V can be identified as the voltage difference between the bottom of the trough (the trough is a well not only in geometric but also in potential terms) and the ridge, while I is the current of electrons moving diffusively from a trough to a ridge. Elementary manipulations then lead to eq. (4.46), where one sees that Y depends on the rate of change of the magnetic field (which is known and constant) and the rate of change of the partial fraction of electrons on the ridges (or the troughs) with respect to the magnetic field.

The partial fraction of electrons on the ridges can be calculated numerically for any given set (n_s, T, B), where n_s denotes the saturated electron density of the TDES (determined from the holding field voltage), T is the temperature and B the magnitude of the magnetic field. In a magnetic field sweep, n_s and T are constant throughout, whereas B is measured in discrete steps. Therefore, it suffices to obtain a discrete set of pairs (B, n), where n is the partial fraction of electrons on the ridges as calculated numerically from eq. (4.45)[2], which can then be interpolated by a continuous function $n(B)$. Numerically differentiating $n(B)$ provides the rate of change of the partial fraction of electrons on the ridges with respect to the magnetic field and allows the admittance Y to be determined theoretically. The theoretical values can thereafter be compared with actual measurements. The procedure is easier to implement in symbolic programming

[2]This equation actually refers to the partial fraction of electrons in the troughs, but an almost identical formula holds for electrons on the ridges, as explained in the text accompanying the equation.

languages like *Mathematica* and execution time for 200 points and the first 40 quantum states should not be more than a minute for vintage PCs.

Electron interactions were ignored in the derivation of the theoretical model and electrons residing in the ridges and the troughs were assumed not to conduct at all. As a result, the admittance of a TDES when the magnetic field remains constant should be zero according to the model, a prediction which is obviously false.

Indeed, electrons in both the ridges and the troughs conduct and electron interactions are important for high electron densities, making the admittance nonzero even when the magnetic field does not change. However, the main result of the model is that a component of the measured admittance should be attributed to a diffusive electron current from and to the troughs as the magnetic field changes. This component will constitute a major part of the measured admittance for low electron densities and low temperatures, but it will be rendered a minority for high electron densities and high temperatures.

Moreover, assuming that the TDES covers the whole area ($1mm^2$) of the substrate and by estimating the number of troughs from the approximation $2r = 800nm$ for the diameter of a trough, the model predicts an admittance which can be directly compared with the measured Y, without the need to employ the transmission line or the equivalent circuit model in order to calculate the conductivity of the TDES.

5.2. Preliminary measurements

Except for the magnetic field, other parameters that influence TDES conductivity include excitation voltage V_{ex}, excitation cyclic frequency ω_{ex}, temperature T, saturated electron density n_s, liquid helium film thickness d and guard voltage V_g.

Of these parameters, V_{ex} and ω_{ex} could be classified as being of a more 'technical' nature, because, although they influence the resolution of measuring signal, they do not alter the physics of TDES *per se*. Their function could be compared to the focusing of a microscope's optical circuit, which sharpens not the studied object itself, but its image.

More specifically, the influence of V_{ex} and ω_{ex} on conductivity σ can be easily predicted by the current mode equations (3.22), (3.23), which lead immediately to

$$\sigma = \sqrt{G_x^2 + (\omega_{ex} C_x)^2} = \frac{1}{V_{ex}} \sqrt{X^2 + Y^2}. \tag{5.1}$$

From the equation above, it becomes obvious that conductivity should be linearly dependent on the excitation cyclic frequency ($\sigma \propto \omega_{ex}$) and inversely proportional to the excitation voltage ($\sigma \propto 1/V_{ex}$). In the upper plot of fig. 5.2, the linear dependence of conductivity on ω_{ex} is verified with an impressive accuracy. In the bottom plot of fig. 5.2, the inversely proportional dependence of

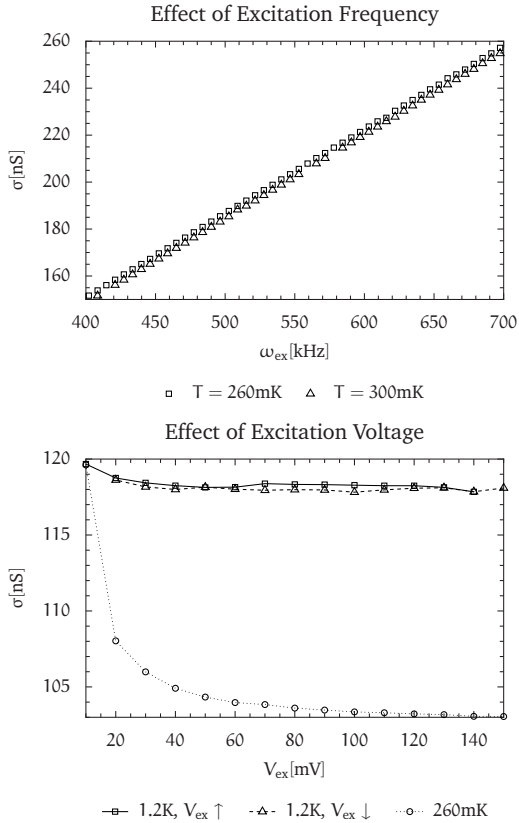

FIGURE 5.2. In the upper plot, conductivity σ plotted against excitation cyclic frequency ω_{ex} at the given temperatures T. In the plot below, σ is plotted against increasing (↑) and decreasing (↓) excitation voltage V_{ex} at the given temperatures. For both plots, the saturated electron density is $n_s = 1.21 \times 10^{13} m^{-2}$ and the holding field voltage, $V_{TB} = 10V$. In the upper plot, the excitation voltage is $V_{ex} = 10mV$ and in the bottom plot, the excitation frequency is $f_{ex} = 55kHz$.

conductivity on V_{ex} is discerned mainly for the low temperature measurement at $T = 0.260K$, because σ remains almost constant for the measurement at $T = 1.2K$. The fact that conductivity is almost independent of excitation voltage for $T \gtrsim 1K$ and varies linearly with excitation frequency means that the precise values of V_{ex} and ω_{ex} are indeed not critical for the physical behavior of a TDES.

Temperature alters the conductivity of a TDES in a nontrivial way. For TDES on bulk liquid helium, conductivity exhibits an exponential increase when T decreases down to approximately 0.7K and a polynomial increase for $T \lesssim 0.7K$ (cf. the discussion on electron mobility in section 1.2).

In fig. 5.3 the conductivity σ of a TDES on a helium film wetting the nanotower is depicted. Evidently, not only σ does not increase exponentially or polynomially for decreasing temperatures but *decreases* instead. Specifically, conductivity exhibits a plateau in the temperature range $0.8K \lesssim T \lesssim 1.3K$ and decreases for temperatures down to 1.3K and below 0.8K. Overall, conductivity has a very low value and does not change significantly.

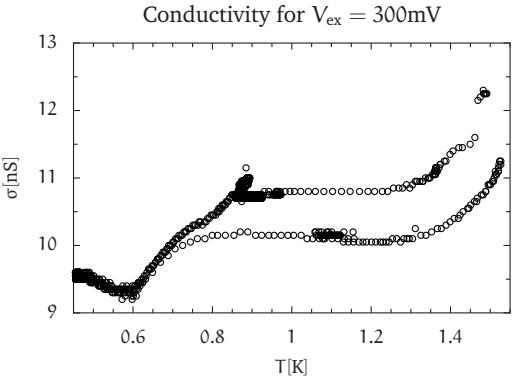

FIGURE 5.3. Temperature dependence for a TDES on a helium film of thickness $d = 39$nm wetting the nanotower substrate. Holding field is 15V, corresponding to a saturated electron density $n_s = 1.83 \times 10^{13} e/m^2$, excitation frequency is $f_{ex} = 65$kHz and excitation voltage is $V_{ex} = 300$mV.

These results appear to be contradictory if it is not realized that electron localization, due to the interaction of the electrons with the dielectric substrate (the nanotower substrate is made of silicon with dielectric constant $\epsilon_{Si} = 11$), is almost complete even in the presence of holding field only, as shown theoretically in section 4.4. If electrons are localized in the presence of holding field only, it should be expected that conductivity would decrease for decreasing temperatures, because the diminishing thermal fluctuations enhance localization.

Guard voltage, depending on its magnitude, confines a TDES to a lesser or greater area, altering in effect the electron density and the degree a TDES covers the whole spatial extent of measuring electrodes. Electron density is a central property of TDES with important consequences on their physical behavior and any influence on it from the value of the guard voltage must therefore be understood.

It was commented in section 1.1.4 that the ability of TDES to screen external fields means that the electric field due to guard voltage does not extend inside the TDES, hence there is no need to apply perturbation methods for electron states parallel to the helium surface (with obvious theoretical advantages).

It also appears in practice that guard voltage affects electron density in a trivial way. More specifically, fig. 5.4 indicates that making V_g more negative increases the conductivity of the TDES, an observation consistent with viewing large negative V_g as "squeezing" the TDES in a smaller area and therefore increasing its density. However, the "squeezing" effect is not pronounced and it saturates after a certain negative voltage, which was never more negative than -6V in the configuration used in the experiments. After that point, making V_g more negative does not have any effect on σ, as seen in fig. 5.4.

Helium film thickness is decisive for the formation of periodic potential wells, especially for low electron densities and films that are thick compared to the trough dimensions (depth and diameter) of a mesoscopic surface. However, the effect of guard voltage on electron density is experimentally found to be

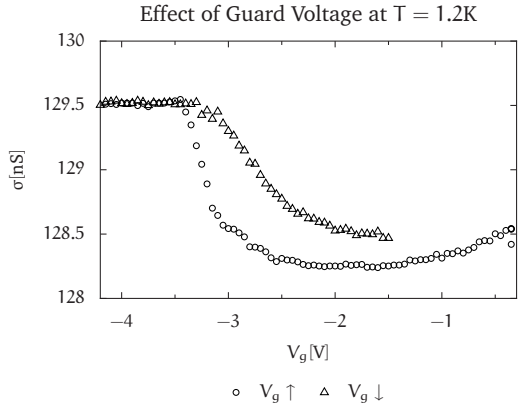

FIGURE 5.4. Conductivity σ of a TDES on the nanotower substrate against guard voltage V_g. Saturated electron density is $7.29 \times 10^{12} m^{-2}$ ($\approx 6.4e$ per trough). Holding field voltage is 6V, excitation voltage is 10mV and excitation frequency is 55kHz. Initial value was $V_g = 1.4V$.

weak, and film thickness cannot be varied in a wide range without encountering problems in charging the liquid helium surface with electrons. For these reasons, guard voltage and bulk liquid helium level—which determines film thickness—remained unaltered throughout most of localization experiments.

5.3. Two estimates for the normalized admittance

The physical quantity that was measured in our experiments was the admittance Y of TDES on deformed liquid helium films. Up to now, apart from the flow admittance Y_f, given by eq. (4.46), which is predicted to be a component of the total admittance, the implications of the model with respect to the total admittance were not explicitly discussed but implied at a qualitative level. In this section, an effort is made to derive a quantitative estimate for the *normalized* admittance (a pure number) based on a modification of the standard Drude model, which was described in section 2.5.1, for TDES on deformed liquid helium films. The Drude model estimates the normalized quantity Y_0/Y, where Y_0 is the admittance for zero magnetic field. In addition, by means of a different physical reasoning, a proportionality is derived for the normalized quantity Y_∞/Y, where Y_∞ is the limiting admittance for extremely strong magnetic fields.

5.3.1. Drude normalized admittance. The basic prediction of the Drude model is the relation $\sigma_0/\sigma = 1 + \mu^2 B^2$, connecting the normalized conductivity σ_0/σ with electron mobility μ and the magnetic field B (the same relation holds for the normalized admittance as well). In the original formulation of the Drude model, the TDES resides on a flat surface and its electrons undergo Landau oscillations. However, the TDES for the particular deformed films considered in chapter 4 partition themselves in two fractions, peak electrons and trough electrons.

If the partial fraction of peak electrons is denoted with n_p, the partial fraction of trough electrons will necessarily be $1-n_p$. Peak electrons perform Landau oscillations and the original Drude model applies without modification, giving a contribution $\left(1+\mu_p^2 B^2\right) n_p$ to the total normalized admittance, where μ_p is electron mobility on the peaks.

Trough electrons on the other hand perform Darwin-Fock oscillations and the derivation of the Drude model outlined in section 2.5.1 no longer applies. Nevertheless, it can be expected that a contribution $F(\mu_t, B)(1-n_p)$ to the total normalized admittance should arise, where $F(\mu_t, B)$ is an as yet unknown function of the magnetic field B that contains electron mobility μ_t in the troughs as a parameter.

Then, the total normalized admittance according to the amended Drude model we propose for TDES on deformed films should be of the form

$$\frac{Y_0}{Y-Y_f} = \left(1+\mu_p^2 B^2\right) n_p + F(\mu_t, B)(1-n_p). \tag{5.2}$$

In the denominator of the normalized admittance the flow admittance Y_f is subtracted from the measured total admittance Y, because its physical origin is different and cannot be described by a Drude model. In the discussion of the experimental data in section 5.5 and especially fig. 5.6 one can easily conclude that the agreement of the model with the experimental data is improved when $Y_0/(Y-Y_f)$ instead of Y_0/Y is considered.

The unknown function $F(\mu_t, B)$ could in principle be calculated by starting off from the Boltzmann equation

$$m\boldsymbol{a} = -\frac{m\boldsymbol{v}}{\tau} - e\nabla(V - \boldsymbol{v}\cdot\boldsymbol{A}), \tag{5.3}$$

which is just eq. (2.14) with the Lorentz force written in terms of the potential V and the vector potential $\boldsymbol{A}$, and following through the steps of the derivation in section 2.5.1 in order to determine the conductivity tensor. However, this approach is no longer straightforward because the potential, except for the AC component $V_0 e^{i\omega t}$ of the lockin amplifier, also contains the DC component given by the general eq. (4.22) due to the deformed topology of the film. For this reason, an approximation of $F(\mu_t, B)$ shall be employed.

More specifically, one can see from eq. (5.2) by setting $B = 0$ that $F(\mu_t, 0) = 1$, since it is $n_p = 0$ and $Y_f = 0$, while by definition $Y = Y_0$ in that case. Let us now generalize and approximate $F(\mu_t, B) = 1$ even for $B > 0$. Then, one can immediately obtain the estimate

$$\frac{Y_0}{Y-Y_f} \approx 1 + \mu_p^2 B^2 n_p \quad \text{when} \quad F(\mu_t, B) = 1, \tag{5.4}$$

for the normalized admittance, which is very similar to the original Drude expression for TDES on flat films.

The effect of the approximation of F was not to ignore any contribution of trough electrons to the total normalized admittance. This would have been the case if it were $F(\mu_t, B) = 0$, leading to the equation $Y_0/(Y - Y_f) = \left(1 + \mu_p^2 B^2\right) n_p$ for the normalized admittance. Essentially, the approximation was to regard the contribution of trough electrons as constant for all magnetic fields. This is correct only if the said contribution is minimal, or equivalently, when trough electrons are very well localized regardless of the magnetic field. It was explained in section 4.4 that for deformed films wetting a dielectric substrate most electrons are already very well localized inside the troughs (and their mobility is correspondingly very small) when a holding field is present even before a magnetic field is applied. The approximation $F(\mu_t, B) = 1$ for $B \geqslant 0$ should therefore not be unjustified.

It has been shown in chapter 4 that n_p is not constant but a function of B among other things. As a consequence, the right-hand side of eq. (5.4) already anticipates that the behavior of the normalized admittance in the left-hand side, which is calculated from the experimental data, will deviate from the straight line one would expect from the normal Drude model, when normalized admittance is plotted against B^2. The open question is whether the anticipated deviation will be predicted in its exact form or not.

5.3.2. Cyclotron radius normalized admittance. One of the initial motivations of localization experiments came about from the intuition that the cyclotron radius of electrons under the influence of a magnetic field $\mathbf{B} = (0, 0, B)$ decreases and promotes their localization. This means that the total measured admittance depends on the cyclotron radius and the form of this dependence should be explored further.

In the context of the model proposed in chapter 4, let peak electrons be characterized by a cyclotron radius $r_c^{(p)}$ and trough electrons by $r_c^{(t)}$. Then, a proportionality

$$Y \propto r_c^{(p)} n_p + r_c^{(t)} (1 - n_p) \tag{5.5}$$

should hold for the total admittance Y.

The generic cyclotron radius is $r = \left(2k_B T/m\omega^2\right)^{1/2}$, where ω is to be substituted with $\omega_c = eB/m$ for peak electrons and $\Omega = \left(\omega_E^2 + \omega_c^2\right)^{1/2}$ for trough electrons (ω_E is defined in eq. 4.26). Even for magnetic fields of several Tesla it is $\omega_c \ll \omega_E$ and one can write $\Omega \approx \omega_E$ with good accuracy. Then, by replacing r_c in eq. (5.5) with the proper expression with respect to ω, it is found that

$$Y \propto \frac{1}{\omega_E} \left(\frac{2k_B T}{m}\right)^{1/2} \times \left(1 + \left(\frac{\omega_E}{\omega_c} - 1\right) n_p\right), \quad \text{for} \quad \omega_c \ll \omega_E. \tag{5.6}$$

For obtaining the normalized admittance one could proceed to divide Y_0 by Y as given in eq. (5.6). However, a more elegant proportionality turns out if

instead the limiting admittance Y_∞ for very strong magnetic fields is used. Of course, at the limit $B \longrightarrow \infty$ it is $Y_\infty = 0$ and therefore a more realistic limit, like the (very strong) B where $\omega_c \approx \omega_E$ should be used, which then leads to the limiting value

$$Y_\infty \longrightarrow \frac{1}{\omega_E}\left(\frac{2k_B T}{m}\right)^{1/2} \quad \text{for} \quad \omega_c \approx \omega_E. \tag{5.7}$$

The proportionality that connects the normalized admittance with $\omega_c = eB/m$ and the partial fraction of peak electrons n_p can then be written down very elegantly as

$$\frac{Y_\infty}{Y - Y_f} \propto \frac{1}{1 + \left(\frac{\omega_E}{\omega_c} - 1\right) n_p}. \tag{5.8}$$

Comparing eqs. (5.4) and (5.8) the following comments can be made:

- Normalized admittance of eq. (5.4) begins with a value of unity and is always a number *greater* than unity for stronger B.
- Normalized admittance of eq. (5.8) is always a number *less* than unity and approaches unity for strong B.
- The opposite behavior of normalized admittance exhibited by eqs. (5.8) and (5.4) can be traced back to the fact that $Y_0 > Y_\infty$.

It should be kept in mind that eq. (5.4) is an approximation, while eq. (5.8) a *proportionality*. By plotting $Y_0/(Y - Y_f)$ there should be an appropriate fit with $1 + \mu_p^2 B^2$, from which electron mobility μ_p can be determined. In contrast, a plot of $Y_\infty/(Y - Y_f)$ must be multiplied by a proportionality factor in order to become comparable with the right-hand side of eq. (5.8). However, after the multiplication by this factor, which cannot be predicted by the model, the form of the two curves should be the same.

5.4. Physical intuition for the behavior of admittance

From the theoretical developments so far, a physical intuition emerges for the behavior of the admittance Y, which will be summarized here for the sake of clarity before we proceed with the discussion of the measurements.

5.4.1. Finite admittance is a result of diffusion. First and foremost, a finite nonzero admittance is the result of electron diffusion and at the limit where diffusion ceases to exist admittance can only be zero or infinite [**82**]. This means that the weakening of diffusive processes leads ultimately to a limiting value of the admittance: if the limiting value is infinite, then admittance necessarily increases, otherwise, admittance must decrease.

For TDES admittance arises from scattering processes between electrons and helium gas atoms (for $T > 0.7$K) or ripplons (for $T < 0.7$K) and its limiting value in the absence of diffusion is zero (this is a general result for two-dimensional

systems [1]). Scattering of electrons by helium gas atoms becomes exponentially weaker with decreasing temperature, while scattering by ripplons only polynomially so[3]. As a result, the admittance of TDES can only decrease when temperature decreases, because diffusive processes, or equivalently scattering mechanisms, weaken.

This behavior is the complete opposite of what is observed for the system of the three-dimensional electron gas in the conduction band of metals, where the admittance of course *increases* for a decreasing temperature. The main (diffusive) scattering mechanism of electrons is collisions with the ion grid, or equivalently the coupling of electrons to phonons, which decreases with decreasing temperature exactly like the coupling of TDES to ripplons. But due to the fact that the limiting value of the admittance in the absence of diffusion is infinite for this system, weakening of diffusive mechanisms actually increases the admittance.

5.4.2. The natural triplet and its effects on the admittance. The physical properties of the admittance in our system are a function of the triplet (T, B, n_s), namely temperature, magnetic field and saturated electron density. Certainly, admittance depends also on parameters like the dielectric constant of the substrate and the thickness of the liquid helium film, or excitation voltage and frequency, but these cannot or will not change in the course of a measurement, in the particular way it was performed at least. Let us further analyze the expected *generic* effect each member of the triplet has on the admittance when the other two are kept constant. Generic means in this context that the complications of electron kinetics, especially diffusion of electrons to and from the peaks of the substrate, which alters the partial fractions of electrons in troughs and peaks, are ignored for the time being. Then, we have the following:

Increasing temperature should lead to a monotonically higher admittance because it weakens electron localization in both troughs and peaks. This can be understood, if one recalls from previous chapters the definition of the cyclotron (classical) radius $r_c = \left(2k_B T/m\omega^2\right)^{1/2}$, which is a measure of electron localization in the sense that larger r_c imply less localized electrons, more prone to diffusive processes and therefore more conductive (see eq. 4.42 and the relevant discussion). The proportionality $r_c \propto T^{1/2}$ means that Y should increase for an increasing temperature and from eq. (5.6) it is seen that $Y \propto T^{1/2}$ as well.

Increasing magnetic field on the other hand should lead to a monotonically lower admittance because it enhances electron localization in both troughs and peaks. Again, this can be understood from the definition of r_c if one recalls

[3] An equivalent formulation occasionally used in the literature is in terms of the *coupling* of TDES to helium gas atoms and ripplons. Then one could say, for example, that the coupling of electrons with ripplons is stronger than the coupling with helium gas atoms for lower temperatures, or that the coupling of electrons with ripplons exhibits a polynomial dependence on temperature.

that $\omega = eB/m$ for electrons on peaks and $\Omega > \omega$ for electrons in troughs[4]. The dependence of cyclotron radius with B now has the form $r_c \propto B^{-1}$ and from eq. (5.6) one gets $Y \propto B^{-1}$ for the admittance.

Increasing saturated electron density enhances Coulomb interactions, which were left out of the theoretical treatment so far. It is therefore not easy to predict their influence when they become important. A quantitative measure of the strength of Coulomb interactions is the Γ parameter, discussed in sections 1.4 and 2.3, which can be calculated by means of the eq. (2.10). A Wigner crystal is theoretically expected for $\Gamma > 125$ but experimentally it is found that it forms for $\Gamma \gtrsim 137$. Gamma parameter is always provided in the caption of measurement plots. For the measurements with a combination of (n_s, T) that allows the formation of a Wigner crystal, admittance does exhibit deviations from what is expected from the theoretical model, the deviations' features and physical interpretation being extensively discussed in sections 5.5.2 and 5.5.3. The conclusion of the relevant discussion is that Coulomb interactions are important when a Wigner crystal is formed but much less so otherwise.

5.4.3. Admittance is mainly due to peak electrons. Another intuition is that electrons in peaks should contribute more to the conductivity—and therefore also the admittance—than electrons in troughs. This follows immediately from the fact that r_c (the classical radius of electron motion) is much greater for peak electrons than troughs electrons because $\omega_c < \Omega$. In turn, this is a consequence of the fact that peak electrons perform *Landau* oscillation while trough electrons perform *Darwin-Fock* oscillations. Therefore, the following are completely equivalent formulations:

- Trough electrons are better localized than peak electrons.
- Peak electrons diffuse more than trough electrons.
- Peak electrons contribute more to conductivity (admittance) than trough electrons.

It is important to realize that the kinetics of electrons proposed here are in sharp contrast to that of the two-fraction model [**56**], where the emerging physical picture considers electrons on rough peaks as essentially "pinned" due to the very strong interaction of those electrons with the underlying dielectric substrate. This, effectively, means that only the "unpinned" part of TDES should be active (i.e trough electrons in our case), or that electrons on rough peaks should not contribute to properties such as electron mobility and conductivity.

However, the size of the peaks, the sufficient thickness of the film on the peaks (approximately 25nm) and the periodical nature of the substrate's surface leads us to adopt a completely different physical picture, namely, that electrons

[4]Electrons in troughs perform *Darwin-Fock* oscillations due to the presence of holding field and Ω is the respective quantum of oscillation.

should be essentially unpinned and mobile in both peaks and troughs, or, to formulate more drastically, the effects of substrate roughness should be disregarded. Therefore, according to our physical picture, which is corroborated by *Valkering et al.* [**110**], electrons are in principle free to move from a peak to a trough and vice versa.

5.4.4. Expected phenomenology. The physical intuition developed so far suggests a rather simple phenomenology for what could be expected from measurements of the form $Y = Y(B)$: admittance should monotonically decrease for increasing B without exhibiting any maxima or minima. Moreover, for $T_1 < T_2 < \ldots < T_m$ there should be a regular ordering $Y_1(B) > Y_2(B) > \ldots > Y_m(B)$, while for $n_s^{(1)} < n_s^{(2)} < \ldots < n_s^{(m)}$ there should also be a general ordering $Y_1(B) < Y_2(B) < \ldots < Y_m(B)$, which could be irregular.

However, a simple inspection of the measurements in figs. 5.5 through 5.11 is enough in order to realize that TDES on a deformed surface seem to exhibit a much richer phenomenology, unless one would adopt the *trivial* approach of dismissing the maxima of Y in several measurements as artifacts, or else adopt the *deus ex machina* approach and attribute them to uncontrolled experimental factors like substrate roughness, pinned charges and the like.

A physical factor that was left out until now is the effect of TDES statistical mechanics and in particular its effect on the partial fractions of electrons in troughs and peaks together with the resulting flow admittance. Indeed, it was shown for TDES on deformed liquid helium films that when the magnetic field changes the distribution of electrons on the peaks and in the troughs changes as well. A TDES should then no longer be regarded as a monolithic entity with a uniform density but rather as made up of three component systems.

5.4.5. The three component systems. A TDES on a deformed liquid helium film and in the presence of holding and magnetic field partitions in three component systems with different contributions to the admittance and different densities. These component systems are the *trough electrons*, the *peak electrons* and the *flowing electrons*.

Flow Electrons: This system comprises of those electrons that move *to* or *from* the troughs of the deformed film at any instant of time. They belong neither to the troughs nor to the peaks and their contribution to the admittance is the flow admittance defined in eq. (4.46). This system ceases to exist when $dB/dt = 0$ and flow admittance becomes zero in that case.

Peak Electrons: This system comprises of all electrons localized on the peaks of the deformed film. They perform *Landau* oscillations and their contribution to the admittance is expected to be of the form $Y \propto B^{-1}$.

Trough Electrons: This system comprises of all electrons localized inside the troughs of the deformed film. They perform *Darwin-Fock* oscillations and as a result r_c is much smaller than that of peak electrons. Consequently, they are better localized and contribute less to the admittance than peak electrons and flow electrons, although it is expected that $Y \propto B^{-1}$ as in the case of peak electrons.

A much richer phenomenology can be accounted for, when the effect of TDES statistical mechanics is included, because the origins of the measured admittance become diverse and can counteract with each other.

In particular—and this is a perfectly possible scenario—, the general decrease of the admittance when the magnetic field increases could be counteracted not only by the flow admittance but also by an increasing partial fraction of peak electrons, which as it was repeatedly stated are more conductive than trough electrons. From eq. (5.6) it is seen that this scenario comes about when $n_p(B)/B$ is an increasing function for an interval of B, for example when n_p is of the form $n_p(B) = aB^2 + bB + c$.

Of course, in the end, the induced localization from the magnetic field takes over in both peaks and troughs of the deformed charged film and for sufficiently high B (say, when Y from peak and trough electrons approaches zero) only flow admittance should be measured. Thus, in that way, a means of calibration and a reality check is obtained for the proposed model because the numeric value of flow admittance should not be far from the measured Y in the limit of strong magnetic fields.

The amended Drude model of eq. (5.4) and the cyclotron radius approximation of eq. (5.8) are complementary with each other, in a sense which we shall try to make more precise. More specifically:

- The amended Drude model, eq. (5.4), could explain minima (values $Y(B) < Y_0$) in the evolution of the admittance, where by definition $Y_0/Y > 1$. But it *cannot* explain or even predict admittance maxima (values $Y(B) > Y_0$) because the right-hand side of eq. (5.4) is always greater than unity.
- The cyclotron radius model, eq. (5.8), could explain admittance maxima (values $Y(B) > Y_\infty$), where by definition $Y_\infty/Y < 1$. But it *cannot* explain or even predict minima in the evolution of the admittance (values $Y(B) < Y_\infty$) because the right-hand side of eq. (5.8) is necessarily less than unity.

These important observations should be kept in mind in the analysis of the experimental data, where one encounters cases where $Y(B) > Y_0$ and $Y(B) < Y_\infty$ (see for example fig. 5.9A and the relevant discussion).

In order to assist the interpretation of the experimental results by means of the physical intuition exposed here, all measurements in section 5.5 are organized in the following manner:

- A plot of $Y = Y(B)$, usually for both increasing and decreasing magnetic field sweeps is given.
- A plot of the partial fraction of peak electrons as a function of B is given, calculated as $1 - n_{v,l}/n_s$, with $n_{v,l}/n_s$ obtained from eq. (4.45).
- A plot of the flow admittance as a function of B, as calculated from eq. (4.46), is given.

Moreover, a plot of the normalized admittance as a function of B^2 is provided, according to eq. (5.4), first for the case when flow admittance is ignored ($Y_f = 0$) and subsequently for when it is included.

The physical intuition built in this section should suffice for the careful reader to interpret the experimental data without further commenting on our part. It is, however, customary to provide a detailed commentary for the measurements, into which we now embark.

5.5. Results and discussion

In this section, measurements are presented and commented, along with predictions of the theoretical model developed in chapter 4, on quasi zero dimensional electron localization on helium films wetting the nanotower substrate.

Bulk liquid helium level was kept 0.5mm below the surface of the nanotower substrate (the nanotower is 0.5mm thick, meaning that the surface of bulk liquid helium is located roughly at the base of the substrate), which by eq. (4.6) means that the suspended helium film is approximately 82nm thick.

Under conditions of constant film thickness and a guard voltage sufficiently negative to ensure the maximum saturated signal, the filament (source of electrons) was fired until saturated electron density was achieved for a given holding field between the top and the bottom plate.

Firing of the filament always took place at temperatures of about 1.35K to 1.40K, to prevent the substrate from being charged with electrons. Indeed, as explained in section 3.3, charging with a filament must proceed with diffused, not ballistic electrons. The temperature then was brought slowly at the desired level and stabilized there before the main measurement began.

The main measurement consisted of *continuous* magnetic field sweeps at a constant rate 0.167T/s from zero up to a maximum value and then back to zero. In this way, the possibility of artifacts was reduced and the reproducibility of the measurements tested.

It must be noted that proper parameters, especially with regard to helium film thickness and electron density (voltage difference between top and bottom plate), proved to be critical for creating a measurable signal out of TDES.

Thinner helium films would not support stable, measurable TDES and electron density could not be altered without significant efforts. Signals of TDES would not be measurable even after extensive pulsing with different combinations of guard voltage, excitation voltage and frequency, sometimes they would appear but not persist as the temperature was reduced, or even disappear and reappear after some time.

The source of these problems could be attributed to the fact that, due to the strong interaction with the dielectric substrate, electrons are strongly localized even without the application of a magnetic field, with the result that their conductivity may become so small as not to be measurable, or insensitive to changes in the magnetic field.

The fact that a film thickness of approximately 80nm proved to be "ideal" for the measurements could then indicate that this thickness is large enough to allow a weaker interaction of the TDES with the substrate, and yet still smaller than the peaks of the nanotower (100nm), so that the periodic potential wells for quasi zero dimensional localization are deep enough.

The sensitivity of the system to the thickness of the helium film and the electron density, as well as its proneness to failure due to substrate charge could be only partially adressed and are by far the most critical impediments to a rich, systematic experimental study. It could well be stated that the presented data were won in the very end from an unruly system that would not let be brought under full command.

An aspect of the data presented in figs. 5.5 through 5.11, which is used as a classification, is their different overall character with respect to temperature. From fig. 5.3 it can be seen that conductivity exhibits a plateau in the temperature range $0.8\text{K} \lesssim T \lesssim 1.3\text{K}$. In this *intermediate* temperature range belong the measurements of figs. 5.9 and 5.11, whereas the measurement of fig. 5.5 belongs to the *low* temperature range and that of fig. 5.7 to the *high* temperature range.

5.5.1. Low temperature and electron density. The behavior of admittance in the low temperature, low electron density regime, both experimentally and theoretically, is depicted in fig. 5.5. At a temperature of 550mK, where electron scattering with helium gas atoms is insignificant, trough electron density is just 3.7e per trough, and a Wigner crystal—as evidenced by an inspection of fig. 2.2—cannot form, it is observed that admittance monotonically decreases for an increasing magnetic field. More specifically, admittance exhibits two regimes in its evolution, one of quick decrease for $0\text{T} \leqslant B \leqslant 0.3\text{T}$ and a second one of slower decrease of $B \geqslant 0.3\text{T}$.

Notice that the onset of the linear regime at $B \approx 0.3\text{T}$ is very near to the magnetic field $B_0 \approx 0.35\text{T}$ where the diffusive electron flow from the troughs to the peaks is reversed. The reversal of electron flow is recognized in fig. 5.5B from the maximum that is exhibited by the partial fraction of peak electrons.

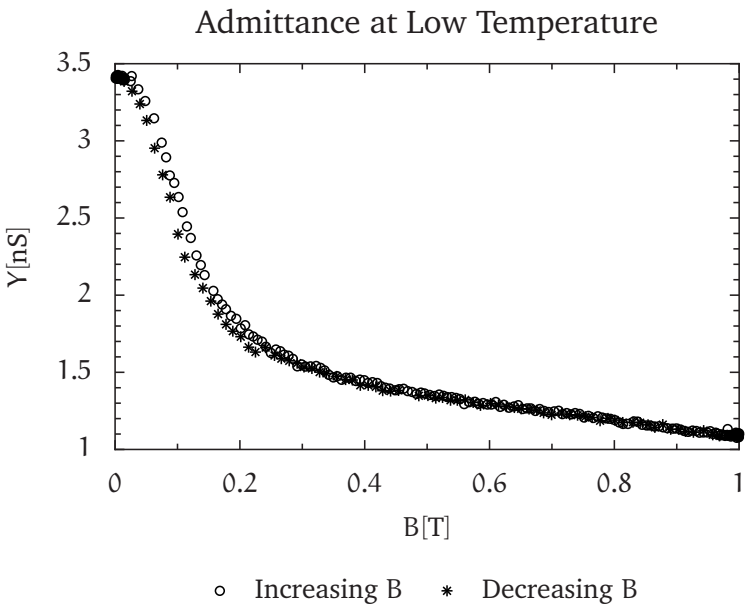

(A) Measured admittance

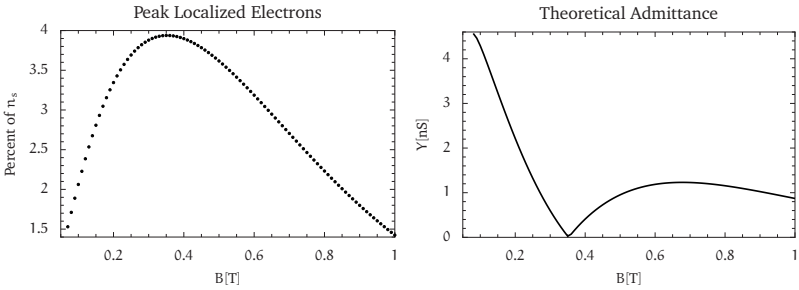

(B) Electrons on substrate peaks

(C) Flow admittance

FIGURE 5.5. Admittance (Y) of a TDES plotted against the magnetic field (B). In (A), the measured admittance at a temperature $T = 550\text{mK}$ is plotted. The saturated electron density is $n_s = 7.29 \times 10^{12}\text{m}^{-2}$, corresponding to $\approx 3.7e$ per trough and $\Gamma = 78$. Holding field voltage is $V_{TB} = 6\text{V}$, excitation voltage is $V_{ex} = 10\text{mV}$ and excitation frequency is $f_{ex} = 55\text{kHz}$, while B was changing at a rate of 0.167T/s. In (B), the dotted curve shows the partial fraction of electrons on the peaks of the nanotower as a function of B. The partial fraction is expressed as a percentage of the n_s. In (C), the flow admittance for the same conditions is plotted. Flow admittance results from the absolute value of the first derivative of an interpolation of the dotted curve in (B) with respect to B according to eq. (4.46).

For magnetic fields weaker than B_0 the partial fraction of peak electrons increases quickly, yet after B_0 the decline of peak electron partial fraction is not as quick. Indeed, peak electrons constitute 1.5% of the total when $B = 0.1$T and their percentage rises to 4% when $B = 0.35$T, making up a mean rate of change of $+10\%$ per Tesla, while the respective mean rate of change for the decline is only -3.65% per Tesla. These different rates of increase (decrease) are reflected in the evolution of the flow admittance, depicted in fig. 5.5C, which is essentially the absolute value of the first derivative of the curve in fig. 5.5B with respect to the magnetic field.

Comparing the magnitude of flow admittance Y_f in fig. 5.5C with the measured admittance in fig. 5.5 it is seen that the theoretical model certainly overestimates the flow admittance, especially for weaker magnetic fields, where Y_f is somewhat larger than the measured admittance. Low temperatures and electron densities are admittedly the physical conditions where the model we propose is expected to be more accurate, but still Y_f cannot be solely responsible for the measured admittance because peak electrons should also contribute to Y.

Turning to eqs. (4.46) and (4.48), it is seen that sources of Y overestimation could be errors in the estimation of electron density and errors in the estimation of the voltage difference between a trough and a peak.

In turn, errors in the estimation of voltage difference arise from errors in the effective diameter of a trough and from the fact that it was considered constant. One could correct the estimation of Y_f in view of the experimental results, but this should be done by means of a convincing procedure. Such a procedure is shown in fig. 5.6, where the upper plot depicts the normalized admittance Y_0/Y without taking into account Y_f at all, while the bottom plot depicts the normalized admittance $Y_0/(Y-Y_f)$ after taking into account flow admittance. The solid line in both plots is a fit according to the amended Drude model eq. (5.4) and it provides us with an estimate of the peak electron mobility μ_p in each case.

An inspection of the upper plot of fig. 5.6 indicates that the almost linear evolution of Y_0/Y cannot be captured by the always more "curvy" Drude fit. One could argue that the ugly fit is a fault of the amended Drude model and that the standard Drude model of eq. (2.21), which is linear in B^2, would have been ideal in this case, but this route would completely fail to address every single measurement to be subsequently presented in this thesis, whose normalized admittance generally does not increase linearly in B^2 but saturates for strong magnetic fields (see for example fig. 5.10). Therefore, it seems more appropriate to use the amended Drude model of eq. (5.4) and include the effects of Y_f in the normalized admittance. This is done in the bottom plot of fig. 5.6, where it is immediately seen that $Y_0/(Y-Y_f)$ becomes more "curvy", making the fit with the amended Drude model much better.

It was noted in the previous paragraphs that Y_f is certainly overestimated by the model. A better estimate can be obtained by trying to obtain a better

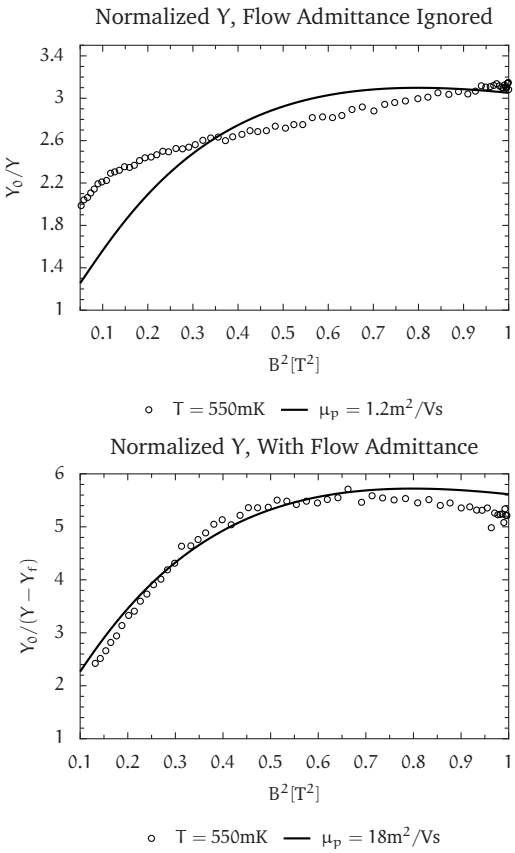

FIGURE 5.6. Normalized admittance of the TDES of the measurement in fig. 5.5 plotted against the square of the magnetic field. In the upper plot flow admittance is ignored, therefore normalized admittance is Y_0/Y where Y_0 is the value when $B = 0$. The solid line is a fit according to the modified Drude model, eq. (5.4) for $Y_f = 0$. The bottom plot shows the same measurement and the corresponding fit when flow admittance Y_f (see fig. 5.5C) is included. The partial fraction n_p of electrons on peaks is for both plots shown in fig. 5.5B. The inclusion of Y_f improves the agreement of the model with the experimental data. Estimated mobility μ_p of peak electrons differs by one order of magnitude.

fit in the bottom plot of fig. 5.6. More specifically, flow admittance was scaled by multiplying the values depicted in fig. 5.5C with a constant scale factor, the best of which appears to be 0.5. This scale factor is always used in the relevant subsequent plots for easier comparison. Flow admittance is a much smaller component of the total admittance for the rest of the measurements, but its inclusion greatly affects the estimated peak electron mobility μ_p in each and every case. The reader can verify that when Y_f is included the estimated μ_p is one order of magnitude greater than otherwise.

Summarily, the information gained from the low temperature, low electron density regime is that the theoretical model is well applicable and that the concept of flow admittance is relevant for a better description of the experimental data, although the data indicate that it should be at least half the theoretically calculated value.

5.5.2. High temperature and intermediate electron density. In the high temperature range and intermediate electron density shown in fig. 5.7A, electron scattering with helium gas atoms dominates, while the higher electron densities in comparison to the measurement of fig. 5.5 means that Coulomb interactions might also be important.

Indeed, just an inspection of the measurements in figs. 5.5A and 5.7A reveals a different evolution with respect to the magnetic field. While obviously in both measurements the admittance ultimately decreases for an increasing B as one would expect, the nature of the decrease is different and actually differs even for the measurements within the high temperature regime, which have two slightly different temperatures ($T = 1.32K$ and $T = 1.35K$) but different electron densities (24.4e and 18.32e per trough).

The different behavior of the two measurements in fig. 5.7A cannot be an artifact, because magnetic field sweeps for each proceeded in both directions (increasing and then decreasing field) without giving different results.

As one would expect, for the measurement at $T = 1.32K$, which is characterized by a higher electron density than that at $T = 1.35K$, admittance has a higher magnitude but it nevertheless diminishes faster for strong magnetic fields.

It should be also noted that the onset of the strong decline of $Y(T = 1.32K)$ at about 0.8T is very near to the maximum exhibited by the percentage of peak electrons at about 1T, as shown in fig. 5.7B. However, a similar maximum of the percentage of peak electrons for $Y(T = 1.35K)$, which has a lower electron density is not associated with the onset of any decline of the admittance, as $Y(T = 1.35K)$ instead exhibits a plateau around that magnetic field (0.9T). In fig. 5.7B, as for the low temperature, low electron density measurement of fig. 5.5B the mean rate of increase of the percent of peak electrons is much greater before the maximum, than the respective mean rate of decrease after the maximum.

Flow admittance is depicted in fig. 5.7C, where it is seen that for both measurements its magnitude is much smaller than the total admittance but not negligible.

Clearly, at a high temperature and electron density it is not as straightforward to apply the physical intuition of the model as in the low temperature, low electron density regime. In particular, the simplifying assumption of no Coulomb interactions certainly no longer holds, but it is not as yet immediately obvious what features of the admittance are affected thereby.

The plots of normalized admittance against B^2, shown in fig. 5.8, turn out to be more revealing for certain features not pronounced in fig. 5.7A, which are very helpful in order to recognize and interpret what the physical aspects of Coulomb interaction influence might be.

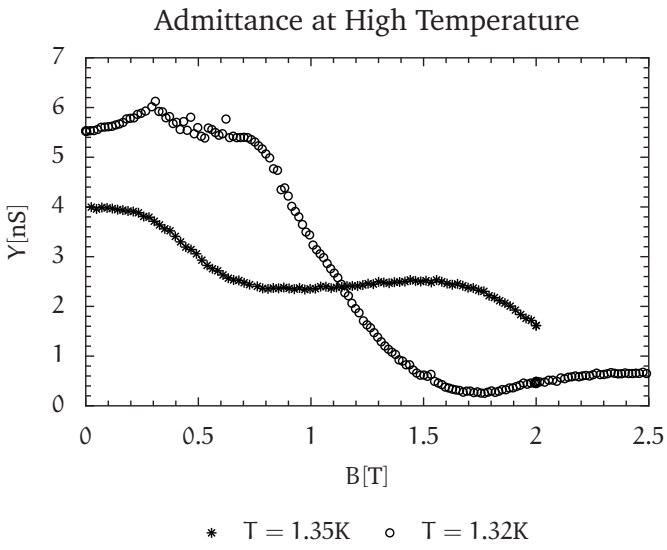

(A) Measured admittance

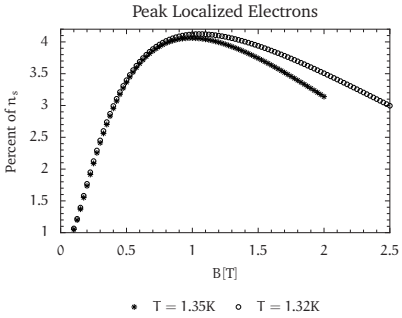

(B) Electrons on substrate peaks

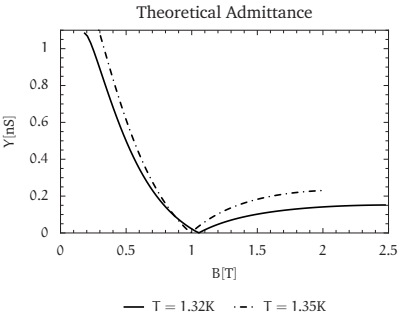

(C) Flow admittance

FIGURE 5.7. Admittance (Y) of a TDES plotted against the magnetic field (B). In (A), the measured admittance at the given temperature T and saturated electron densities $n_s = 4.86 \times 10^{13} m^{-2}$ ($T = 1.32K, \Gamma = 142$) and $n_s = 3.64 \times 10^{13} m^{-2}$ ($T = 1.35K, \Gamma = 115$), corresponding respectively to $\approx 24.4e$ and $\approx 18.32e$ per trough is plotted. Holding field voltage is $V_{TB} = 40V$, excitation voltage is $V_{ex} = 10mV$ and excitation frequency is $f_{ex} = 65kHz$, while B was changing at a rate of $0.167T/s$. In (B), the curves show the partial fraction of electrons on the peaks of the nanotower as a function of B. The partial fraction is expressed as a percentage of the respective n_s. In (C), the flow admittance for the same conditions is plotted. Flow admittance results from the absolute value of the first derivative of an interpolation of the curves in (B) with respect to B according to eq. (4.46).

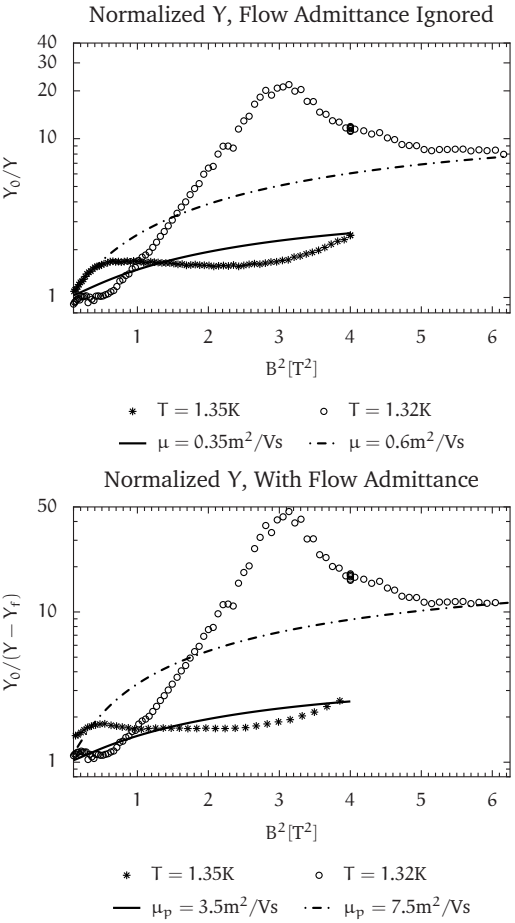

FIGURE 5.8. Normalized admittance of the TDES of the measurement in fig. 5.7 plotted against the square of the magnetic field. In the upper plot flow admittance is ignored, therefore normalized admittance is Y_0/Y where Y_0 is the value when $B = 0$. The solid line is a fit according to the modified Drude model, eq. (5.4) for $Y_f = 0$. The bottom plot shows the same measurement and the corresponding fit when flow admittance Y_f (see fig. 5.7C) is included. The partial fraction n_p of electrons on peaks is for both plots shown in fig. 5.7B. The inclusion of Y_f does not improve the agreement of the model with the experimental data, but the estimated mobility μ_p of peak electrons differs by one order of magnitude.

The measurement $Y(T = 1.35K)$ in the upper plot of fig. 5.8, where flow admittance is not taken into account, overshoots the amended Drude fit (solid line) for weaker magnetic fields and undershoots it for stronger B. This behavior is not qualitatively different than that exhibited by the low temperature, low electron density measurement in the upper plot of fig. 5.6, but as evidenced in the bottom plot of fig. 5.8 it still persists even when flow admittance is included. Of course, as it can be discerned from fig. 5.7C, flow admittance contributes much less to the total Y than in the case of the low temperature measurement and its influence in correcting the discrepancy of the normalized admittance and the fit is damped. But in principle it would have been possible to obtain a much better agreement of $Y_0/(Y-Y_f)$ with the Drude fit, if Y_f were much larger but preserved the same form as in 5.7C.

Flow admittance by definition is proportional to the rate of change of the partial fraction of peak electrons with respect to the magnetic field (dn_p/dB) and inversely proportional to the voltage difference between a trough and a peak. A value of Y_f larger than what the model predicts[5] would necessarily mean that:

- The flow of electrons from the troughs to the peaks is underestimated and is actually larger than what the model predicts. This would affect the calculation of $n_p(B)$ (see section 4.5) and the very form of the equation of statistical equilibrium.
- The voltage difference between a trough and a peak is overestimated and is actually less than what the model predicts. This has an effect only in the calculation of Y_f and does not affect $n_p(B)$ or the equation of statistical equilibrium (see section 4.5).

Physically, these two effects are not completely independent, because a smaller peak-trough voltage difference would make the potential barrier for trough electrons easier to overcome, with the result that electron flow to the peaks would be enhanced and its rate increased. After all, the existence of a potential barrier between a trough and a peak is precisely what ultimately leads to the two different systems (trough and peak electrons) and the equilibrium between them through electron flow.

But then, what are the physical reasons for the trough-peak voltage difference to be smaller than what the model predicts?

Obviously, the only relevant physical factors that differ for the measurement in fig. 5.6 and $Y(T = 1.35K)$ in fig. 5.8 are *temperature* and *electron density*. Temperature is adequately taken into account in the model, but Coulomb interactions among electrons when trough electron density increases are totally ignored. It is not easy to foresee the effect of Coulomb interactions in the equation of statistical equilibrium—the effects on the form of $n'_p(B)$—but it is very probable that the peak-trough voltage difference should be expected to be generally *reduced* for an increasing trough electron density. Indeed, a peak electron would be more likely to be repelled and not so easily reenter a trough when many electrons are already there. Complementary, it would be no longer so difficult for a trough electron to escape to a peak because the repelling force of the other trough electrons would help it. If this is the case, then the peak-trough voltage difference would be less, flow admittance Y_f would be much higher and the agreement of the normalized admittance for the measurement at $T = 1.35K$ with the amended Drude model is almost guaranteed to be as good as in the bottom plot of fig. 5.6.

The features of the measurement $Y(T = 1.32K)$ depicted in fig. 5.8 are of a different kind. In both the upper and the bottom plot of fig. 5.8 (without and with

[5]Notice that the general correction of Y_f by a scale factor of 0.5 as discussed in section 5.5.1 is already included. Here, the emphasis is in physical factors that were not considered in the model and would make trough-peak voltage difference smaller for this specific measurement.

the inclusion of Y_f respectively) normalized admittance undershoots the Drude fit curve for magnetic fields up to 1.22T ($B^2 = 1.5T^2$) and then greatly overshoots the fit curve for stronger fields. This is the exact opposite behavior from what the measurement $Y(T = 1.35K)$ exhibits and obviously the proposed remedy for a better fit of that measurement (greater Y_f due to increased trough electron density), while also applicable for $Y(T = 1.32K)$, would actually exacerbate the exhibited behavior and not correct it. Clearly, something else is at play here.

It should be recalled that an undershoot of the *normalized* admittance means that the admittance is *larger* than it should be, while similarly an overshoot of the normalized admittance indicates that the admittance is less than it should be. A plot $Y = Y(B)$ is inverted and in a certain sense stretched larger in both the abscissa and the ordinate (notice the logarithmic scale) when it is plotted in the form $Y = Y_0/Y(B^2)$.

Therefore, we are after physical factors that would cause the TDES to be more conductive (diffusive) for weak fields and much less conductive (diffusive) for stronger fields than what the amended Drude model suggests.

A closer look in the parameters of the measurements laid out in the caption of fig. 5.7 and especially the respective Γ parameters[6] furnishes the decisive physical factor, namely Wigner crystallization. It is seen that $\Gamma = 142$ for the measurement $Y(T = 1.32K)$, a value safely above 137, which is the critical Γ for the formation of a Wigner crystal. Measurement $Y(T = 1.35K)$ has $\Gamma = 115$ and therefore it can be claimed with some confidence that no Wigner crystal is formed, although the temperature and electron density are very close with those of $Y(T = 1.32K)$.

In sections 1.4 and 2.3 of the theoretical part of the thesis it was explained that the formation of a Wigner crystal is a result of TDES statistical mechanics and especially Coulomb interactions. A crystallized TDES has a much *lower* admittance than an uncrystallized one because diffusive processes are minimized precisely due to the crystallization of the TDES.

Recall that lower admittance implies a *higher* value of the respective normalized admittance, meaning that the formation of a Wigner crystal should be visible as a marked peak in a plot of $Y_0/Y(B^2)$. Similarly, the destruction of a Wigner crystal should be visible as a marked trough in a plot $Y_0/Y(B^2)$. The magnetic field does not enter as a term in eq. (2.10) and therefore Γ parameter is independent of B. As a consequence, whenever $\Gamma > 137$, a Wigner crystal has already formed for $B = 0$.

Let us turn our attention once more to the measurement $Y(T = 1.32K)$ in fig. 5.8. According to the analysis in the previous paragraphs, the evolution of this measurement can be interpreted in the following manner:

[6] All Γ parameters were calculated from eq. (2.10) and they do not depend on B.

- The TDES starts off as a Wigner crystal for $B = 0$ with all electrons residing in the troughs.
- As B starts to increase, the Wigner crystal is disturbed or fractured and electrons escape to the peaks, giving rise to a strong Y_f. Peak electrons are not crystallized and their admittance is high. As a result normalized admittance undershoots the Drude fit.
- As B continues to increase, peak electrons 'stabilize', flow admittance is low and a Wigner crystal encompassing peak electrons is formed so that admittance declines once more. This is revealed as an increase of the normalized admittance up to a maximum in fig. 5.8.
- From that point onwards, admittance slowly increases due to Y_f and slowly moves towards a limiting value. This regime coincides with the decline of the normalized admittance after the maximum in fig. 5.8.

It is remarkable how an innocent-looking variation in the parameters (n_s, T) could lead to such a markedly different evolution. Also important, is the fact that the magnetic field *de*stabilizes localization (in the form of a Wigner crystal or otherwise) in the first stages of the sweep, due to electrons escaping in the peaks.

Summarily, the information gained from the high temperature, intermediate electron density regime is that the model overestimates the peak-trough voltage difference, when electron density is not low, and as a result flow admittance is lower than it should. The agreement of the model with the experimental data when flow admittance is corrected is expected to be good and comparable to that of the low temperature regime. When a Wigner crystal is formed, the evolution of normalized admittance cannot be captured by the model. However, the effects due to the formation or destruction of a Wigner crystal can be recognized from the areas where the normalized admittance is higher or lower than the amended Drude fit.

5.5.3. Intermediate temperatures, different electron densities. The importance of TDES Coulomb interactions in general and Wigner crystallization in particular was manifest in measurement $Y(T = 1.32K)$ shown in figs. 5.7 and 5.8. But as it currently stands, that measurement is still an outlier and further corroborating data are needed in order to confirm the interpretation put forth in section 5.5.2 regarding the influence of Wigner crystallization on the behavior of the admittance.

Thus, in this section admittance measurements made at very similar temperatures are presented, where the parameter Γ corresponds to TDES that should be deep into the Wigner crystallization regime. Once more, the plot $Y = Y(B)$ for those measurements, depicted in fig. 5.9A, does not reveal all physical aspects are present in the evolution of the admittance. Therefore, a complementary plot of the normalized admittance against B^2 is also provided in fig. 5.10. Recall that a plot $Y_0/Y(B^2)$ is an *inverted* and *stretched larger* version of $Y(B)$.

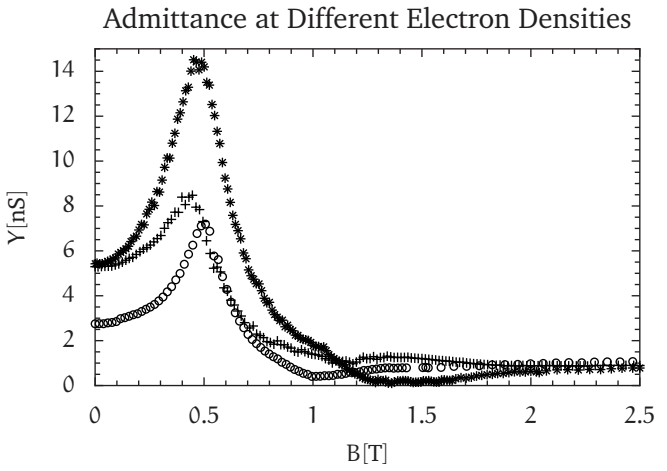

(A) Measured admittance

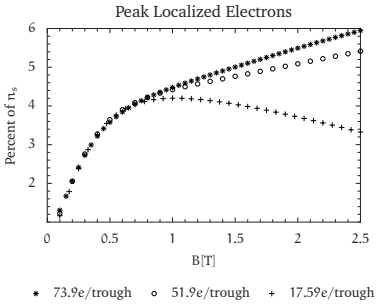

(B) Electrons on substrate peaks

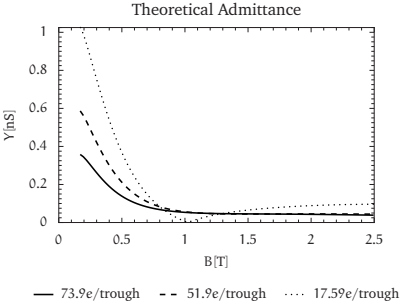

(C) Flow admittance

FIGURE 5.9. In (A), the admittance (Y) of TDES at similar temperatures T but different electron densities is plotted against the magnetic field (B). Saturated electron densities are $n_s = 1.47 \times 10^{14} m^{-2}$ ($T = 1.09K, \Gamma = 322$) corresponding to 73.9e per trough, $n_s = 1.03 \times 10^{14} m^{-2}$ ($T = 1.1K, \Gamma = 263$) corresponding to 51.9e per trough and $n_s = 6.08 \times 10^{13} m^{-2}$ ($T = 1.14K, \Gamma = 188$) corresponding to 17.59e per trough. These n_s were generated with holding field voltage of 121V, 85V and 50V, respectively. Excitation voltage and frequency were set at $V_{ex} = 10mV$ and $f_{ex} = 65kHz$ for all measurements. In (B), the respective curves show the partial fraction of electrons on the peaks of the nanotower as a function of B. The partial fraction is expressed as a percentage of the respective n_s. In (C), the flow admittance for the same conditions is plotted. Flow admittance results from the absolute value of the first derivative of an interpolation of the curves in (B) with respect to B according to eq. (4.46).

Inspection of fig. 5.9A reveals that all measurements exhibit a pronounced admittance maximum in the interval $(0.4T, 0.5T)$, a much less pronounced admittance minimum, which takes place at magnetic fields of about 1T for $Y(n_s = 51.9e/\text{trough})$, 1.15T for $Y(n_s = 17.59e/\text{trough})$ and 1.5T for $Y(n_s = 73.9e/\text{trough})$ and a minor increase of the admittance after the minimum, towards a saturation value for ever stronger magnetic fields.

The percentage of peak electrons as a function of B is shown in fig. 5.9B. One sees that the percentage of peak electrons reaches a maximum (at $B = 0.8T$) only for measurement $Y(n_s = 17.59e/\text{trough})$. For the other two measurements, characterized by a very high saturated electron density, fig. 5.9B implies that electrons continue to flow on the peaks for ever increasing B. However, the rate of electron flow to the peaks decreases markedly after a magnetic field of approximately 0.5T. The magnetic field where the rate of electron flow changes and the position of admittance maxima for the respective measurements is very close.

Of course, flow admittance, depicted in fig. 5.9C, inherits the features of 5.9B as it is essentially the first derivative of the percent of peak electrons with respect to the magnetic field. Notice that the calculated flow admittance, in the range of weak B, is lower for the measurements with higher electron densities. Flow admittance forms a small but not negligible component of the measured admittance, consistent with what is expected for the admittance of TDES outside the low temperature and low electron density regime.

The values of Y_f in fig. 5.9C are results directly out of eq. (4.46), but as argued in section 5.5.1, calibration of Y_f with data from the low temperature and density regime, indicates that Y_f must be at least half what is calculated by eq. (4.46). Moreover, as discussed in section 5.5.2, except for the general scaling of Y_f that affects all measurements, for high electron density measurements the peak-trough voltage difference should be lower (perhaps significantly so) than what is calculated from eq. (4.47) and this would make flow admittance higher.

The plots of the normalized admittance against B^2 with and without Y_f, shown in the upper and lower plot of fig. 5.10 respectively, invert and 'magnify' the evolution of the admittance as a function of the magnetic field. Admittance maxima for weak magnetic fields, which were so prominent in fig. 5.9A, are now narrow minima that are visible right at the beginning of the plots. On the contrary, admittance minima for stronger magnetic fields, which were barely visible in fig. 5.9A, are now wide maxima so imposing they can be fully captured only with a logarithmic scale of the ordinate.

Data representation in terms of the $Y_0/Y(B^2)$ is extremely suitable for tracing the influence of Coulomb interactions, which must be huge, considering the values of Γ in the caption of fig. 5.9 (a TDES forms a Wigner crystal for $\Gamma > 137$). Let once more be reiterated that Γ is calculated by eq. (2.10) and is independent of the magnetic field, meaning that each TDES starts off in the Wigner crystal state

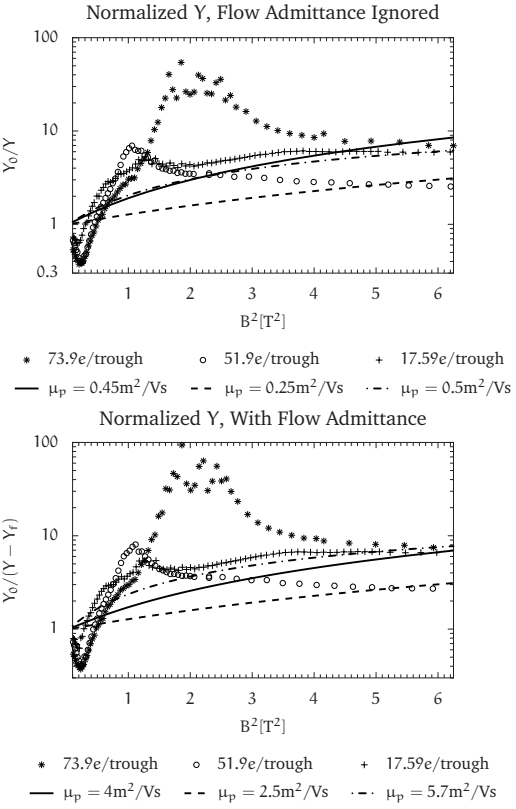

FIGURE 5.10. Normalized admittance of the TDES of the measurement in fig. 5.7 plotted against the square of the magnetic field. In the upper plot flow admittance is ignored, therefore normalized admittance is Y_0/Y where Y_0 is the value when $B = 0$. The solid line is a fit according to the modified Drude model, eq. (5.4) for $Y_f = 0$. The bottom plot shows the same measurement and the corresponding fit when flow admittance Y_f (see fig. 5.9C) is included. The partial fraction n_p of electrons on peaks is for both plots shown in fig. 5.9B. The inclusion of Y_f does not improve the agreement of the model with the experimental data, but the estimated mobility μ_p of peak electrons differs by one order of magnitude.

already for zero field. Obviously then, the admittance Y_0 for zero field refers to the admittance of a Wigner crystal, which is much lower than that of a TDES in the liquid state. In turn, this means that a disruption or fracturing of the Wigner crystal toward the liquid state, which has a higher admittance, is associated with a *decrease* of the normalized admittance because in that case $Y_0 < Y$ and $Y_0/Y < 1$. Opposite conclusions hold for the case when a TDES in the liquid state forms a Wigner crystal, because in that case normalized admittance should *increase*.

The amended Drude model fit of eq. (5.4), which is depicted as solid, dashed and dot-dashed curves in the bottom plot of fig. 5.10, provides a guide of what the evolution of the normalized admittance would be without effects due to the Coulomb interaction[7]. Clearly, this evolution is far off from what is observed and it immediately implies a scenario similar to that outlined for measurement $Y(T = 1.32K)$ in section 5.5.2.

[7]Zero field admittance Y_0 refers to the admittance of a Wigner crystal, where the Drude model, which ignores Coulomb interactions, cannot be really applied. But this is not known *a priori*.

All TDES start off in the state of a Wigner crystal with their electrons localized inside the troughs. When the magnetic field increases, an electron flow from the troughs to the peaks sets in. As a result, the partial fraction of peak electrons increases, flow admittance is large (but quickly diminishes) and the Wigner crystal in the troughs is disturbed or fractured. Peak electrons do not yet have the necessary density to immediately form a Wigner crystal on the peaks (which would be possibly connected with the crystal in the troughs) and as a result the admittance of the TDES increases sharply. The observed admittance maxima should then be attributed exclusively to the relatively free peak electrons and the increased flow admittance. This increase of Y means in turn that normalized admittance decreases sharply (because $Y_0 < Y$, which makes $Y_0/Y < 1$) and this explains the narrow minima in fig. 5.10.

However, as the magnetic field continues to increase, the density of peak electrons and their localization reaches a point where a Wigner crystal forms on the peaks as well. Flow admittance is also much lower and as a result the admittance collapses again to a much smaller value. Correspondingly, normalized admittance increases sharply to a maximum.

Then, both Y_0/Y and Y tend asymptotically to a saturated value consistent with what would be expected by a slow but steady electron flow to the peaks and the associated flow admittance.

Summarily, the information gained from the intermediate temperature, high density regime is that Wigner crystallization greatly affects the evolution of the admittance, making the fit between measured data and the amended Drude model problematic. Nevertheless, the problematic areas can be interpreted and almost completely be accounted for by carefully comparing the measured data, which make Coulomb interactions manifest, with the statistical equilibrium model, which ignores them.

5.5.4. Intermediate temperatures, same electron density. In this section a pair of measurements is presented, where a TDES is created and then a magnetic field sweep up to 2T is performed by keeping the temperature constant at 1K, whereupon the temperature is warmed up to 1.16K and a reverse sweep toward zero magnetic field is undertaken. Electron density of the TDES remains constant throughout, but the change of temperature means that parameter Γ, calculated from eq. (2.10), will be different. In particular, measurement $Y(T = 1K)$ has $\Gamma = 151$, a value indicating Wigner crystallization, while $Y(T = 1.16K)$ has $\Gamma = 130$, a value below 137, indicating therefore a TDES that should be in the liquid state.

Inspection of fig. 5.11A reveals that the evolution of Y for *both* measurements is similar to that of a TDES starting off in the Wigner crystal state at zero field.

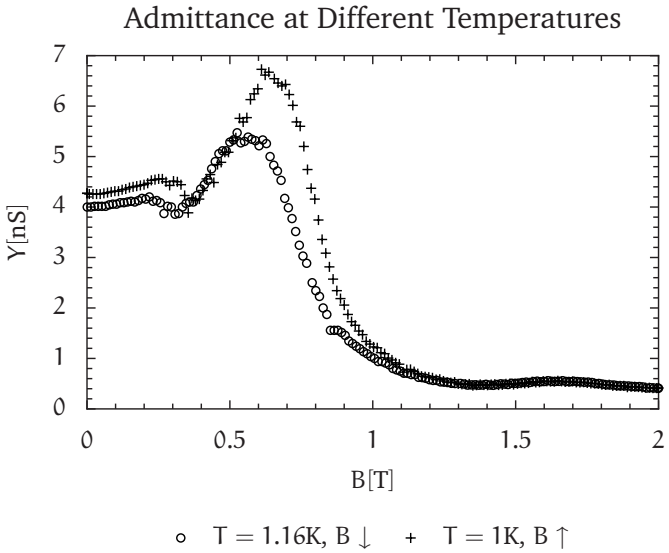

(A) Measured admittance

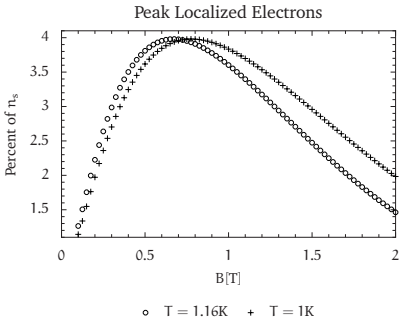

(B) Electrons on substrate peaks

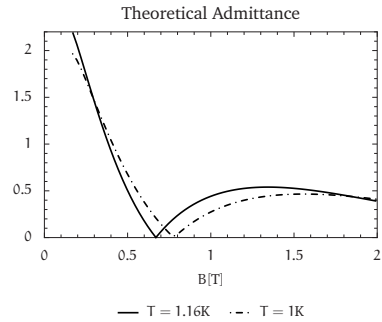

(C) Flow admittance

FIGURE 5.11. Admittance (Y) of a TDES plotted against the magnetic field (B). In (A), the measured admittance at temperatures T = 1K (increasing B) and T = 1.16K (decreasing B) is plotted. The saturated electron density is $n_s = 3.50 \times 10^{13} m^{-2}$, corresponding to $\approx 17.59e$ per trough and $\Gamma = 151$ (T = 1K) and $\Gamma = 130$ (T = 1.16K). Holding field voltage is $V_{TB} = 28.8V$, excitation voltage is $V_{ex} = 10mV$ and excitation frequency is $f_{ex} = 65kHz$, while B was changing at a rate of 0.167T/s. In (B), the respective curves show the partial fraction of electrons on the peaks of the nanotower as a function of B. The partial fraction is expressed as a percentage of n_s. In (C), the flow admittance is plotted. Flow admittance results from the absolute value of the first derivative of a continuous interpolation of the curves in (B) with respect to B according to eq. (4.46).

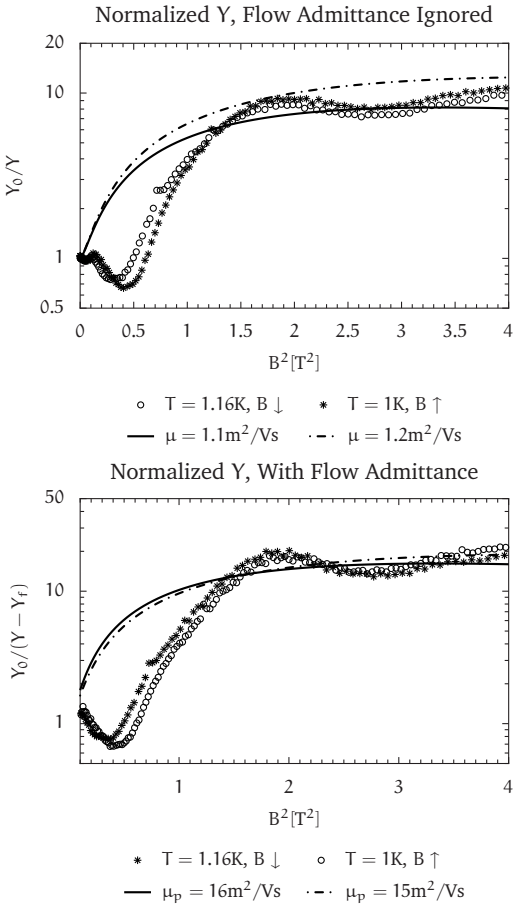

FIGURE 5.12. Normalized admittance of the TDES of the measurement in fig. 5.7 plotted against the square of the magnetic field. In the upper plot flow admittance is ignored, therefore normalized admittance is Y_0/Y where Y_0 is the value when $B = 0$. The solid line is a fit according to the modified Drude model, eq. (5.4) for $Y_f = 0$. The bottom plot shows the same measurement and the corresponding fit when flow admittance Y_f (see fig. 5.11C) is included. The partial fraction n_p of electrons on peaks is for both plots shown in fig. 5.11B. The inclusion of Y_f does not improve the agreement of the model with the experimental data, but the estimated mobility μ_p of peak electrons differs by one order of magnitude.

Qualitatively, no new feature comes up in figs. 5.11 and 5.12 that was not encountered, described and interpreted in similar measurements like those in section 5.5.3 and $Y(T = 1.32K)$ in section 5.5.2: for this reason a more detailed analysis on those plots seems superfluous[8] and will not be attempted.

However, while it seems that the TDES remains at the Wigner crystal state for both magnetic field sweeps, this really should not be the case for $Y(T = 1.16K)$, because for that measurement $\Gamma < 137$.

The absolute lower theoretical limit for Wigner crystallization of a TDES is calculated [**83**] to be $\Gamma = 125$, but this calculation ignores extrinsinc diffusive

[8]We became aware that *E. Fermi* is said to have once remarked that we should "never underestimate the joy people derive from hearing something they already know". But we remain sceptical.

mechanisms that couple with the TDES, like ripplon and gas atom scattering. Those diffusive mechanisms disturb the formation of a Wigner crystal and Γ must be necessarily higher than 125. Moreover, gas atom scattering cannot be dismissed for $Y(T = 1.16K)$, because temperature is high enough that it remains important and the critical $\Gamma = 137$ is fairly well supported by many independent measurements. Therefore, while permissive as an explanation of last resort, the *ad hoc* hypothesis that experimental errors made the determination of Γ incorrect, will not be employed.

A more plausible explanation would certainly consider what experimental conditions are different for $Y(T = 1.16K)$ compared to all the other measurements. Following this trace, one sees that for all measurements except $Y(T = 1.16K)$, the TDES was created directly in the Wigner crystal state for zero magnetic field and—more critically—the physical factors that determine Γ were not altered in the course of each measurement. However, measurement $Y(T = 1.16K)$ was unusual in that the temperature (a physical factor that influences Γ) was increased while the TDES was at a strong magnetic field. Magnetic field definitely enhances localization and it is not unnatural to suggest that the Wigner crystal was not destroyed precisely due to the strong magnetic field where temperature increase took place.

The fact that the TDES remained more or less a crystal while the magnetic field decreased, indicates that the onset of the Wigner crystal state probably takes place at a lower Γ in the presence of a magnetic field, for TDES on deformed films at least and this is the information gained from the intermediate temperature, same electron density regime.

5.6. Final Scholium

The theoretical and experimental analysis presented in this thesis, outlines a coherent framework for working with, and understanding dynamic and kinetic properties of TDES on periodically deformed liquid helium films.

Original motivation of these experiments was that electrons of TDES in the horizontal plane would start moving in circular orbits when a uniform magnetic field in the z-direction were applied, the radius of this circular orbit becoming smaller with an increasing field magnitude. The application of such a magnetic field would not have been yet sufficient to ensure electron localization, because the various scattering mechanisms would cause the centers of the circular orbits to obviate perpetually and execute a diffusive, spatially unconstrained random walk motion. This spatially unconstrained motion of the centers of circular orbits was thought it could be averted when the surface of liquid helium were no longer flat, but instead exhibited periodically positioned lows (troughs) and highs (peaks). Such a periodical structure were to be ensured by using a substrate whose surface had been crafted with periodically positioned troughs and peaks. Since superfluid liquid helium is a universal wetting agent, it follows that a

liquid helium film (whose thickness can be easily regulated) will always wet the substrate surface and have the same periodic structure.

Period, depth (height) and diameter of the troughs (peaks) are important, as they influence film structure before and—more critically—after a TDES has been formed (TDES also influence film structure). Capillary effects must be taken into account in the design of a structured substrate, as well as the range of TDES density one wishes to study and the range of the experimentally feasible magnetic field for the onset of localization. These considerations limit the dimensions of surface characteristics in the mesoscopic range (tens or hundreds of nanometer).

An important finding in this thesis is that the use of dielectric substrates *greatly* influences electron localization, not only because the developing image charges on the surface of the substrate reduce electron mobility: the effect of a structured dielectric substrate is especially pronounced when a holding field is applied. It was shown in the theoretical part of this thesis that electron localization in the troughs of the periodic substrate in this case is almost complete *even in the absence of a magnetic field*. This is in sharp contrast to nondielectric structured substrates, where electron interaction with the substrate is minimal or nonexistent and extremely strong holding fields must be applied in order to localize a minute fraction of electrons in the troughs and only for temperatures in the 10^{-2}K range.

Electron localization due to the combination of a dielectric substrate and a holding field is problematic, because it greatly reduces the measurable admittance signals and meddles with electron localization from the magnetic field. Perhaps contrary to intuition, the theory and the experimental results presented suggest that the magnetic field actually *delocalizes* part of TDES electrons, especially for weak magnetic fields, and so enhance the measured admittance.

Indeed, the model developed in the present thesis predicts that a constant holding field would localize most electrons of a TDES inside the troughs in some Fock-Darwin state. If, however, an increasing magnetic field is applied in addition to the holding field, the fraction of electrons on the peaks of the substrate will increase. Equivalently, localized electrons from the troughs will move to the peaks and occupy a regular Landau state there[9].

The diffusive electron flow from the troughs to the peaks, induced by the changing magnetic field[10], is a current and it should therefore contribute to the admittance. The developed model gives a quantitative result with regard to that contribution—the *flow admittance* Y_f—, which can be compared with the experimental data. Moreover, it provides an amended Drude model of the form

[9]Electron potential on a peak can be arbitrarily defined as zero. A consequence of such a selection is that a trough obtains a negative potential, becoming thus a potential well.

[10]The motion from the troughs to the peaks is the result of a complicated summation of quantum states. Nevertheless, it can be crudely motivated by the fact that larger magnetic fields increase the angular momentum L_z, which directs electrons 'upwards' (out of the troughs).

$1+\mu_p^2 B^2 n_p(B)$ for the normalized admittance $Y(0)/(Y(B)-Y_f(B))$, where μ_p is peak electron mobility and $n_p(B)$ the partial fraction of peak electrons as a function of the magnetic field.

For regimes other than the low temperature and low electron density, flow admittance is only a small part of the measured one. This means that most of the measured admittance should rather be attributed to electrons in the troughs, or electrons on the peaks, or both. However, the evolution of the partial fraction of electrons on the peaks with respect to the magnetic field indicates that the fraction of electrons on the peaks is the active part responsible for most of the measured admittance. The main reasons are that first, the partial fraction of peak electrons increases when the admittance increases or retains a large value (at weak magnetic fields) and second that the partial fraction declines when the admittance decreases (at strong magnetic fields).

Even in the exceptional case where the partial fraction of peak electrons increases at a lower rate in strong magnetic fields, Landau localization of peak electrons becomes much better and reduces their contribution to the admittance. Overall, at the limit of strong magnetic fields the admittance always declines and its evolution tends asymptotically to flow admittance $Y_f(B)$. Therefore, for strong magnetic fields electrons are well localized either inside the troughs or on the peaks and the measured admittance should only be due to electrons which flow from the troughs to the peaks or conversely.

The preceding analysis has made clear that quasi zero dimensional electron localization is possible, and that transport properties of localized electrons are heavily influenced by the interplay of temperature, magnetic field, holding field and electron density. Nontrivial physical insight was gained even by using a simple theoretical model that ignores Coulomb interactions, because the comparison of experimental data on TDES where Coulomb interactions dominate (Wigner crystallized TDES) with the model, revealed the precise form of the influence of Wigner crystallization on the admittance. It was shown that TDES statistical mechanics are critical, in the sense that the TDES can no longer be regarded as a monolithic entity but rather as a system made up of three distinct subsystems (peak electrons, trough electrons, flow electrons) whose dynamic equilibrium determines transport properties.

Future experimental research, benefiting from the presented framework, would undoubtedly extend the measurements of admittance for higher magnetic fields and many more combinations of electron density and temperature. A more elaborate theoretical modeling could perhaps incorporate Coulomb interactions and propose a quantitative result for the admittance of electrons in the troughs (in the context of the Drude model or beyond). This would allow a comparison with the admittance of peak electrons, explaining thus completely the features of the measured admittance.

APPENDIX A

A Single Electron on a Dielectric Liquid

A.1. Bound states of an electron on the surface of a dielectric liquid

The wavefunction $\psi(x,y,z)$ of an electron on the surface of a dielectric liquid is the solution of Schrödinger equation

$$-\frac{\hbar^2}{2m}\nabla^2\psi(x,y,z)-\frac{\Lambda}{z}\psi(x,y,z)=E\psi(x,y,z)\Longrightarrow \tag{A.1}$$

$$\nabla^2\psi+\left(\frac{2m\Lambda}{\hbar^2 z}+\frac{2mE}{\hbar^2}\right)\psi=0, \tag{A.2}$$

where it is reminded that Λ has been defined in eq. (1.1) and E denotes the eigenenergies of the bound states, meaning that $E<0$; for negative eigenenergies, it can be demanded that the wavefunction will be zero at the origin ($z=0$) and at infinity ($z\longrightarrow\infty$).

The laplacian is separable in cartesian coordinates, and the substitution $\psi(x,y,z)=f(x,y)\phi(z)$ into eq. (A.1) leads to a wave equation for (x,y). Decomposing the total eigenenergy into the sum $E=E_k+E_\nu$, one gets

$$\nabla^2 f(x,y)=\frac{2mE_k}{\hbar^2}f(x,y). \tag{A.3}$$

This equation can be further separated into two one-dimensional wave equations whose solutions are plane waves $e^{ik_x x}$ and $e^{ik_y y}$ (here, the wavenumbers $k_{x,y}=\hbar^2k^2/2m$, for $k=1,2,\ldots$ were introduced, such that $E_k=\hbar^2k^2/2m$).

Next, we define the "natural dimensions" of the problem, by setting

$$a=\frac{2\hbar^2}{m\Lambda}\approx 78\text{Å},\quad \lambda=\sqrt{-\frac{2mE}{\hbar^2}},\quad \nu=\frac{1}{\lambda a},\quad \zeta=\lambda z. \tag{A.4}$$

Observe that the parameter a (the "Bohr radius" of the problem) has dimensions of length, while λ has dimensions of inverse length, making the product λa dimensionless. Moreover, the new argument ζ of $\phi(\cdot)$ is dimensionless as well.

These transformations, lead to a dimensionless form of the differential equation for $\phi(\zeta)$, which is suitable for further mathematical manipulations. The dimensionless form is

$$\phi''(\zeta)+\left(\frac{1}{\lambda a\zeta}-\frac{1}{4}\right)\phi(\zeta)=0\Longrightarrow\phi''(\zeta)+\left(\frac{\nu}{\zeta}-\frac{1}{4}\right)\phi(\zeta)=0. \tag{A.5}$$

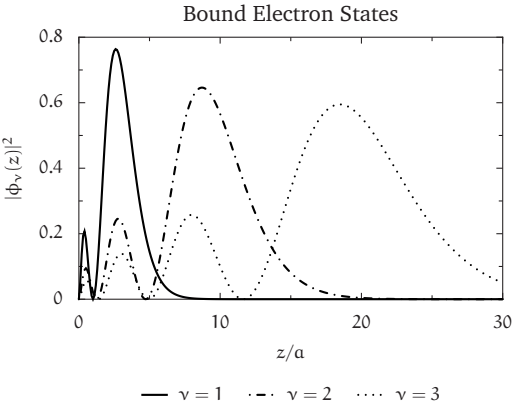

FIGURE A.1. Probability densities $|\phi_\nu(z)|^2$ of bound states ν for a single electron above the surface of liquid ^{4}He, as a function of the normalized distance z/a, where $a = 78$Å (cf. eq. A.9). The average electron of the ground state is found approximately 78Å above the surface of liquid helium.

The previous ordinary differential equation is not yet recognized as belonging to one of the known solvable forms, but by means of the transformation

$$\phi(\zeta) = \zeta e^{-\zeta/2} u(\zeta), \tag{A.6}$$

it is recasted into the Laplace differential equation

$$\zeta u''(\zeta) + (2-\zeta)u'(\zeta) - (1-\nu)u(\zeta) = 0. \tag{A.7}$$

The general solution of the Laplace differential equation above is given in terms of the confluent hypergeometric function[1] ${}_1F_1$, as

$$u(\zeta) = c_0 {}_1F_1(1-\nu;2;\zeta) + c_1 \zeta^{-1} {}_1F_1(-\nu;0;\zeta). \tag{A.8}$$

Basic properties of the confluent hypergeometric function can be used to show that the expression $\zeta^{-1} {}_1F_1(-\nu;0;\zeta)$ diverges, and therefore it must be necessarily $c_1 = 0$. In the same manner, it can be shown that ${}_1F_1(1-\nu;2;\zeta)$ is equal, up to a proportionality constant, to the associated Laguerre polynomial[2] $L^1_\nu(\zeta)$. Finally, the solution in terms of the original function $\phi(z)$ is,

$$\phi_\nu(z) = 2c_0 \frac{z}{\nu a} \exp\left(-\frac{z}{\nu a}\right) L^1_\nu\left(\frac{2z}{\nu a}\right) \quad \nu = 1, 2, \ldots \tag{A.9}$$

An inspection of eq. (A.9) reveals that the boundary condition $\phi(0) = 0$ is trivially satisfied; the condition $\phi(z \longrightarrow \infty) = 0$ on the other hand is satisfied, because $L^1_\nu(z)$ are polynomials increasing as $\mathcal{O}(z^\nu)$, slower than the exponential decay of order $\mathcal{O}(e^{-z})$. The normalization constant c_0 is determined by the condition $c_0^2 \int_0^\infty dz |\phi_\nu(z)|^2 = 1$. The first three bound states can be seen in fig. A.1.

[1] We are referring to the *Mathematica* function Hypergeometric1F1[a, b, z].

[2] Generalized, or associated Laguerre polynomials are called with the help of the *Mathematica* function LaguerreL[a, b, z].

The eigenenergies E_ν can be calculated from,

$$E_\nu = -\frac{m\Lambda^2}{8\hbar^2}\frac{1}{\nu^2} \approx -\frac{7.23 k_B}{\nu^2}, \quad \nu = 1,2,\dots \tag{A.10}$$

It is very convenient to express the energies E in terms of the temperature of the corresponding thermal energy resulting from $E = k_B T$. Then, the "temperature difference" between the first excited and ground state is 3.6K. Since the temperature of TDES on the surface of liquid helium can be $\approx$ 2K at most, all electrons will be found at the ground state and it is impossible to excite electrons thermally.

A.2. Perturbative solution in the presence of holding field

The presence of a holding electric field $E_\perp$ along the z-direction is enough to make Schrödinger equation intractable analytically. Approximate methods must be used and the most common is perturbation method. This method is applicable whenever the hamiltonian of the problem can be written in the form $\hat{\mathcal{H}} = \hat{\mathcal{H}}_0 + \delta\hat{\mathcal{V}}$, where $\hat{\mathcal{H}}_0$ possess an analytical solution and $\delta\hat{\mathcal{V}}$ can be considered a 'small' perturbation, in the sense that $\delta \ll 1$.

Assuming $\delta \ll 1$, one can expand both the eigenenergies $E_\nu^{(s)}$ and the eigenfunctions $|\phi_\nu^{(s)}\rangle$ of $\hat{\mathcal{H}}$ in a power series with respect to δ. Usually, the first order correction $(s = 1)$ is a very accurate approximation and it will be calculated by means of the formulas,

$$E_\nu^{(1)} = E_\nu^{(0)} + \delta\langle\phi_\nu|\hat{\mathcal{V}}|\phi_\nu\rangle, \tag{A.11a}$$

$$|\phi_\nu^{(1)}\rangle = |\phi_\nu^{(0)}\rangle + \delta\sum_{k\neq\nu}\frac{\langle\phi_k^{(0)}|\hat{\mathcal{V}}|\phi_\nu^{(0)}\rangle}{E_\nu^{(0)} - E_k^{(0)}}|\phi_k^{(0)}\rangle. \tag{A.11b}$$

These formulas are valid only for nondegenerate eigenstates, because otherwise it might happen that $E_\nu^{(0)} = E_k^{(0)}$ for two distinct eigenstates $|\phi_\nu^{(0)}\rangle, |\phi_k^{(0)}\rangle$.

It is a common practice in experiments involving TDES on liquid helium to impose a static electric field $E_\perp$ along z-direction. The hamiltonian of an electron on the surface of liquid ^{4}He takes the form

$$\hat{\mathcal{H}} = -\frac{\hbar^2}{2m}\nabla^2 - \frac{\Lambda}{z} - eE_\perp z, \tag{A.12}$$

whereby it is immediately obvious that $eE_\perp z$ is a candidate perturbation term. It was shown that $\hat{\mathcal{H}}$ can be decomposed into a part involving only (x, y) and a part involving the height z; the perturbation term affects only the z-coordinate, and any corrections will be therefore constrained to $|\phi_\nu(z)\rangle$ and the corresponding eigenenergies E_ν.

If the perturbation term is written as a function of the dimensionless parameter ζ (defined in eq. A.4), such that $\mathcal{V} = -2e\lambda E_\perp \zeta$, then

$$\delta = -2e\lambda E_\perp \Longrightarrow \delta = -\frac{2eE_\perp}{\nu a} \approx -8.20 \times 10^{-11}\,\frac{E_\perp}{\nu} \quad \text{[SI]}, \tag{A.13}$$

which is indeed much less than unity for every conceivable holding field magnitude $E_\perp$, whose maximum value cannot be larger than $10^4 \mathrm{V/m}$.

Values of $\langle \phi_k^{(0)}(\zeta)|\zeta|\phi_\nu^{(0)}(\zeta)\rangle$

$k = \ldots$	1	2	3	4
$\nu = 1$	12	$-5\sqrt{2}$	$\sqrt{3}$	0
$\nu = 2$	$-5\sqrt{2}$	9	$-7\sqrt{6}/3$	$\sqrt{2}$

An inspection of first order perturbation formulas eqs. (A.11) reveals already that the energy spectrum will be shifted to more negative values, but no splitting will occur because there is no degeneracy to be lifted in the z-direction. For obtaining quantitative results, expressions of the form

$$\langle \phi_k^{(0)}|\zeta|\phi_\nu^{(0)}\rangle = c_k c_\nu \int_0^\infty d\zeta\, \zeta^3 e^{-\zeta} L_k^1(\zeta) L_\nu^1(\zeta), \tag{A.14}$$

need to be calculated. The integration is easy to do and for reference purposes the values of $\langle \phi_k^{(0)}|\zeta|\phi_\nu^{(0)}\rangle$ for various ν, k are provided in tabular form. An extremely fortuitous result that should be kept in mind is that all other values for $k > 4$ are equal to zero, and the summation in eq. (A.11b) is actually finite, consisting of only two terms for the ground state correction, $\nu = 1$.

APPENDIX B

Landau Quantization

The hamiltonian of an electron moving in the presence of a magnetic field $\mathbf{B} = \nabla \times \mathbf{A}$, has the general form

$$\hat{\mathcal{H}} = \frac{1}{2m}(\hat{\mathbf{p}} + e\hat{\mathbf{A}})^2 = \frac{\hat{\mathbf{p}}^2}{2m} + \frac{e}{2m}(\hat{\mathbf{p}}\hat{\mathbf{A}} + \hat{\mathbf{A}}\hat{\mathbf{p}}) + \frac{e^2}{2m}\hat{\mathbf{A}}^2, \tag{B.1}$$

if, as a first approximation valid for low gyration frequencies, electron spin does not interact with the magnetic field.

Consider an electron of a TDES that is constrained to move in the xy-plane and a homogeneous magnetic field along the z-axis. Then, the momentum operator is $\hat{\mathbf{p}} = (\hat{p}_x, \hat{p}_y, 0)$ and the vector potential can be chosen[1] to be either $\mathbf{A} = (0, B\hat{x}, 0)$ (the Landau gauge) or $\mathbf{A} = -\mathbf{r} \times \mathbf{B}/2$ (the symmetric gauge).

Expanding the hamiltonian and substituting for the cyclotron frequency $\omega_c = eB/m$ wherever possible, one arrives at the expression

$$\hat{\mathcal{H}} = \frac{\hat{\mathbf{p}}^2}{2m} + \frac{m}{2}\left(\frac{\omega_c}{2}\right)^2 \left(x^2 + y^2\right) + \frac{\omega_c}{2}\hat{\mathcal{L}}_z \quad \text{for the symmetric gauge,} \tag{B.2}$$

and

$$\hat{\mathcal{H}} = \frac{\hat{p}_x^2}{2m} + \frac{1}{2}m\omega_c^2\left(\hat{x} + \frac{\hbar k_y}{m\omega_c}\right)^2 \quad \text{for the Landau gauge.} \tag{B.3}$$

In eq. (B.3), $\hat{\mathcal{L}}_z$ is the z-component of the angular momentum. The form of the hamiltonian in eq. (B.3) is identical to that of a one-dimensional harmonic oscillator, when the transformations $\hat{x}' \longrightarrow \hat{x} + \hbar k_y/m\omega_c$ and $\hat{p}'_x \longrightarrow \hat{p}'_x$ are performed. As a consequence, the energy eigenvalues will be given by

$$E_\nu = \left(\nu + \frac{1}{2}\right)\hbar\omega_c \quad \nu = 0, 1, \ldots \quad \text{(Landau levels).} \tag{B.4}$$

Each Landau level is degenerate, containing up to

$$\eta = s\frac{eB}{2\pi\hbar}, \quad \text{or} \quad \eta = 2.418 \times 10^{14} sB \tag{B.5}$$

electron states: except for the expected dependence of η on the surface s of the TDES, the degree of degeneracy is an increasing function of the magnetic field.

[1] The choice is governed by the desire to derive a magnetic field with the particular form $\mathbf{B} = (0, 0, B)$ from $\nabla \times \mathbf{A}$.

Even for moderate magnetic fields the degree of degeneracy is comparable to the electron densities encountered in TDES, with the effect that the overlap between different Landau levels is minimal.

The thermal energy of a TDES can be compared with the quantum $\hbar\omega_c$ of Landau levels by means of

$$\frac{\hbar\omega_c}{k_B T} \approx 1.34 \frac{B}{T} \quad [\text{SI}]. \tag{B.6}$$

For typical temperatures of 1K and magnetic fields less than about 1T, the TDES occupies the ground Landau level ($\nu = 0$) only. Higher Landau levels ($\nu > 0$) get increasingly occupied for weaker magnetic fields, or higher temperatures, or both.

The hamiltonian of eq. (B.2) is the quantum analogue of the classical hamiltonian that describes helical motion around the z-axis. If electrons were free to move in the z-direction, they would be driven by the nonzero $\widehat{\mathcal{L}}_z$ to move towards positive z for $\omega_c > 0$ and negative z for $\omega_c < 0$ (the sign of ω_c reflects the direction of the magnetic field). But the electrons of a TDES are constrained in a strictly two-dimensional motion and therefore $\widehat{\mathcal{L}}_z$ is irrelevant[2] (not zero!) for their motion.

Then, the relevant part of the hamiltonian in eq. (B.2) is that of a two-dimensional harmonic oscillator, which corresponds to uniform circular motion about a fixed center. The eigenvalues of the hamiltonian in eq. (B.2) are

$$E_\nu = (\nu_x + \nu_y + 1)\frac{\hbar\omega_c}{2} = (2\nu + 1)\frac{\hbar\omega_c}{2} = \left(\nu + \frac{1}{2}\right)\hbar\omega_c, \quad \nu = 0, 1, \ldots \tag{B.7}$$

In the previous equation, the quantum numbers ν_x and ν_y for each degree of freedom were set equal (to a common quantum number ν), because the hamiltonian in eq. (B.2) is symmetric in the swap $x \leftrightsquigarrow y$. Observe that the resulting eigenvalue spectrum is the same as in the case of the Landau gauge. This must be the case, because the energy spectrum is a measurable physical quantity and it cannot be dependent upon the choice of the vector potential. An extensive and detailed discussion of Landau quantization can be found in the book of *Cohen-Tannoudji* [**18**].

[2] One could wonder whether the angular momentum of our universe is nonzero and whether a nonzero value would have had any observable consequences.

APPENDIX C

Zusammenfassung

Elektronen können sich auf der Oberfläche dielektrischen Substanzen, z.B suprafluiden flüssigen Heliums (LHe), versammeln, und darauf stabile zweidimensionale Systeme gestalten [**116**]. Zweidimensionale Systeme von Elektronen auf flüssigem Helium wurden intensiv sowohl theoretisch als auch experimentell untersucht [**10**].

Aus theoretischer Sicht bilden Elektronen auf flüssigem Helium ein entartetes zweidimensionales Fermionengas wessen Teile durch Coulomb'sche Kräfte wechselwirken. Es kann theoretisch gezeigt werden [**90**], dass solche zweidimensionale Elektronensysteme sich, abhängig von ihrem Dichte und herrschenden Temperatur, in flüssigem oder festem Zustand befinden. Ein Phasenübergang, dass der Kosterlitz-Thouless Theorie [**58**] gehorcht, findet zwischen beiden Zuständen statt [**39**]. Ein weiterer Phasenübergang von dem festen zu dem gasförmigen Zustand wird erwartet, wenn man die Elektronendichte auf ungefähr $10^{16}\mathrm{e/m}^2$ erhöht. Dieser Phasenübergang kann nicht beobachtet werden, denn solch eine hohe Elektronendichte macht die Oberfläche von flüssigem Helium instabil: Nur Heliumfilme bleiben bei hohen Elektronendichten stabil, da sie mit dem benetzten dielektrischen Substrat durch van-der-Waals'sche Kräfte wechselwirken.

Verschiedene experimentelle Versuche probten eine noch stärkere Lokalisierung von Oberflächenzustandselektronen (OZE) auf LHe in einem bzw. null Raummaße [**61**]. Lokalisierung in diesem Sinne bedeutet, dass die unterbundenen Raummaße eine viel kleinere Längeskala als die der nicht unterbundenen Raummaße besitzen.

In dieser Dissertation erforschen wir die OZE-Dynamik auf deformierten LHe-Filme und berichten von Messungen der Admittanz solcher OZE für verschiedene Elektronendichten und Temperaturen als Funktion eines der Filmoberfläche senkrecht gerichteten Magnetfelds. Die Messungen wurden mithilfe einer Sommer-Tanner Elektrodenanordung erfasst [**101**].

Der LHe-Film benetzt ein Substrat aus Silizium, dessen freie Oberfläche periodische Mulden und Erhebungen aufweist. Das Profil des Heliumfilms leiten wir aus der Young-Laplace'schen Gleichung ab. Dann berechnen wir das Potenzial auf dem deformierten Heliumfilm als Funktion des Magnetfelds und eines

konstanten elektrischen Feldes. Wir zeigen, dass die Elektronen in den Mulden durch einen parabolischen Potenzialschacht erfasst sind, weil das Potenzial auf den Erhebungen konstant ist.

Elektronen sollen Landau-Schwingungen auf den Erhebungen des Substrats und Darwin-Fock Schwingungen in den Mulden des Substrats ausführen. Sowohl Landau als auch Darwin-Fock Schwingung kann klassisch als eine Umdrehung dargestellt werden. Der Halbmesser der (klassischen) Umdrehung hängt von dem Magnetfeld und der Temperatur ab und ist generell kleiner im Falle der Darwin-Fock Schwingung. Höhere Magnetfelder und niedrigere Temperaturen machen den Halbmesser der Umdrehung kleiner und umgekehrt, sodass die Elektronen sich unter solchen Bedingungen besser lokalisieren. Es folgt also, dass die idealen Bedingungen für Lokalisierung in den Mulden des Substrats unter niedriger Temperatur und starkem Magnefeld stattfinden.

Elektronen auf flüssigem Helium bilden ein stark korreliertes N-Teilchen Fluid, dass nur begrenzt von Landaus *Fermi-Flüssigkeit* Theorie beschrieben werden kann. Das hat zur Folge, dass man die Ergebnisse der quantenmechanischen Betrachtung eines einzigen Elektrons nicht unbedingt auf N-Elektronen zuführen darf. Dennoch ergibt sich durch den *Speicherfunktionformalismus* [**82**] ein Bild, dass im wesentlichen von der Fermi-Flüssigkeit Theorie nicht unterscheidet. Experimente zeigen [**72**], dass der Speicherfunktionformalismus von der Fermi-Flüssigkeit Theorie nur für Magnetfelder über 10T und Elektronendichten über $10^{13}\,e/m^2$ abweicht.

Da in unseren Experimenten Magnetfelder bis 2T und Elektronendichten bis $10^{14}\,e/m^2$ erzeugt wurden, durften wir ein statistisches Modell auslegen, dass die Coulomb'sche Wechselwirkung der OZE auslässt.

Dieses statistische Modell basiert sich auf folgenden Grundsätzen und Vereinfachungen:

- Die Rauigkeit des Substrats wird nicht berücksichtigt, sodass Elektronen sich als ungestört in ihrer Bewegung betrachten lassen.
- Coulomb'sche Wechselwirkungen sind schwach.
- Elektronen führen Landau-Schwingugen in den Erhebungen und Darwin-Fock Schwingungen in den Mulden durch.
- Die Teilbrüche n_p und n_t der Elektronen auf jeweils Erhebungen und Mulden werden durch eine statistische Gleichgewichtgleichung berechnet und hängen von der Temperatur, das Magnetfeld und die gesättigte Elektronendichte ab.

Wesentliche Voraussagen dieses statistischen Modells, wenn man annimmt, dass die Teilbrüche konstant bleiben, sind folgende:

Steigendes Magnetfeld: Soll bei konstanter Temperatur und gesättigter Elektronendichte zu einer monoton niedrigeren Admittanz führen, weil alle Elektronen besser lokalisieren lassen.

Steigende Temperatur: Soll bei konstantem Magnetfeld und konstanter gesättigter Elektronendichte zu einer monoton höheren Admittanz führen, weil die Lokalisierung der Elektronen schwächer wird.

Steigende Elektronendichte: Nur hier wird der Einfluss der Coulomb'schen Wechselwirkung wichtig. Man könnte annehmen, dass für niedrige Elektronendichten solche Wechselwirkungen doch nicht so stark sein dürften, weil dagegen sich steigende Elektronendichten die Lokalisierung der Elektronen stören und somit die Admittanz bei konstanter Temperatur und konstantem Magnetfeld höher machen.

Die Teilbrüche der Elektronen auf die Erhebungen und Mulden bleiben jedoch nicht konstant bei einem sich ändernden Magnetfeld und dies hat als Folge einen diffusen Elektronenfluss zwischen Erhebungen und Mulden, der die Admittanz erhöht. Ferner, kann es vorkommen, dass ein genügend starker Elektronenfluss zu den Erhebungen, wo die Lokalisierung schwach ist, die Admittanz nicht absteigen läßt, oder sie sogar erhöht, auch bei einem sich steigenden Magnetfeld.

Die experimentellen Daten der Admittanz als Funktion des Magnetfeldes weisen in der Tat ein nicht monotones Verhältnis auf, dass bei Temperaturen um 1K und Magnetfelder um 0.5T besonders deutlich hervortritt. Elektronendichte scheint nur das allgemeine Niveau und nicht die Form des Admittanzmaximums zu beeinflussen.

Das beobachtete nicht monotone Verhältnis der Admittanz als Funktion des Magnetfeldes kann man also auf den stattgefundenen diffusen Elektronenfluss von den Mulden zu den Erhebungen zurückführen.

Bibliography

1. E. Abrahams, P. W. Anderson, D. C. Licciardello, and T. V. Ramakrishnan, *Scaling theory of localizations: absence of quantum diffusion in two-dimensions*, Phys. Rev. Lett. **42** (1979), 673. (Cited on pages 3 and 113)
2. P. W. Adams and M. A. Paalanen, *Localization in a non-degenerate two-dimensional electron gas*, Phys. Rev. Lett. **58** (1987), 2106. (Cited on page 45)
3. Y. Alhassid, *The statistical theory of quantum dots*, Rev. Mod. Phys. **72** (2000), 895. (Cited on page 4)
4. B. L. Altshuler, D. Khmel'nitzkii, A. I. Larkin, and P. A. Lee, *Magnetoresistance and Hall effect in a disordered two-dimensional electron gas*, Phys. Rev. B **22** (1980), 5142. (Cited on page 42)
5. B. L. Altshuler and P. A. Lee, *Disordered electronic systems*, Physics Today **41** (1988), 36. (Cited on page 43)
6. P. W. Anderson, *Absence of diffusion in certain random lattices*, Phys. Rev. **109** (1958), 1492. (Cited on page 43)
7. T. Ando, A. Fowler, and F. Stern, *Electronic properties of two-dimensional systems*, Rev. Mod. Phys. **54** (1982), 437. (Cited on pages 3, 33, and 38)
8. T. Ando and Y. Uemura, *Theory of quantum transport in a two-dimensional electron system under magnetic fields. I. Characteristics of level broadening and transport under strong magnetic fields*, J. Phys. Soc. Japan **36** (1974), 959. (Cited on page 38)
9. E. Y. Andrei, *Observation of the polaronic transition in a two-dimensional electron system*, Phys. Rev. Lett. **52** (1984), 1449. (Cited on page 33)
10. E. Y. Andrei (ed.), *Two-dimensional electron systems on helium and other cryogenic substrates*, Kluwer Academic Publishers, 1997. (Cited on pages 12, 22, 35, 70, and 143)
11. J. F. Babb, *Long-range atom-surface interactions for cold atoms*, J. Phys.: Conf. Ser. **19** (2005), 1. (Cited on page 60)
12. G. Bergmann, *Weak localization in thin films*, Phys. Rep. **107** (1984), 1. (Cited on page 45)
13. T. R. Brown and C. C. Grimes, *Observation of cyclotron resonance in surface-bound electrons on liquid helium*, Phys. Rev. Lett. **29** (1972), 1233. (Cited on pages 25 and 46)
14. V. A. Buntar, V. N. Grigor'ov, O. I. Kirichek, Yu. P. Monarkha, Yu. Z. Kovdrya, and S. S. Sokolov, *Kinetic properties of surface electrons over helium under strong electron-electron interaction*, J. Low Temp. Phys. **79** (1990), 323. (Cited on page 18)
15. H. B. G. Casimir and D. Polder, *The influence of retardation on the London-van der Waals forces*, Phys. Rev. **73** (1948), 360. (Cited on page 61)
16. E. Cheng, M. W. Cole, and M. H. Cohen, *Binding of electrons to the surface of liquid helium*, Phys. Rev. B **50** (1994), 1136. (Cited on pages 9 and 10)
17. E. Cheng, M. W. Cole, W. F. Saam, and J. Treiner, *Helium prewetting and nonwetting on weak-binding substrates*, Phys. Rev. Lett. **67** (1991), 1007. (Cited on page 59)
18. C. Cohen-Tannoudji, B. Diu, and F. Laloë, *Quantum mechanics (vols. 1-2)*, A Wiley-Interscience Publication, 1977. (Cited on page 142)

19. M. W. Cole, *Properties of image-potential-induced surface states of insulators*, Phys. Rev. B **2** (1970), 4239. (Cited on pages 3, 17, and 25)
20. ———, *Electronic surface states of liquid helium*, Rev. Mod. Phys. **46** (1974), 451. (Cited on pages 12, 13, and 14)
21. M. W. Cole and M. H. Cohen, *Image-potential-induced surface bands in insulators*, Phys. Rev. Lett. **23** (1969), 1238. (Cited on page 3)
22. E. Collin, W. Bailey, P. Fozooni, P. G. Frayne, P. Glasson, K. Harrabi, M. J. Lea, and G. Papageorgiou, *Microwave saturation and the Rabi frequency of the Rydberg states of electrons on helium*, Physica E **18** (2003), 186. (Cited on page 50)
23. E. Collin, W. Bailey, P. Fozooni, P. J. Frayne, P. Glasson, K. Harrabi, M. J. Lea, and G. Papageorgiou, *Microwave saturation of the Rydberg states of electrons on helium*, Phys. Rev. Lett. **89** (2002), 245301. (Cited on page 50)
24. R. S. Crandall and R. Williams, *Properties of electron surface states on liquid helium*, Phys. Rev. A **5** (1972), 2183. (Cited on pages 12 and 25)
25. A. J. Dahm, *Possibility of ripplon induced weak localization of electrons*, Low Temp. Phys. **23** (1997), 480. (Cited on page 45)
26. A. J. Dahm, J. A. Heilman, I. Karakurt, and T. J. Peshek, *Quantum computing with electrons on helium*, Physica E **18** (2003), 169. (Cited on pages 50 and 51)
27. S. Datta, *Electronic transport in mesoscopic systems*, Cambridge University Press, 1995. (Cited on page 3)
28. J. G. Daunt, D. O. Edwards, F. J. Milford, and M. Yaqub (eds.), *Low temperature physics (LT9)*, Plenum Press, 1965. (Cited on page 37)
29. D. P. DiVincenzo, *The physical implementation of quantum computation*, Fortschr. Phys. **48** (2000), 771. (Cited on page 48)
30. G. Dresselhaus, A. F. Kip, and C. Kittel, *Cyclotron resonance of electrons and holes in silicon and germanium crystals*, Phys. Rev. **98** (1955), 368. (Cited on page 46)
31. M. I. Dykman and L. S. Khazan, *Effect of the interaction between nondegenerate electrons localized in a thin surface layer on the cyclotron resonance*, JETP **50** (1979), 747. (Cited on page 39)
32. M. I. Dykman, M. J. Lea, P. Fozooni, and J. Frost, *Magnetoresistance in 2D electrons on liquid helium: Many-electron versus single-electron kinetics*, Phys. Rev. Lett. **70** (1993), 3975. (Cited on page 39)
33. M. I. Dykman and P. M. Platzman, *Quantum computing using electrons floating on liquid helium*, Fortschr. Phys. **48** (2000), 1095. (Cited on pages 49, 50, and 51)
34. C. Enss and S. Hunklinger, *Tieftemperaturphysik*, Springer, 2000. (Cited on page 54)
35. H. Etz, W. Gombert, W. Idstein, and P. Leiderer, *Stability of charged ^{4}He films*, Phys. Rev. Lett. **53** (1984), 2567. (Cited on pages 29 and 62)
36. L. H. Germer, *The distribution of initial velocities among thermionic electrons*, Phys. Rev. **25** (1925), 795. (Cited on page 64)
37. D. C. Glattli, E. Y. Andrei, and F. I. B. Williams, *Thermodynamic measurement on the melting of a two-dimensional electron solid*, Phys. Rev. Lett. **60** (1988), 420. (Cited on page 23)
38. C. C. Grimes and G. Adams, *Observation of two-dimensional plasmons and electron-ripplon scattering in a sheet of electrons on liquid helium*, Phys. Rev. Lett. **36** (1976), 145. (Cited on pages 24, 25, 26, and 49)
39. ———, *Evidence for a liquid to crystal transition in a classical, two-dimensional sheet of electrons*, Phys. Rev. Lett. **42** (1979), 795. (Cited on pages 4, 22, 23, and 143)
40. C. C. Grimes and T. R. Brown, *Direct spectroscopic observation of electrons in image-potential states outside liquid helium*, Phys. Rev. Lett. **32** (1974), 280. (Cited on pages 9, 10, and 49)
41. C. C. Grimes, T. R. Brown, M. L. Burns, and C. L. Zipfel, *Spectroscopy of electrons in image-potential-induced surface states outside liquid helium*, Phys. Rev. B **13** (1976), 140. (Cited on page 15)

42. B. I. Halperin and D. R. Nelson, *Theory of two-dimensional melting*, Phys. Rev. Lett. **41** (1978), 121. (Cited on page 21)
43. D. Herman, I. Karakurt, H. Mathur, and A. J. Dahm, *Damping of quantum interference of electrons on helium*, Phys. Rev. B **68** (2003), 033402. (Cited on page 46)
44. D. Herman, H. Mathur, and A. J. Dahm, *Dephasing of electrons on helium by collisions with gas atoms*, Phys. Rev. B **63** (2001), 115418. (Cited on page 46)
45. A. J. G Hey and R. Allen (eds.), *Feynman lectures on Computation*, Perseus Press, 1996. (Cited on page 48)
46. X. L. Hu and A. J. Dahm, *Stability of charged thin helium films*, Phys. Rev. B **42** (1990), 2010. (Cited on pages 29, 30, and 66)
47. H. Ikezi and P. M. Platzman, *Stability of helium films charged with electrons*, Phys. Rev. B **23** (1981), 1145. (Cited on pages 28 and 29)
48. Y. Iye, *Mobility of electrons in the surface state of liquid helium*, J. Low Temp. Phys. **40** (1980), 441. (Cited on pages 25 and 26)
49. Y. Iye, K. Kono, K. Kajita, and W. Sasaki, *Escape rate of two-dimensional electrons on a liquid helium surface around* 1*K*, J. Low Temp. Phys. **34** (1979), 539. (Cited on page 11)
50. ———, *Electron escape from the image-potential-induced surface states on liquid helium*, J. Low Temp. Phys. **38** (1980), 293. (Cited on page 11)
51. H. W. Jiang, M. A. Stan, and A. J. Dahm, *Phase diagrams and melting in a screened two-dimensional system: electrons on helium films*, Surf. Sci. **196** (1988), 1. (Cited on page 33)
52. I. Karakurt and A. J. Dahm, *Weak localization of electrons on a helium surface*, J. Low Temp. Phys. **113** (1998), 1091. (Cited on pages 43 and 45)
53. ———, *Dephasing times due to 2D electron-vapor atom scattering*, Physica B **284** (2000), 1924. (Cited on page 45)
54. I. Karakurt, D. Herman, H. Mathur, and A. J. Dahm, *Dephasing times in a non-degenerate two-dimensional electron gas*, Phys. Rev. Lett. **85** (2000), 1072. (Cited on page 46)
55. J. Klier, T. Günzler, A. Würl, P. Leiderer, G. Mistura, E. Teske, P. Wyder, and V. B. Shikin, *Two-fraction electron system on a thin helium film*, J. Low Temp. Phys. **122** (2001), 451. (Cited on page 34)
56. J. Klier, A. Würl, P. Leiderer, G. Mistura, and V. B. Shikin, *Cyclotron resonance for two-dimensional electrons on thin helium films*, Phys. Rev. B **65** (2002), 165428. (Cited on pages 34, 47, and 114)
57. K. Kono, U. Albrecht, and P. Leiderer, *Surface state electrons on a hydrogen film. 2. influence of adsorbed helium films*, J. Low Temp. Phys. **85** (1991), 423. (Cited on page 33)
58. J. M. Kosterlitz and D. J. Thouless, *Long-range order and metastability in two-dimensional solids and superfluids. (application of dislocation theory)*, J. Phys. C **5** (1972), 1124. (Cited on pages 21 and 143)
59. ———, *Ordering, metastability and phase transition in two-dimensional systems*, J. Phys. C **6** (1973), 1181. (Cited on pages 3 and 21)
60. L. P. Kouwenhoven, D. G. Austing, and S. Tarucha, *Few-electron quantum dots*, Rep. Prog. Phys. **64** (2001), 701. (Cited on page 92)
61. Yu. Z. Kovdrya, *One-dimensional and zero-dimensional electron systems on liquid helium (review)*, Low Temp. Phys. **29** (2003), no. 2, 77–104. (Cited on page 143)
62. Yu. Z. Kovdrya, V. A. Nikolaenko, S. P. Gladchenko, and S. S. Sokolov, *Linear electron chains on the liquid helium surface: Carrier transport*, J. Low Temp. Phys. **113(5-6)** (1998), 1109. (Cited on pages 4 and 103)
63. ———, *Linear electron chains on the surface of superfluid helium*, Low Temp. Phys. **24(11)** (1998), 837. (Cited on pages 4 and 103)
64. H. Kroemer, *A proposed class of heterojunction lasers*, Proc. IEEE **51** (1963), 1782. (Cited on page 2)

65. E. Krotscheck and M. Miller, *Generic electron mobility in surface states on thin helium films*, Phys. Rev. B **75** (2007), 205440. (Cited on page 33)
66. L. D. Landau and E. M. Lifshitz, *Electrodynamics of continuous media*, Pergamon Press, 1984. (Cited on page 89)
67. ———, *Fluid mechanics*, Pergamon Press, 1987. (Cited on page 83)
68. E. Lassner and W. D. Schubert, *Tungsten: Properties, chemistry, technology of the element, alloys and chemical compounds*, Kluwer Academic/Plenum Publishers, 1999. (Cited on page 62)
69. R. B. Laughlin, *Anomalous quantum Hall effect: An incompressible quantum fluid with fractionally charged excitations*, Phys. Rev. Lett. **50** (1983), 1395. (Cited on page 3)
70. M. J. Lea, P. G. Frayne, and Yu. Mukharsky, *Could we quantum compute with electrons on helium?*, Fortschr. Phys. **48** (2000), 1109. (Cited on page 51)
71. M. J. Lea, A. O. Stone, P. Fozooni, and J. Frost, *The ac response of a 2-D electron gas on liquid helium in a magnetic field*, J. Low Temp. Phys. **85** (1991), 67. (Cited on pages 73, 76, 77, and 78)
72. P. Lea, M. J. Fozooni, P. J. Richardson, and A. Blackburn, *Direct observation of many-electron magnetoconductivity in a nondegenerate 2D electron liquid*, Phys. Rev. Lett. **73** (1994), 1142. (Cited on pages 37 and 144)
73. J. L. Levine and T. M. Sanders, *Mobility of electrons in low-temperature helium gas*, Phys. Rev. **154** (1967), 138. (Cited on page 24)
74. L. B. Lurio, T. A. Rabedeau, P. S. Pershan, I. F. Silvera, M. Deutsch, S. D. Kosowsky, and B. M. Ocko, *Liquid-vapor density profile of helium: An x-ray study*, Phys. Rev. Lett. **68** (1992), 2628. (Cited on page 9)
75. ———, *X-ray specular reflectivity study of the liquid-vapor density profile of ^4He*, Phys. Rev. B **48** (1993), 9644. (Cited on page 9)
76. J. M. Luttinger, *An exactly soluble model of a many-fermion system*, J. Math. Phys. **4** (1963), 1154. (Cited on page 4)
77. M. Masili and A. F. Starace, *Static and dynamic dipole polarizability of the helium atom using wave functions involving logarithmic terms*, Phys. Rev. A **68** (2003), 012508. (Cited on page 61)
78. R. Mehrotra and A. J. Dahm, *Analysis of the Sommer technique for measurement of the mobility for charges in two dimensions*, J. Low Temp. Phys. **67** (1987), 115. (Cited on pages 73, 77, and 78)
79. R. Mehrotra, M. Guenin, and A. J. Dahm, *Ripplon-limited mobility of a two-dimensional crystal of electrons: Experiment*, Phys. Rev. Lett. **48** (1982), 9. (Cited on pages 22, 23, 49, and 73)
80. G. Mistura, O. Tress, E. Teske, V. B. Shikin, P. Wyder, and P. Leiderer, *Microwave study of surface electrons on helium films in a magnetic field*, J. Low Temp. Phys. **110** (1998), 243. (Cited on page 34)
81. Yu. P. Monarkha and K. Kono, *Two-dimensional Coulomb liquids and solids*, Springer, 2004. (Cited on page 3)
82. Yu. P. Monarkha, E. Teske, and P. Wyder, *Quantum magnetotransport in two-dimensional Coulomb liquids*, Phys. Rep. **370** (2002), 1. (Cited on pages 37, 39, 41, 42, 47, 103, 112, and 144)
83. R. H. Morf, *Temperature dependence of the shear modulus and melting of the two-dimensional electron solid*, Phys. Rev. Lett. **43** (1979), 931. (Cited on pages 22, 23, and 133)
84. P. J. Nacher and J. Dupont-Roc, *Experimental evidence for nonwetting with superfluid helium*, Phys. Rev. Lett. **67** (1991), 2966. (Cited on page 59)
85. V. A. Nikolaenko, Yu. Z. Kovdrya, and Yu. Mukharskii, *Possible spatial ordering of particles in electron chains over liquid helium*, Low Temperature Physics **32** (2006), 617. (Cited on page 103)
86. H. Oberst, Y. Tashiro, K. Shimizu, and F. Shimizu, *Quantum reflection of He^* on silicon*, Phys. Rev. A **71** (2005), 052901. (Cited on page 60)
87. R. M. Ostermeier and K. W. Schwarz, *Surface-bound electrons on liquid helium—a negative result*, Phys. Rev. Lett. **29** (1972), 25. (Cited on pages 12, 13, 14, and 46)

88. G. Papageorgiou, P. Glasson, K. Harrabi, V. Antonov, E. Collin, P. Fozooni, P. G. Frayne, M. J. Lea, Y. Mukharsky, and D. G. Rees, *Counting individual electrons on liquid helium*, ArXiv.org, cond-mat/0405084, 2007. (Cited on page 51)
89. F. M. Peeters, *Two-dimensional wigner crystal of electrons on a helium film: Static and dynamical properties*, Phys. Rev. B **30** (1984), 159. (Cited on page 32)
90. F. M. Peeters and P. M. Platzman, *Electrons on films of helium: A quantum mechanical two-dimensional fermion system*, Phys. Rev. Lett. **50** (1983), 2021. (Cited on pages 28 and 143)
91. P. M. Platzman and M. I. Dykman, *Quantum computing with electrons floating on liquid helium*, Science **284** (1999), 1967. (Cited on pages 3, 48, and 49)
92. H. Rupprecht, J. M. Woodall, and G. D. Pettit, *Efficient visible electroluminescence at* 300°K *from* $Ga_{1-x}Al_xAs$ *p-n junctions grown by liquid-phase epitaxy*, Appl. Phys. Lett. **11** (1967), 81. (Cited on page 2)
93. A. S. Rybalko, Yu. Z. Kovdrya, and B. N. Esel'son, *Electron mobility near the surface of liquid helium at temperatures down to* $0.5K$, JETP Lett. **22** (1976), 280. (Cited on page 25)
94. M. Saitoh, *Melting temperature of two-dimensional electron crystals trapped on thin-film liquid he*, Phys. Rev. B **40** (1989), 810. (Cited on pages 31 and 32)
95. D. Savignac and P. Leiderer, *Charge-induced instability of the* ^{4}*He solid-superfluid interface*, Phys. Rev. Lett. **49** (1982), 1869. (Cited on page 20)
96. V. B. Shikin, *Motion of helium ions near a vapour-liquid surface*, Sov. Phys. JETP **31** (1970), 939. (Cited on page 3)
97. ———, *Cyclotron resonance for electrons over helium in a resonator*, JETP Lett. **75** (2002), 29. (Cited on page 47)
98. ———, *Mobility of electrons on a liquid-helium film with a rough substrate*, JETP Lett. **76** (2002), 355. (Cited on page 34)
99. V. B. Shikin, J. Klier, I. Doicescu, A. Würl, and P. Leiderer, *Dip problem of the electron mobility on a thin helium film*, Phys. Rev. B **64** (2001), 073401. (Cited on page 34)
100. K. Shirahama and K. Kono, *Dynamical transition in the Wigner solid on a liquid helium surface*, Phys. Rev. Lett. **74** (1995), 781. (Cited on page 49)
101. W. T. Sommer and D. J. Tanner, *Mobility of electrons on the surface of liquid* ^{4}*He*, Phys. Rev. Lett. **27** (1971), 1345. (Cited on pages 12, 13, 14, 24, 25, 46, 70, 73, and 143)
102. M. J. Stephen, *Weak localization and the conductivity of nondegenerate electrons*, Phys. Rev. B **36** (1987), 5663. (Cited on pages 42 and 46)
103. B. Tanatar and T. Hakioglu, *Superconductivity of two-dimensional electrons on the surface of liquid helium films*, Sol. St. Comm. **88** (1993), 115. (Cited on page 3)
104. E. Teske, *Coulomb effects in magnetotransport of a non-degenerate two-dimensional electron system*, Ph.D. thesis, University of Konstanz, 2004. (Cited on pages 41 and 47)
105. E. Teske, Yu. P. Monarkha, M. Seck, and P. Wyder, *Coulomb narrowing of the quantum cyclotron resonance in a nondegenerate two-dimensional electron liquid*, Phys. Rev. Lett. **82** (1999), 2772. (Cited on page 47)
106. D. J. Thouless, *Electrons in disordered systems and the theory of localization*, Phys. Rep. **13** (1974), 93. (Cited on page 3)
107. H. Totsuji, *Numerical experiment on two-dimensional electron liquids. Thermodynamic properties and onset of short range order*, Phys. Rev. A **17** (1978), 399. (Cited on page 11)
108. D. C. Tsui, H. L. Stormer, and A. C. Gossard, *Two-dimensional magnetotransport in the extreme quantum limit*, Phys. Rev. Lett. **48** (1982), 1559. (Cited on page 3)
109. K. v. Klitzing, G. Dorda, and M. Pepper, *New method for high-accuracy determination of the fine-structure constant based on quantized Hall resistance*, Phys. Rev. Lett. **45** (1980), 494. (Cited on pages 3, 37, and 38)

110. A. M. C. Valkering, H. Yayama, and R. W. van der Heijden, *Mobility of electrons on a helium film capillary condensed on a 2d-grating*, J. Low Temp. Phys. **113(5-6)** (1998), 873. (Cited on pages 33, 103, 104, and 115)
111. C. Vicente, W. Yao, H. J. Maris, and G. M. Seidel, *Surface tension of liquid* ^{4}He *as measured using the vibration modes of a levitated drop*, Phys. Rev. B **66** (2002), 214504. (Cited on page 84)
112. M. Wanner and P. Leiderer, *Charge-induced ripplon softening and dimple crystallization at the interface of* ^{3}*He-*^{4}*He mixtures*, Phys. Rev. Lett. **42** (1979), 315. (Cited on page 19)
113. J. D. Weeks, *Volume change on melting for systems with inverse-power-law interactions*, Phys. Rev. B **24** (1981), 1530. (Cited on page 21)
114. W. Wigner, *On the interaction of electrons in metals*, Phys. Rev. **46** (1934), 1002. (Cited on page 3)
115. L. Wilen and R. Giannetta, *Cyclotron resonance of the two-dimensional electron crystal*, Phys. Rev. Lett. **60** (1988), 231. (Cited on page 47)
116. F. I. B. Williams, R. S. Crandall, and A. H. Willis, *Surface states of electrons on liquid helium*, Phys. Rev. Lett. **26** (1971), 7. (Cited on pages 3, 12, 13, 14, and 143)
117. A. Würl, *Dissertation preprint*, Ph.D. thesis, University of Konstanz, 2004. (Cited on pages 47 and 62)
118. A. P. Young, *Melting and the vector Coulomb gas in two dimensions*, Phys. Rev. B **19** (1979), 1855. (Cited on page 21)
119. J. Zinn-Justin, *Quantum field theory and critical phenomena*, Clarendon Press, 1996. (Cited on page 3)

Acknowledgements

This work would not have come to being without the help and guidance of

- **Prof. Dr. Paul Leiderer** who accepted me in his group and provided me with his invaluable knowledge, but above all, a difficult example to follow.
- **Prof. Dr. Johannes Boneberg** who very kindly accepted to be the second tutor.
- **Dr. Géza Szeghy** who worked as a postdoctoral fellow for the largest part of this project, his experience and guidance being critical for the success of the measurements.
- **Priv. Doz. Dr. Jürgen Klier** who was working as a senior scientist for the project.

Special thanks deserve to the able and kind *Louis Kukk*, the technician of the Chair, who always managed to transform vague mechanical concepts into concrete, working devices.
The Helium Team, consisting of *Hartmut Görig* and *Ralf Siebert* were always there for the timely and efficient procurement of liquid helium, for a cryostat that needed quite a lot of it.
Many thanks also to the other members of the Low Temperature group, but especially to *Michael Köppl* (and *Tanja Weller*), *Jörg Angrik*, *Masoud Sohaili* and *Andreas Würl*.

During the time of my stay in Konstanz and later in Freiburg, I had the joy and privilege to get to know friends like *Κώστα Μουτζούρη*, *Αλέξανδρο Καρύδα*, *Στέλιο Χρονόπουλο*, *Μανώλη Χαβάκη* and *Αντώνη Παπαπαντολέων* who profoundly influenced me both directly and indirectly.

Όμως πάνω απ΄ όλα, θα ήθελα να ευχαριστήσω την οικογένειά μου για την στήριξή της όλα αυτά τα χρόνια και τον αδιάσπαστο δεσμό αγάπης και σεβασμού που μας ενώνει.